VILNIUS GEDIMINAS TECHNICAL UNIVERSITY

Justė ROŽĖNĖ

APPLICATION OF *SACCHAROMYCES CEREVISIAE* YEAST IN BIOFUEL CELLS

DOCTORAL DISSERTATION

TECHNOLOGICAL SCIENCES
MATERIALS ENGINEERING (T 008)

Vilnius, 2022

Doctoral dissertation was prepared at Vilnius Gediminas Technical University in 2018–2022.

Supervisor

Dr Inga MORKVĖNAITĖ-VILKONČIENĖ (Vilnius Gediminas Technical University, Materials Engineering – T 008).

The Dissertation Defence Council of Scientific Field of Materials Engineering of Vilnius Gediminas Technical University:

Chairman

Dr Viktor GRIBNIAK (Vilnius Gediminas Technical University, Materials Engineering – T 008).

Members:

Assoc. Prof. Dr Birutė SAPIJANSKAITĖ-BANEVIČ (Kaunas University of Technology, Chemistry – N 003),
Prof. Dr Habil. Roman Adam SZEWCZYK (Warsaw University of Technology, Poland, Materials Engineering – T 008),
Assoc. Prof. Dr Jelena ŠKAMAT (Vilnius Gediminas Technical University, Materials Engineering – T 008),
Prof. Dr Vytautas TURLA (Vilnius Gediminas Technical University, Mechanical Engineering – T 009).

The dissertation will be defended at the public meeting of the Dissertation Defence Council of Materials Engineering in the Senate Hall of Vilnius Gediminas Technical University at **1 p. m. on 15 June 2022**.

Address: Saulėtekio al. 11, LT-10223 Vilnius, Lithuania.
Tel.: +370 5 274 4956; fax +370 5 270 0112; e-mail: doktor@vilniustech.lt

A notification on the intended defending of the dissertation was send on 13 May 2022. A copy of the doctoral dissertation is available for review at Vilnius Gediminas Technical University repository http://dspace.vgtu.lt and at the Library of Vilnius Gediminas Technical University (Saulėtekio al. 14, LT-10223 Vilnius, Lithuania).

Vilnius Gediminas Technical University book No 2022-023-M

doi:10.20334/2022-023-M

juste.rozene@vilniustech.lt

VILNIAUS GEDIMINO TECHNIKOS UNIVERSITETAS

Justė ROŽĖNĖ

MIELIŲ *SACCHAROMYCES CEREVISIAE* TAIKYMAS BIOKURO ELEMENTUOSE

DAKTARO DISERTACIJA

TECHNOLOGIJOS MOKSLAI,
MEDŽIAGŲ INŽINERIJA (T 008)

Vilnius, 2022

Disertacija rengta 2018–2022 metais Vilniaus Gedimino technikos universitete.

Vadovas

dr. Inga MORKVĖNAITĖ-VILKONČIENĖ (Vilniaus Gedimino technikos universitetas, medžiagų inžinerija – T 008).

Vilniaus Gedimino technikos universiteto Medžiagų inžinerijos mokslo krypties disertacijos gynimo taryba:

Pirmininkas

dr. Viktor GRIBNIAK (Vilniaus Gedimino technikos universitetas, medžiagų inžinerija – T 008).

Nariai:

doc. dr. Birutė SAPIJANSKAITĖ-BANEVIČ (Kauno technologijos universitetas, chemija – N 003),
prof. habil. dr. Roman Adam SZEWCZYK (Varšuvos technologijos universitetas, Lenkija, medžiagų inžinerija – T 008),
doc. dr. Jelena ŠKAMAT (Vilniaus Gedimino technikos universitetas, medžiagų inžinerija – T 008),
prof. dr. Vytautas TURLA (Vilniaus Gedimino technikos universitetas, mechanikos inžinerija – T 009).

Disertacija bus ginama viešame Medžiagų inžinerijos mokslo krypties disertacijos gynimo tarybos posėdyje **2022 m. birželio 15 d. 13 val.** Vilniaus Gedimino technikos universiteto senato posėdžių salėje.

Adresas: Saulėtekio al. 11, LT-10223 Vilnius, Lietuva.
Tel.: (8 5) 274 4956; faksas (8 5) 270 0112; el. paštas doktor@vilniustech.lt

Pranešimai apie numatomą ginti disertaciją išsiųsti 2022 m. gegužės 13 d.

Disertaciją galima peržiūrėti Vilniaus Gedimino technikos universiteto talpykloje http://dspace.vilniustech.lt ir Vilniaus Gedimino technikos universiteto bibliotekoje (Saulėtekio al. 14, LT-10223 Vilnius, Lietuva).

Abstract

With the rapid growth of research into the performance and applicability of biofuel cells, a remaining crucial factor is ensuring their efficiency and increasing the current output and power relative to the fuel cell area. To improve the efficiency indicators, many new scientific tasks have to be solved, such as improving the charge transfer by selecting materials and examining their impact on the performance of the biofuel cell and the viability of the microorganisms.

To create and investigate a microbial fuel cell by modifying its anodic part and using yeast as a catalyst, theoretical and analytical studies were first performed to elucidate the primary data useful for research and find solutions to the problem examined in previous studies. Experimental studies were also performed with the yeast *Saccharomyces cerevisiae* modified with 9,10-phenanthrenequinone (PQ), 2-methyl-1,4-naphthoquinone (MD) quinones, and multilayer carbon nanotubes. The investigation and evaluation focused on the viability of different yeasts under the influence of redox mediators and multi-walled carbon nanotubes (MW-CNTs). Electrochemical properties were investigated by cyclic voltammetry, and the local electrochemical properties were examined by scanning electrochemical microscopy (SECM). Mechanical properties were studied by atomic force microscopy. To this end, an atomic force microscopy model was developed to evaluate the image quality of the test results and to determine the artefacts, considering the tip geometry, scanning speed, and sample material. Investigations of the developed biofuel cells were performed at thirteen different load resistances, measuring the voltage and calculating the generated power. All the obtained data were analysed at the end of the work, and conclusions with recommendations were presented.

The obtained research results expand research possibilities and the use of biofuel cells. The study on applying yeast *Saccharomyces cerevisiae* in biofuel cells reveals the opportunities of redox medium immobilisation, the efficiency of new materials applied in biofuel cells and the benefits of selecting the parameters of the atomic force microscope used for research. Using the developed atomic force microscopy model and setting the scan parameters, the image quality of any cell can be determined before measurement if the surface material and structure are known. The atomic force microscope (AFM) operator can enter the parameters of the model surface structure and select the optimal scanning speed and the most reliable interaction force. In addition, the results determined by the AFM can be compared with the theoretically calculated from the proposed model. Also, in this research, the presented methods of applying redox mediators in biofuel cells can increase the efficiency of future biofuel cells.

Reziumė

Sparčiai didėjant tyrimų, kuriuose nagrinėjamas biokuro elementų veikimas ir taikymo galimybės, jų efektyvumo užtikrinimas ir generuojamos srovės bei galios santykiniam kuro elemento plotui didinimas vis dar išlieka esminiu faktoriumi. Siekiant gerinti efektyvumo rodiklius tenka išspręsti nemažai naujų mokslinių uždavinių, tokių kaip elektros krūvio pernašos gerinimas parenkant medžiagas ir jų išnagrinėjant jų įtaką biokuro elemento veikimui bei pačių mikroorganizmų gyvybingumui.

Siekiant sukurti ir ištirti biokuro elementą modifikuojant jo anodinę dalį ir kaip katalizatorių naudojant mieles darbe pirmiausia atlikta literatūros analizė siekiant išsiaiškinti pirminius duomenis eksperimentiniams tyrimams ir rasti nagrinėjamos problematikos sprendimo būdus. Taip pat atlikti eksperimentiniai tyrimai, kai *Saccharomyces cerevisiae* mielės buvo modifikuotos 9,10-fenantrenchinonu, 2-metil-1,4-naftochinonu ir (arba) daugiasieniais anglies nanovamzdeliais. Ištirtas ir įvertintas skirtingų mielių gyvybingumas paveikus jas elektronų pernašos tarpininkais bei daugiasieniais anglies nanovamzdeliais. Ciklinės voltamperometrijos metodu buvo tiriamos elektrocheminės savybės. Lokalios elektrocheminės savybės buvo tiriamos skenuojančiu elektrocheminiu mikroskopu (SECM). Mechaninės savybės buvo tiriamos atominių jėgų mikroskopijos metodu, taikant sukurtą dinaminį modelį, atsižvelgiant į zondo geometriją, skenavimo greitį ir mėginio medžiagą. Sukonstruotų biokuro elementų tyrimai buvo atliekami esant skirtingoms apkrovos varžoms, matuojant įtampos kritimą ir skaičiuojant generuojamą galią. Visi gauti duomenys buvo analizuojami ir pateikiamos išvados bei rekomendacijos.

Gauti tyrimų rezultatai praplečia biokuro elementų tyrimų ir panaudojimo galimybes. Mielių *Saccharomyces cerevisiae* taikymo biokuro elementuose tyrimas atskleidžia elektronų pernašos tarpininko imobilizavimo ant elektrodo galimybes, naujų medžiagų taikymo biokuro elementuose efektyvumą bei tyrimams naudojamo atominių jėgų mikroskopo parametrų parinkimo naudą. Taikant sukurtą atominių jėgų mikroskopo modelį ir pasirenkant skenavimo parametrus galima nustatyti vaizdo kokybę prieš matavimą, jei žinoma paviršiaus medžiaga ir struktūra. Atominių jėgų mikroskopo operatorius gali lengvai įvesti modelio paviršiaus struktūros parametrus, pasirinkti optimaliausią nuskaitymo greitį ir patikimiausią sąveikos jėgą. Be to, atominių jėgų mikroskopo nustatytus rezultatus galima palyginti su teoriniais, apskaičiuotais siūlomu modeliu. Taip pat pasitelkus pasirinktų ir pritaikytų tyrimuose elektronų pernašos tarpininkų taikymo biokuro elementuose būdus galima padidinti šių efektyvumą.

Notations

Symbols

E_s – Young's module of silicon (page 42);
h_c – damping of cantilever (page 42);
h_k – damping of contact between surface and tip (page 42);
h_s – damping of scanner (page 42);
h_v – damping of control latency DOF (page 42);
k_c – stiffness of cantilever (page 42);
k_s – stiffness of scanner (page 42);
k_v – stiffness of control latency DOF (page 42);
m_c – mass of cantilever $m = \rho V$ (page 42);
mM – millimolar (page 22);
m_s – mass of scanner (page 42);
P – Poisson's ratio of silicon (page 42);
Pt – platinum (page 11);
ρ – density of cantilever material (page 42).

Abbreviations

AFM – atomic force microscope/microscopy;
BFC – biofuel cell;
BS – phosphate-acetate buffer solution;

CFU – colony-forming units;
CV – cyclic voltammogram;
DNA – deoxyribonucleic acid;
DOF – degree of freedom;
FCN – potassium ferricyanide;
MD – 2-methyl-1,4-naphthoquinone, menadione;
MFC – microbial fuel cell;
MW-CNT – multi-walled carbon nanotube;
OD – optical density;
PI – propidium iodide;
PMMA – poly (methyl methacrylate);
PQ – 9,10-phenanthrenequinone;
RBM – radial breathing mode;
RNA – ribonucleic acid;
ROS – reactive oxygen species;
SEM – scanning electron microscopy;
UV-VIS – ultraviolet-visible;
XRD – X-ray diffraction analysis;
YPG – yeast extract peptone glucose.

Contents

Introduction

Problem Formulation

In recent years, the rapid growth in demand for energy resources and environmental pollution monitoring has led to a shift towards alternative energy sources. However, only recently, biofuel cells have started to be considered an alternative energy source, especially in addressing the energy consumption of wastewater treatment. The food and beverage industry has been using biofuel cells to treat wastewater, generating power from 50 to 2000 $\mu W/cm^2$.

Electrodes used as anodes and cathodes are becoming the leading and most crucial aspect of biofuel cells. Therefore, a material with high biocompatibility, must be selected as essential aspects. When choosing electrodes, it is also necessary to select catalysts: enzymes, bacteria or microorganisms.

Therefore, it is essential to consider the properties of redox mediators: electrochemical activity; non-toxicity to microorganisms; easy penetration through the cell membrane; adequate redox potential for electron transfer mediation; soluble and chemically stable anolyte; rapid kinetics of the oxidation process at the electrode surface. Also, a system of two mediators is commonly used to ensure proper electron transfer from microorganisms towards the electrode.

Thus, the main problem, which is still being addressed, is ensuring the efficiency of biofuel cells by selecting required materials and their application method

to improve electric charge transfer from the cell to the anode in an alternative energy source.

Relevance of the Thesis

With the rapid growth of research into the performance of biofuel cells and their potential applications, their low efficiency remains a significant problem. Many new scientific challenges need to be addressed to increase biofuel cell performance.

The study on applying yeast *Saccharomyces cerevisiae* in biofuel cells reveals possibilities of diminishing the toxic effect of quinones on the microorganisms by immobilising them on the electrode instead of adding them into the working solution. Additionally, the application of such new materials as multiwalled carbon nanotubes in biofuel cells is expected to increase biofuel cell efficiency.

Research Object

The object of the present study is a biofuel cell and its performance.

Aim of the Thesis

The aim of the thesis is to develop and investigate an MFC with the anode based on yeast, quinones and MW-CNTs.

Tasks of the Thesis

In order to achieve the objective of the thesis, the following tasks had to be solved:

1. To develop and evaluate a methodology for viability assessment, electrochemical activity and visualisation of living cells.
2. To create a dynamical model for an AFM electromechanical system to determine the parameters suitable for living cell visualisation and estimation by atomic force microscopy while working in the contact mode.
3. To evaluate lipophilic redox mediators and (or) multilayer carbon nanotubes' effects on the viability and electrochemical activity of yeast used in biofuel cells.

4. To determine the efficiency of developed MFC with yeast as a catalyst, PQ, MD, and MW-CNTs using a system based on two redox mediators in the anode compartment.

Research Methodology

The thesis first includes a literature analysis to find the primary data useful for research and solutions to similar problems. The found information was classified and summarised. Next, experimental studies were continued by modifying *Saccharomyces cerevisiae* with quinones and/or MW-CNTs. The viability of different yeast cells was assessed by optical microscopy, and the electrochemical properties were evaluated by cyclic voltammetry. Local electrochemical properties were examined by scanning electrochemical microscopy (SECM), and the visualisation was made using atomic force microscopy. Also, MFC performance was investigated at different loads by measuring voltage and calculating the generated power. The obtained data were analysed at the end of the work, resulting in conclusions and recommendations.

Scientific Novelty of the Thesis

During the research on the dissertation topic, the following new knowledge for the science of materials engineering was obtained:

1. The created AFM model can be used for AFM scanning optimisation by considering the tip's geometry and the sample's material.
2. For the first time, the applicability was evaluated of PQ in MFCs based on *Saccharomyces cerevisiae* baker's yeast strain and *Saccharomyces cerevisiae* 21PMR (MATα leu2 ura3-52) strain, and charge transfer aspects were described between living yeast cells and electrodes.
3. For the first time, the effects were evaluated of MD exposure on the viability of the *Saccharomyces cerevisiae* baker's yeast strain, *Saccharomyces cerevisiae* 21PMR (MATα leu2 ura3-52) strain and the possibility of using this MD compound as the redox mediator in the MFC.
4. For the first time, the influence was investigated of the MW-CNTs and PQ/MW-CNTs application in MFCs on the *Saccharomyces cerevisiae* baker's yeast strain and *Saccharomyces cerevisiae* 21PMR (MATα leu2 ura3-52) strain cells.

Practical Value of the Research Findings

The obtained research results expand research possibilities and the use of biofuel cells. Also, the results enable new research methods. Using the developed atomic force microscopy model and selecting the scanning parameters, the image quality can be determined before measurement if the surface material and structure are known. The AFM operator can enter the surface structure parameters, and the optimal scanning speed and the most reliable interaction force will be selected. In addition, the results determined by the AFM can be compared with the theoretically calculated from the proposed model.

Methods for applying quinones as redox mediators in biofuel cells, selected and used in research, can also lead to higher efficiency biofuel cells.

Defended Statements

The following statements based on the results of the present investigation may serve as the official hypotheses to be defended:

1. Using the developed dynamic AFM model for biofuel cell research, input parameters can be selected for measurement by atomic force microscopy to improve the visualisation of living cells while using the developed dynamic AFM model for biofuel cell research.
2. The immobilised 2.5 μL drop of quinones or MW-CNTs instantly improves electrical charge transfer between yeast and anode in yeast-based MFC.
3. The system based on two redox mediators is well suitable for charge transfer in an MFC when the anode is modified by PQ or MD.
4. The concentration of quinones and MW-CNTs used to modify yeast in biofuel cells should be selected according to the results of yeast viability and electrochemical activity experiments.

Approval of the Research Findings

Seven scientific articles were published on the topic of the dissertation.

The author gave ten presentations at eleven scientific conferences:

The 16th International Conference *Mechatronic Systems and Materials (MSM 2021*). Vilnius, Lithuania.

The 23rd International Conference – school *Advanced materials and technologies*. Palanga, Lithuania.

The International Conference *2021 IEEE Open Conference on Electrical, Electronic and Information Sciences (eStream)*. Vilnius, Lithuania

The International Conference *Automation 2021. Recent Achievements in Automation, Robotics and Measurement Techniques*. Warsaw, Poland.

The Fourteenth International Conference *The vital nature sign*. Kaunas, Lithuania.

The 22nd International Conference – school *Advanced materials and technologies*. Palanga, Lithuania.

The International Conference *Automation 2020. Towards industry of the future*. Warsaw, Poland.

The 62nd International Conference for Students of Physics and Natural Sciences *Open readings 2019*. Vilnius, Lithuania.

The 9th International Conference of Young Scientists *Interdisciplinary Research in Physical and Technological Sciences*. Vilnius, Lithuania.

The International Conference *The immunosensors based on scanning electrochemical microscopy // 10th International workshop on SECM and related techniques* 2019. Paris, France.

The International *Automation 2019. Progress in automation, robotics and measurement techniques* Conference. Warsaw, Poland.

The Structure of the Dissertation

The dissertation is structured around three main chapters.

Chapter 1 presents the overview and analysis of all the components necessary for biofuel cells. First, different types of biofuel cells designed in the past few years are discussed. Also, various electron transfer mediators chosen for the biofuel cell research are described: PQ, MD; MW-CNTs. The analysis also includes the *Saccharomyces cerevisiae* yeast cells. Finally, the chapter presents the application of atomic force microscopy in living cell studies.

Chapter 2 reviews the methods used for the investigation and materials, including a graphite electrode, yeast cells and MW-CNT suspension preparation. The preparation of yeast cells is described for the experiments with redox mediators and MW-CNTs. A part of the chapter is devoted to describing the electrochemical measurements and characterisation of nanoparticles.

Chapter 3 presents experimental investigation results on the application of yeast *Saccharomyces cerevisiae* in biofuel cells. Based on the methods discussed

in Chapter 2, this chapter presents the results of modelling and the electrochemical studies of a yeast-modified biofuel cell.

The study is summarised by general conclusions and recommendations. It closes with an extensive list of references and a list of 4 publications by the author on the dissertation topic.

Acknowledgement

Throughout the writing of this dissertation, I have received a great deal of support and assistance.

First, I would like to thank my supervisor, Dr. Inga Morkvėnaitė-Vilkončienė, whose expertise was invaluable in formulating the research questions and methodology. Your insightful feedback encouraged me to sharpen my thinking and brought my work to a higher level.

I want to acknowledge my colleagues at Vilnius Gediminas Technical University for their extraordinary collaboration. The department of Robotics, Mechatronics and Digital Manufacturing was my support team during the most challenging times. Special thanks go to the Head of the department, Prof. Dr Vytautas Bučinskas.

I want to acknowledge my internship colleagues at the Institute of Physical Chemistry for their wonderful collaboration. Special thanks go to my supervisor Wojciech Nogala. Wojciech, thank you for your patient support and all of the opportunities I was given to further my research.

I also thank my colleagues from Vilnius University and the Center for Physical Sciences and Technology for their valuable guidance throughout my studies. You provided me with the tools to choose the right direction and successfully complete my dissertation.

I am grateful to every co-author of the articles, reviewers and consultants, and the staff of the doctoral department.

Also, I want to extend my appreciation to my family and relatives for their wise counsel and a sympathetic ear. You are always there for me.

Finally, I could not have completed this dissertation without the support of my friends, who provided stimulating discussions and happy distractions to rest my mind outside my research.

1

Overview and Analysis of Biofuel Cells

Chapter 1 reviews the types of biofuel cells and the experiments with different types of cells and redox mediators. The power density and other efficiency parameters from past experiments were collected and reviewed. All the chosen redox mediators (PQ and MD), carbon nanotubes and *Saccharomyces cerevisiae* yeast cells were analysed. Also, the chapter reviews the application of atomic force microscopy in living cell studies. It concludes by formulating the main objective and tasks of the present investigation.

Seven scientific articles by the author have been published on this chapter topics (Morkvenaite-Vilkonciene et al., 2019, 2019b, Bruzaite et al., 2020a, Rozene et al., 2020, 2021a, 2021b, 2022).

1.1. Biofuel Cells and their Types

Nowadays, generating sustainable and environmentally clean energy from renewable sources is becoming extremely important. In this context, biofuel cells (BFCs) based on enzymes (Ramanavicius et al., 2015) and microorganisms

(Bruzaite et al., 2020a)* are of particular interest because they can convert chemical energy into electrical (Ramanavicius et al., 2005). BFCs use substrates from renewable sources (Krikstolaityte et al., 2013); therefore, they have a high conversion efficiency (Babanova et al., 2011). BFCs can be applied in several areas, e.g., in wireless biosensors for environmental monitoring or the powering of implantable or attachable sensors and biosensors (Ruzgas et al., 2019).

A microbial fuel cell is a bio-electrochemical appliance with microorganisms converting chemical energy into electric energy, primarily acting at the anode compartments (Rahimnejad et al., 2011, 2015a). The advantage of MFCs over enzymatic BFCs is that microbes are less susceptible to poisoning and loss of activity under normal operating conditions (Davis and Higson, 2007). Furthermore, in MFCs, mixed cultures of microorganisms can be used, such as *R. ferrireducens*, *E. coli*, *Shewanella oneidensis*, or even a mixed community (Slate et al., 2019).

Microbes used in MFCs offer significant advantages over enzymes because of their viability, regeneration-ability, versatile catalytic properties, reduced sensitivity to poisoning compounds, and activity (Davis and Higson, 2007). In addition, during the generation of electrical energy, some designed MFCs can efficiently perform in wastewater treatment (Schaetzle et al., 2008) and convert the chemical energy of some hazardous compounds into electrical ones (Ramanavicius and Ramanaviciene, 2009; Kisieliute et al., 2019). Moreover, microorganism-based MFCs can be well used to design some attractive educational tools. In MFC, redox-active microorganisms are exploited as versatile "biocatalysts" suitable for bioelectricity production (Bruzaite et al., 2020a). Most microorganisms are used to design anode compartments of MFCs, which can be either aerobic (Kisieliute et al., 2019) or anaerobic (Rahimnejad et al., 2011, 2015b). Significant electric charge can be generated during the metabolic redox process, which occurs in living microorganisms (Davis and Higson, 2007; Liu et al., 2018). Yeast cells are widely accessible and suitable for redox-active microorganisms relevant for MFCs (Raghavulu et al., 2011). However, the generation of such "bioelectricity" is limited by the cell membrane and cell wall, which significantly reduce yeast cells' ability to transfer charge generated during metabolic processes. Therefore, there is tremendous demand to increase the electrical conductivity of the cell membrane and/or cell wall. In the scientific literature, the modified cell membranes of different microorganisms, such as *Aspergillus niger* (Stirke et al., 2016; Apetrei et al., 2018, 2019) and some strains of the yeast cells (Ramanavicius et al., 2016; Andriukonis et al., 2018; Kisieliute et al., 2019) can be found. This technique enabled the increase of the charge transfer through the cell membrane and/or cell wall because the conducting polymer mainly was formed within the

*The reference is given in the list of publications by the author on the topic of the dissertation.

cell membrane and/or between the cell membrane and cell wall. The power generated by an MFC heavily depends on charge transfer efficiency from microorganisms towards electrodes; therefore, significant attention should be paid to this issue during a BFC design (Hubenova and Mitov, 2015).

An essential part of an MFC is the anode compartment, in which electric charge generated during metabolic processes running inside of microorganisms should be transferred towards the electrode. However, the high internal resistance of the cell wall of microbes reduces power production by MFCs (Sharma and Li, 2010). Therefore, power and current densities generated by MFCs are still relatively low (Sekrecka-Belniak and Toczyłowska-Mamińska, 2018) because one of the significant factors limiting the performance of MFCs is a restricted charge transfer from the living cells to the anode (Kisieliute et al., 2019).

A comparison of the MFC efficiency data revealed that the highest power of 2520 mW/m^2 was observed in the MFC with graphene oxide aerogel-graphite fibre brush and *S. oneidensis* MR-1 in the anode compartment, and graphite felt in the cathode compartment without any redox mediators in solution (Table 1.1). MFCs with *Escherichia coli* generated the power range from 980 mW/m^2 to 1624 mW/m^2; using *S. putrefaciens,* the power was from 1025 mW/m^2 to 1735 mW/m^2. One research reported *S. cerevisiae* based BFC generated power of 146.71 mW/m^3. However, this power value was calculated in the volume of the platinum mesh anode. Therefore, data are difficult to compare due to different conditions.

Table 1.1. Open circuit voltage (OCV) and maximal power output data collected from references reporting MFC investigations

Anode compartment	Cathode compartment	OCV, mV	Maximal power output, mW/m^2	Reference
Carbon felt / *C. melibiosica*	carbon felt in BS			(Babanova et al., 2011)
Mediatorless		345	20	
Methyl orange		360	137	
Methyl red		380	113	
Methylene blue		513	640	
Neutral red		679	89	
Bromocresol green		774	46	
Ni-modified carbon felts/ *C. melibiosica*	carbon felt in BS	400	390 720	(Hubenova et al., 2010)
Carbon felt / *C. melibiosica*			36	

Table 1.1 continued

Anode compartment	Cathode compartment	OCV, mV	Maximal power output, mW/m^2	Reference
Platinum mesh electrode/ *S. cerevisiae* / methylene blue, $K_3[Fe(CN)_6]$	platinum mesh electrodes in BS	500	130 (μW)	(Walker and Walker Jr, 2006)
Reticulated vitreous carbon / *S. cerevisiae* / methylene blue, $K_3[Fe(CN)_6]$	reticulated vitreous carbon	383.6	146.71 (mW/m^3)	(Gunawardena et al., 2008)
Graphite rod / *Saccharomyces cerevisiae* in cellulose acetate membrane without methylene blue with methylene blue	graphite rod	 46.5 233	-	(Rossi et al., 2016)
Carbon felt modified with polyethyleneimine / *Saccharomyces cerevisiae* no mediator methylene blue methyl red	carbon felt	 755 611 505	 254.52 429.29 282.77	(Christwardana et al., 2018a)
Carbon felt with polyethylenimine/ *Saccharomyces cerevisiae* without methylene blue with methylene blue	carbon felt	 688 521	 340.9 374.4	(Christwardana et al., 2018b)
PQ and yeast modified graphite electrode / *S. cerevisiae* / $K_3[Fe(CN)_6]$	graphite electrode in $K_3[Fe(CN)_6]$	178	22.2	(Rozene et al., 2021a)*
MD and yeast modified graphite electrode / *S. cerevisiae* / $K_3[Fe(CN)_6]$	graphite electrode in $K_3[Fe(CN)_6]$		0.408	(Rozene et al., 2021b)*

*The reference is given in the list of publications by the author on the topic of the dissertation.

Table 1.1 continued

Anode compartment	Cathode compartment	OCV, mV	Maximal power output, mW/m^2	Reference
Polyaniline and Titanium dioxide / *Escherichia coli* / $K_3[Fe(CN)_6]$	carbon cloth in BS	410	1495	(Qiao et al., 2008a)
Polyaniline / Titanium dioxide / *Escherichia coli*	carbon cloth in BS	340	1300	(Qiao et al., 2008b)
Tungsten trioxide, Polyaniline, carbon felt /*Escherichia coli*	Pt in BS	864	980	(Wang et al., 2013)
Tin oxide nanoparticles on graphene oxide /*Escherichia coli*	Pt rod in BS	580	1624	(Mehdinia et al., 2014)
Carbon fibre paper modified with Eucalyptus leaves / *Escherichia coli* / 2-hydroxy-1,4-naphthoquinone	carbon fibre paper in BS	-	1158	(Zhou et al., 2019)
Carbon paper/ *Geobacter metallireducens*	carbon paper, coated by Pt in BS	604	40	(Min et al., 2005)
Biogenic palladium - carbon cloth / *S. oneidensis* MR-1	carbon paper in BS	780	500	(Quan et al., 2015)
Tartaric acid doped polyaniline modified carbon cloth / *S. oneidensis* MR-1	plain carbon cloth in $K_3[Fe(CN)_6]$	10	490	(Liao et al., 2015)
Nano-flower/ polyaniline-carbon cloth / *S. oneidensis* MR-1	carbon felt, $K_3[Fe(CN)_6]$ in KCl solution	-	388.6	(Liu et al., 2017)
Graphene oxide aerogel-graphite fibre brush *S. oneidensis* MR-1	graphite felt in BS	-	2520	(Yang et al., 2016)
Graphene oxide/ polyaniline-carbon plate / *S. oneidensis* MR-1	graphite felt in aqueous solution	334 and 324	381	(Sun et al., 2017)

End of Table 1.1

Anode compartment	Cathode compartment	OCV, mV	Maximal power output, mW/m^2	Reference
Graphene riboflavin - Graphite plate / *S. oneidensis* MR-1	graphite felt in riboflavin solution	381 and 259	257	(Wang et al., 2017)
Molybdenum carbide-carbon felt / *S. putrefaciens* CN32	carbon fibre brush	10	1025	(Zou et al., 2017)
The graphite felt modified by polypyrrole (ppy) and polythiophene (pth) nanoparticles / *S. putrefaciens*	graphite felt in BS	-	1220 ppy 800 pth	(Sumisha and Haribabu, 2018)
Polydopamine - Macroporous graphitic carbon foam / *S. putrefaciens*	graphite felt in M9 buffer solution	700	1735	(Jiang et al., 2017)
Poly (3,4- ethylenedioxythiophene) - carbon cloth / *S. loihica* PV-4	carbon paper in BS	10	140	(Liu et al., 2015)

1.2. Redox Mediators Used in the Biofuel Cells

Redox mediators are essential for improving the efficiency of electrochemical energy storage and conversion systems. Mediators may exchange electrons with fuels or oxidants at the reaction sites of biocatalysts, then diffuse to the electrode surface and exchange electrons there during a bioelectrocatalysis process (Babanova et al., 2011).

1.2.1. 9,10-Phenanthrenequinone as Redox Mediator in the Biofuel Cell

An artificial mediator to be used in an MFC should satisfy several requirements: (i) it should be electrochemically active; (ii) it must be non-toxic for microorganisms applied in MFCs; (iii) it should penetrate the cell membrane easily; (iv) its redox potential should be appropriate for mediated electron transfer; (v) it should be soluble and chemically stable in both forms oxidised and reduced; and (vi) the

kinetics of the oxidation process at the electrode surface should be fast (Babanova et al., 2011; Kisieliute et al., 2019). Some of the best recently known artificial mediators are thionine, methylene blue, neutral red, 2,6-dichlorophenolindophenol, safranine-O, phenothiazine, and benzyl viologen (Babanova et al., 2011). Some conducting and organic polymers can be chosen as redox mediators because of their charge transferability (Hao Yu and Scott, 2010; Oztekin et al., 2011). In some research, nanoparticles were used to modify anode using different nanoengineering techniques to improve electron transfer (Scott et al., 2007; German et al., 2012). Carbon nanotubes (CNTs) can improve the electron transfer and amplify electrode surface area by utilising carbon nanotube/polyaniline nanostructure composite as anode materials because CNTs are sufficiently conductive to provide fast electron transfer from microbial cells to the electrode. To ensure the advanced electron transfer from the yeast cells to the electrode, a two mediator-based redox system is usually applied: one redox mediator is lipophilic and can penetrate the cell membrane and interact with the intracellular redox centres; another mediator is hydrophilic and accepts electrons from the lipophilic mediator and passes them to the electrode (Morkvenaite-Vilkonciene et al., 2016a; Kisieliute et al., 2019). Some quinones can be applied as lipophilic mediators; however, some are very toxic and can damage and inactivate microorganisms. Although the ability of quinones to act as redox mediators in some electrochemical systems is well established, the degree to which these quinones contribute to overall cytotoxicity is still unclear and is highly dependent on their chemical properties and the conditions of cellular exposure (Hossain et al., 1989; Ishioka et al., 2001; Le Comte et al., 2015; Brousse et al., 2018; Genys et al., 2019). Lipophilic redox compound – PQ – can act intracellularly when reduced and diffuse back through the membrane into the solution (Rodriguez et al., 2008; Yamashoji, 2016). Therefore, in this case, to ensure effective electron transfer to the electrode, the second redox mediator (e.g., ferricyanide) is required (Morkvenaite-Vilkonciene et al., 2016a). Some research demonstrated the possibility of using yeast as a probe to assess redox and electrophile-based toxicities (Rodriguez et al., 2004). Two types of redox mediators are required because one of them acts as an intracellular redox mediator, which transfers the charge across the cell membrane (Hubenova et al., 2010).

The possibility of applying PQ as a redox mediator to evaluate yeast viability was shown in our previous research (Morkvenaite-Vilkonciene et al., 2016a; Ramanavicius et al., 2017; Kisieliute et al., 2019). The research used PQ to image yeast by scanning electrochemical microscopy (SECM) and determined a sufficiently high electrochemical signal compared to p-benzoquinone, 2,6-dichlorophenolindophenol sodium salt hydrate, 10-phenanthroline-5,6-dione. Based on the results, it was predicted that PQ could be suitable for the design of yeast-based

MFC to improve charge transfer through the yeast membrane and cell wall towards the electrode.

1.2.2. 2-Methyl-1,4-naphthoquinone as Redox Mediator in the Biofuel Cell

The charge transfer from the microorganisms to the electrode issue can be solved by adding suitable mediators and optimising the cell design and the electrode. To be used in MFCs, a mediator with appropriate properties must be used. It must be electrochemically active, soluble, chemically stable, non-toxic to microorganisms, easily permeable to the cell membrane, and have a redox potential adequate for electron transfer with a rapid oxidation process at the electrode surface (Qiao et al., 2007; Babanova et al., 2011). Some of the best known artificial mediators are thionine, methylene blue, 2-methyl-1,4-naphthoquinone (MD), thionine, Meldola's Blue, and neutral red (Babanova et al., 2011). Furthermore, conductive polymers can be used as redox mediators (Hao Yu and Scott, 2010). In this case, the anode can be modified by conductive polymers, and polymerisation can be performed by the redox processes occurring in living cells. Electron transfer can be improved, and the area of the electrode (anode) can be increased by modifying it with nanomaterials or nanomaterials and polymers (Scott et al., 2007). Carbon nanotubes (CN) can improve the electrode's charge transfer and working area. The composite of CN and polyaniline nanostructure might be used as the material for the anode electrode to achieve the best operating parameters to maintain the potential value (Bruzaite et al., 2020b). The anode can be modified by lipophilic redox mediators to avoid organic solvents in the solution and to ensure a redox mediator concentration that is as low as possible. With low concentration, it becomes possible to use more than just non-toxic redox mediators in this case. Earlier research showed that PQ (Morkvenaite-Vilkonciene et al., 2016b; Kisieliute et al., 2019) and MD (Petroniene et al., 2020a, 2020b) at low concentrations could be used as redox mediators. MD is reduced intracellularly and diffused back through the membrane into the solution (Rodriguez et al., 2008; Yamashoji, 2016). The second redox mediator, such as ferricyanide, should be used to ensure effective electron transfer to the electrode (Morkvenaite-Vilkonciene et al., 2016b). This is called a two-mediator-based system: one mediator is lipophilic, which interacts with the intracellular redox centres; another mediator is hydrophilic, which takes an electron from the lipophilic mediator and passes it to the electrode (Hubenova et al., 2010). Some of the quinones can be used as a lipophilic mediator and are associated with bone marrow toxicity; additionally, quinones formed by oxidation of polycyclic aromatic hydrocarbons may form adducts with deoxyribonucleic acid (DNA) and ribonucleic acid (RNA), and quinone compounds have been used as anti-cancer drugs (Brunmark and Cadenas,

1989; O'Brien, 1991; Monks and Lau, 1992; Bolton et al., 2000). Quinones can form reactive oxygen species (ROS), such as superoxide (O^{2-}) or hydrogen peroxide (H_2O_2), which can be deleterious (O'Brien, 1991; Monks and Lau, 1992; Kumagai et al., 2002). The effect of quinones on living cells is still unclear and depends on the conditions of cellular exposure.

1.2.3. Carbon Nanotubes as Redox Mediator in the Biofuel Cell

Carbon nanotubes are widely used in chemical/biological sensors, electronics, biomedicine (Cheng et al., 2009) and applied in the production of conducting fibres to cover various sports equipment, which is possible due to their exclusive mechanical, electrical, thermal, and chemical properties (100 times stronger than steel, best field emission emitters, the ability to maintain the current density of more than 10 nA/cm^2, thermal conductivity comparable to diamonds' (Chandrasekhar, 2018)). Therefore, it is predicted that one of the ways to improved charge transfer efficiency in an MFC is to advance the conductivity of these cellular structures by modifying the microorganisms' membrane with carbon nanotubes. According to the information in the reviewed literature, the positive and negative effects of carbon nanotubes on living cells can be noticed. Studies conducted over the past years have provided compelling evidence that various nanoparticles, including metal oxides, fullerenes, and carbon nanotubes, can cause toxic effects on different cells (Kisin et al., 2007; Handy et al., 2008). Some published data suggest stimulating cellular growth by carbon nanotubes (Ghafari et al., 2008). However, the data of other research groups indicate the increase in their mortality towards some kinds of cells, such as murine bone marrow-derived dendritic cells, 3T3 fibroblasts, bronchial epithelial cells and RAW macrophages, human bronchial epithelial cells line (Handy et al., 2008; Francis and Devasena, 2018; Yuan et al., 2019; Mohanta et al., 2019). Yeast *Saccharomyces cerevisiae* cells are widely used in cellular biology studies and molecular biology because of their analogy to the cells of higher eukaryotic organisms. However, there is a lack of knowledge concerning the viability of yeast cells treated by carbon nanotubes.

1.3. *Saccharomyces Cerevisiae* Yeast Cells in Biofuel Cells

Baker's yeast and *Saccharomyces cerevisiae* are used rarely but successfully (Bruzaite et al., 2020b; Rozene et al., 2021a)*. MFCs are environmentally friendly and suitable for compensating for the energy used to treat various industrial

*The reference is given in the list of publications by the author on the topic of the dissertation.

wastewater, and they do not require strict conditions (Babanova et al., 2011; Pandey et al., 2016). MFCs' output is restricted, while high internal resistance considerably decreases the energy produced by MFCs (Sharma and Li, 2010). The main factor determining the MFCs efficiency is the charge transfer from the microorganisms to the electrode (Babanova et al., 2011).

During the last few years, yeast, such as *Saccharomyces cerevisiae*, has been reported as biocatalysts in fuel cells. The yeasts have been utilised for centuries in numerous biotechnological processes in the food industry, which generate enormous amounts of wastewaters rich in organic matter. BFCs are considered an alternative for purifying such wastewaters (Hubenova and Mitov, 2015). The yeast as biocatalyst is ideal for this purpose because of its properties: (i) similarity to mammalian systems homology; (ii) predictable sensitivity/resistance to quinones; (iii) ability to survive in a variety of conditions; and (iv) easy availability and relatively low cost (Baronian, 2004; Rodriguez et al., 2004).

1.4. Application of Atomic Force Microscopy in Living Cell Studies

Atomic force microscopy is a type of scanning probe microscopy (SPM) that can be applied in various surface studies. It is beneficial for surface characterisation at the nanoscale (Morkvenaite-Vilkonciene et al., 2013; Schillers et al., 2017; Janickis et al., 2018; Khedmati et al., 2018). The AFM technique was first developed in 1986 by G. Binnig et al. with a lateral resolution of 30 Å and a vertical resolution of 1 Å in contact mode (Binnig et al., 1986, 1987). Since then, new applications and new AFM modes have been invented (Santos et al., 2011; Lai et al., 2016); the most common AFM modes are: (i) static (contact), (ii) dynamic (tapping) mode; (iii) non-contact mode (Yang et al., 2007) and (iv) contact resonance (Hurley, 2010; Yablon et al., 2012; Kocun et al., 2015)). The main problem in contact mode AFM is the loss of actual contact with the surface of the sample, and this problem very often appears at high scanning velocity. If contact-related issues are resolved, scanning velocity can be increased by up to ten-fold (Bučinskas et al., 2016b; Dzedzickis et al., 2018).

The resolution of AFM images depends on the properties of a combination of scanner and probe, consisting of a tip formed/mounted on a cantilever (Sedin and Rowlen, 2001; Shaik et al., 2016). The scanner's properties directly influence the AFM scan rate, resolution, and, therefore, the overall quality of the image. The number of parameters affects the quality of the AFM image, including ambience, temperature, scanning velocity (Nievergelt et al., 2017), forces applied to the cantilever/probe, the geometry of the used tip, quality (wearing and contamination) of the tip (Frederix et al., 2009), and the material of the sample (Marinello et al.,

2010). Some of these parameters, such as temperature and other environmental conditions, can be controlled easily. The influence of these parameters on the image quality is not very high. However, some very sensitive parameters, such as scanning velocity and applied force, are usually controlled by the user, and, mostly, both these parameters are optimised intuitively.

A decisive parameter is the type and quality of the cantilever and probe because this parameter affects the accuracy of AFM-based measurements and image quality (Wade et al., 2004; Dai et al., 2006; Tranchida et al., 2006). There can be sound reasons to select a particular cantilever type when examining a hard surface, e.g., silicon-based cantilever. However, the AFM-based probing of polymers or living cells usually should account for some result errors (Jones et al., 2002). In addition, a worn tip of the probe can generate various artefacts, which are influenced by the tip geometry or unstable contact of the tip with the surface (Hutter and Bechhoefer, 1993). Image quality may also be affected by the tip contamination, which may not be identified on time (Taatjes et al., 1999).

Moreover, the tip's geometry can vary over time, especially if hard or contaminated surfaces are imaged and wearing cannot be identified experimentally during the measurement (Sedin and Rowlen, 2001; Liu et al., 2010). It is impossible to distinguish wearing from contamination while measuring because an image obtained with a worn or contaminated tip results in poor image quality. Normally, a calibration grid can be used to determine the suitability of a cantilever for measurement (Markiewicz and Goh, 1995), although the grid will provide information only if the tip is "good" or "bad"; the problem of wearing or contamination will remain unresolved. Apart from the tip, both the scanning speed and scanning range (horizontal and vertical) are the sources of AFM image artefacts, which depend on scanner type. This study used Nanosurf AFMs equipped with electromagnetic scanners rather than the commonly used piezoelectric type. This AFM can achieve a vertical stroke up to 21 μm, operates at low voltage and has a simple positioning of the probe (Howald, 2003). Nanosurf AFMs are universal, are notable for their price to performance ratio and are helpful for the imaging of a wide variety of samples. This type of scanner overcomes most of the limitations of the piezoelectric scanners, but scanning velocity is limited. Generally, the imaging velocity of the AFM is determined by numerous and specific dynamic factors related to the properties of the selected cantilever and sample, as well as the nature of the tip and surface interaction. Attempts to increase the scanning velocity inevitably lead to impaired image quality and the appearance of artefacts caused by dynamic errors (Zhao et al., 2008). Moreover, various surface properties and imaging goals require distinctive scanning strategies, which are unique and different from piezoelectric AFM types. At high scanning speeds, the quality of the AFM image resolution can be improved by increasing vertically applied force

(Bučinskas et al., 2016b, 2016a), although this is only possible when the dynamic characteristics of the moving scanner are known.

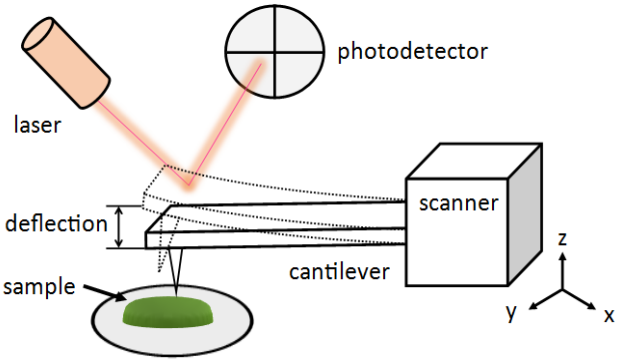

Fig. 1.1. Simplified AFM scheme (Morkvenaite-Vilkonciene et al., 2019a) *

The general AFM scheme is shown in Fig. 1.1. The AFM probe consists of the tip and the cantilever. The diameter of the curvature of the tip is usually in the range of 1–50 nm. The tip's apex angle is typically in the 10–20° range. Cantilevers made from silicon compounds (SiO_2 or Si_3N_4) used photolithography and etching methods for experiments. The tip interacts with the surface during the scan due to Van der Waals interatomic forces. The AFM tip scanned the sample line by line in the horizontal plane (x and y directions). Depending on the tip-surface interaction force, the cantilever has deflected. The optical system measured this deflection by way of the laser beam, which was reflected from the cantilever and was detected by photodiodes. Control electronics engage the feedback control accordingly and adjust the z-axis value if required. Thus, the feedback loop was used to keep the set-point interaction force between the tip and surface of interest. The computer processed the cantilever deflection signal from the detector, and a corresponding line-by-line image was formed.

1.5. Conclusions of Chapter 1 and Formulation of the Thesis Tasks

An analysis of the literature led to the following conclusions:

1. Some quinones applied as lipophilic mediators are toxic and, therefore, can damage and inactivate microbial cells. However, the degree to which

*The reference is given in the list of publications by the author on the topic of the dissertation.

these quinones contribute to overall cytotoxicity is still unclear and is highly dependent on their chemical properties and the conditions of cellular exposure. Lipophilic redox compound — PQ — can act intracellularly when reduced and diffuse back through the membrane into the solution. Baker's yeast in combination with PQ has not been used in MFCs before.

2. The anode of the MFC can be modified by lipophilic redox mediators to avoid organic solvents in the solution and to ensure a redox mediator concentration as low as possible. It becomes possible to use more than just non-toxic redox mediators in this case. Menadione is reduced intracellularly and diffused back through the membrane into the solution. The MD effect on living cells is still unclear and depends on the conditions of cellular exposure.
3. The second redox mediator (e.g., potassium ferricyanide (FCN)) is required to ensure effective electron transfer to the electrode. Two types of redox mediators are necessary because one is lipophilic, which interacts with the intracellular redox centres and transfers the charge across the cell membrane, and another is hydrophilic, which takes an electron from the lipophilic mediator and passes it to the electrode.
4. Any possible toxicity of the carbon nano-compounds for the microorganisms is still poorly investigated. Various nanoparticles, can cause toxic effects on different cells. Some published data suggest the stimulation of cellular growth by carbon nanotubes. Therefore, nanomaterials with much higher conductivity are required for this purpose. Good candidates for this are carbon-based nanomaterials such as graphene or carbon nanotubes, which possess excellent conductivity range from 10^2–10^8 S/m.
5. The main problem in contact mode AFM is the loss of actual contact with the sample's surface at high scanning velocity. The number of parameters affects the quality of the AFM image, including ambience, temperature, scanning velocity, forces applied to the cantilever/probe, the geometry of used tips, quality of the tip, and the material of the sample. However, some very sensitive parameters, such as scanning velocity and applied force, are usually controlled by the user, and, mostly, both of these parameters are optimised intuitively.

After evaluating the issues examined in the scientific literature and considering the aim of the dissertation, it is expedient to solve the following tasks:

1. To evaluate the viability of living cells and charge transfer aspects between living yeast cells and electrodes while using PQ in MFCs based on *Saccharomyces cerevisiae* baker's yeast strain and *Saccharomyces cerevisiae* 21PMR (MATα leu2 ura3-52) strain.

2. To evaluate the *Saccharomyces cerevisiae* baker's yeast strain and *Saccharomyces cerevisiae* 21PMR (MATα leu2 ura3-52) strain cells' viability after MD exposure and the possibility to use of this compound as the redox mediator in the MFC.
3. To evaluate the power density of the two-mediator-based system applied to the MFC.
4. To investigate the influence of the MW-CNTs on the viability of yeast *Saccharomyces cerevisiae* baker's yeast strain cells and power density in the MFCs.
5. To create the dynamic model of AFM to optimise the input parameters to increase the living cells' observability for MFC research.

2

Preparation of the Materials and Methodology

This chapter lists the methods and materials used in the studies, including graphite electrodes, different yeast cells and the MW-CNTs suspension. The description includes the electrochemical measurements with varying redox mediators or MW-CNTs and the characterisation of nanoparticles. It depicts the methodology for improving the electromagnetic actuator-based atomic force microscope operating accuracy. Also, the chapter represents the calculations used for the electrochemical measurements and evaluation of the experimental data by a mathematical model. The dynamic model of the system is included.

Seven scientific articles by the author have been published on this chapter topics (Morkvenaite-Vilkonciene et al., 2019, 2019b, Bruzaite et al., 2020a, Rozene et al., 2020, 2021a, 2021b, 2022).

2.1. Materials

Whatman® Nuclepore (Sigma–Aldrich, Steinheim, Germany) track-etched membrane was purchased from Merck (Carrigtohill, Ireland), and graphite electrodes and chemicals (D-glucose powder, yeast extract, peptone powder, and carbon

nanotubes) were bought from Sigma–Aldrich (Steinheim, Germany). Experiments used *Saccharomyces cerevisiae* 21PMR (MAT leu2 ura3-52). Commercially available baker's yeast was purchased from a food supplier, "Dr. Oetker Lietuva" (Vilnius, Lithuania). Yeast *Saccharomyces cerevisiae* 21PMR (MATα leu2 ura3-52) strain was obtained from Dr. E. Serviene (Nature Research Centre, Lithuania). Double distilled water has been used throughout the experimental work.

The 0.5 M phosphate-acetate buffer solution (BS, pH 6.8) was prepared dissolving 0.05 M CH_3COONa; 0.05 M NaH_2PO_4; 0.05 M Na_2HPO_4, and 0.1 M KCl in distilled water. Glucose (≥98%) and FCN (≥99.0%) were prepared in this BS, and both were purchased from Riedel (Vilnius, Lithuania). Before investigations, glucose solutions were allowed to mutarotate overnight. PQ was purchased from Sigma-Aldrich (Steinheim, Germany) and dissolved in 97% ethanol purchased from "UAB Vilniaus Degtine" (Vilnius, Lithuania).

MD was dissolved in distilled water. MD was purchased from Sigma-Aldrich (Steinheim, Germany).

2.2. Graphite Electrode Preparation

Graphite electrode (a rod 150 mm in length, 3 mm in diameter, low density, and 99.995% trace metals basis) was sanded with paper with three different grinding bead sizes to receive the smooth surface end-effect and washed with distilled water and 97% ethanol. The yeast 0.125g/mL (2.5 µL drop) was immobilised on the electrode modified by baker's yeast (Fig. 2.1a).

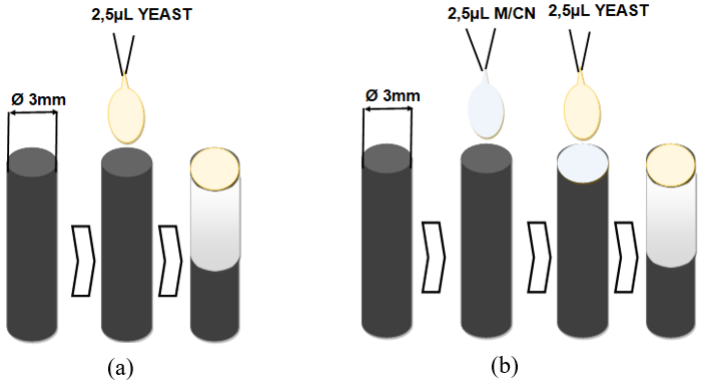

Fig. 2.1. Scheme of the immobilisation of different materials on the graphite electrode: (a) yeast immobilisation; (b) redox mediator or carbon nanotubes and yeast immobilisation

In this case, if a redox mediator with a 3.75 mM concentration or MW-CNTs stock suspension of 10 mg/mL was used, it was immobilised onto the prepared graphite electrode before yeast immobilisation, 2.5 μL drop (Fig. 2.1.b).

2.3. Preparation of Yeast Cells

Saccharomyces cerevisiae 21PMR (MAT leu2 ura3-52) yeast strain and *Saccharomyces cerevisiae* baker's yeast strain cells were grown in a liquid yeast extract peptone glucose (YPG) medium (1% (w/v) yeast extract, 2% (w/v) peptone, and 3% (w/v) glucose) on a rotary shaker at 120 rpm at 20 °C and 30 °C for 16 h. The culture of yeast cells was incubated on a Heidolph Uni-max 1011 shaker with an incubator (Schwabach, Germany).

For electrochemical and MFC measurements, baker's yeast was prepared by adding 500 mg of baker's yeast to the 1 g suspension of YPG mixed with 20 mL distilled water (concentration = 50 g/L). Then, a different culture was grown on a rotary shaker at 200 rpm and 30 °C for 20–24 h.

2.4. Preparation of Multi-Walled Carbon Nanotube Suspension

The MW-CNTs stock suspension of 10 mg/mL was prepared in deionised water cleaned by a multi-purpose water purification system, Adrona Crystal EX (Riga, Latvia), ultrasonicated for 30 min by ultrasound bath Sonorex Digitec from Bandelin electronic GmbH & Co. KG (Berlin, Germany) and then stored in the dark at +4 °C before use.

2.5. Preparation of Yeast Cells for Viability Assays

First, optical density (OD) measurements of microbial and cell growth are among the most common methods used in a microbiology lab to determine the optimal time at which to harvest, the determination of the optimal time to induce a culture when running a protein expression protocol or the monitoring of cloning procedures.

The growth of cells, bacteria or yeast (cell density, bacterial growth, yeast growth) in liquid culture media is commonly controlled by measuring the optical density at 600 nm (OD600). OD600 measurements are typically used to determine the growth stage of a bacterial culture; these measurements help ensure that cells

are harvested at an optimum point that corresponds to an appropriate density of live cells.

Since optical density in the case of OD600 measurements results from light scattering rather than light absorption, size and shape and dead cells and debris of a cell may add to light dissipation. Distinctive cell types that are at densities of the same level (e.g., cells/mL) may therefore show varying values OD600 when estimated on a similar instrument. The growth of bacterial cells typically progresses through consecutive phases, including lag, log, stationary, and decline.

In general, cells should be harvested towards the end of the log phase, using the optical density of the samples to determine when this point has been reached. Cells are grown routinely until the absorbance at 600 nm (known as OD600) reaches approximately 0.4 before induction or harvesting ("The OD600 Basics | Best OD600 Tool To Generate Microbial Growth Curves," n.d.).

2.5.1. Preparation of Yeast Cells for the Experiments with 9,10-Phenanthrenequinone

Agar well diffusion method. Flasks with cultures of (i) yeast *Saccharomyces cerevisiae* and (ii) baker's yeast were inoculated overnight (~16 h), and the initial culture optical density (OD) at 600 nm was 1.2 ± 0.01, which corresponds to 3.6×10^7 of CFU/mL (CFU colony-forming units). Then 0.1 mL suspension of yeast cells was poured into a 9 cm sized Petri dish, after 10 mL of YPG agar medium was poured into this same plate and smoothly stirred. Holes of 8 mm diameter were made on the cooled and frozen YPG agar medium. Then, using a sterile pipette, 0.025 mL PQ solution (0.676 mM, 0.75 mM, 3.75 mM) was added to the well. Ethanol was used as a control. Petri plates were incubated in Laminar airflow box LaboGene SCANLAF Mars (Lillerød, Denmark) at 22.5 °C temperature and 30 °C temperature for 24 hours.

Determination of yeast growth efficiency. The yeast *Saccharomyces cerevisiae* cells and baker's yeast cells were inoculated in the presence of PQ or MD solution with a 3.75 mM concentration. In the control sample, PQ was absent. 1 mL of overnight cultivated yeast cells cultures were transferred to 9 mL fresh liquid YPG medium (OD was observed at 600 nm and was equal to 0.1) and cultivated for 4 h at 30 °C and for 5 h at 22.5 °C (after these procedures OD registered at 600 nm and was equal to 0.5÷0.55). Then, 100 µL of PQ solution was added to the prepared yeast cell suspensions and were incubated on a shaker at 22.5 °C and 30 °C for 5 h with 120 rpm. The OD of the yeast cell cultures was measured within 5 hours at 1-hour intervals between measurements. The wavelength of the spectrophotometer was set at 600 nm and blanked a cuvette with 1 mL sterile YPG medium. Then, the suspension of yeast cells was easily shaken, and 1 mL of suspension was pipetted into the cuvette. The OD of suspension was recorded. This

process was carried out by the determining OD of the yeast cells using a spectrophotometer Genesys 10S ultraviolet-visible (UV-VIS) from Thermo Fisher Scientific (Mettler Toledo, Singapore).

2.5.2. Preparation of Yeast Cells for the Experiments with 2-Methyl-1,4-naphthoquinone

For the agar well diffusion method, the cultures of (i) *Saccharomyces cerevisiae* yeast and (ii) baker's yeast were inoculated in the flask overnight (~16 h). The initial OD of the culture at a 600 nm wavelength was 1.2 ± 0.01, which corresponds to 3.6×10^7 of CFU per mL. Then, 0.1 mL of the yeast cell suspension was transferred to a 9 cm Petri dish. After that, 10 mL of YPG agar medium was added to the same plate and mixed smoothly. The holes (~8 mm in diameter) were made on the cooled and frozen YPG agar medium. Then, 0.025 mL of 3.75 mM concentration MD solution was introduced to the well. Ethanol was used as a control solution. Petri dishes were incubated in a laminar airflow box (LaboGene ScanLaf Mars) (Lillerød, Denmark) at 20 °C and 30 °C for 24 h.

Regarding the determination of total cell number by culture OD, for this experimental investigation, the *Saccharomyces cerevisiae* yeast cells and baker's yeast cells were inoculated in the presence of the 3.75 mM concentration MD solution. Yeast cells unaffected with MD were served as the control. 1 mL of overnight yeast cell cultures were transferred to 9 mL of fresh liquid YPG medium (OD measured at 600 nm was ~0.1) and cultivated for 4 h at 30 °C and 5 h at 20 °C (OD measured at 600 nm was 0.51 ÷ 0.55). After that, 100 μL of MD solution was added to the prepared yeast cell suspensions, and the suspensions were incubated at 20 °C and 30 °C for 26 h. The OD cultures of the yeast cells were determined within 26 h at 2 h intervals between measurements. Yeast cell numbers were monitored on liquid YPG media by measuring the light absorbance by the YPG medium sample with the cells using a Genesys 10S UV-VIS spectrophotometer from Thermo Fisher Scientific (Mettler Toledo, Singapore).

2.5.3. Preparation of Yeast Cells for the Experiments with Multi-Walled Carbon Nanotubes

The yeast *Saccharomyces cerevisiae* cells were incubated with aeration in the liquid YPG medium containing 1% of yeast extract, 2% of peptone, 3% of glucose for 24 h at 30 °C. Possible toxic effects of present MW-CNTs (of 2, 50 or 100 μg/mL concentrations) were determined by the atomic force microscopy, cell count (yeast cells stained with the methylene blue solution and monitored by light microscope (Zamaleeva et al., 2010), the cells were stained with propidium iodide (PI) and monitored by fluorescence microscope) and culture OD.

All experiments were carried out in duplicate or triplicate.

2.6. Electrochemical Measurements

All electrochemical measurements were performed using an "Autolab PGSTAT 30 Potentiostat/Galvanostat" (Utrecht, Netherlands) and "NOVA" software. All experiments were conducted at ambient temperature (20 °C) while stirred in the phosphate-acetate buffer solution, pH 6.8, under aerobic conditions. Measurements were performed in a three-electrode electrochemical cell designed using Metrohm AG's components (Herisau, Switzerland) (Fig. 2.2).

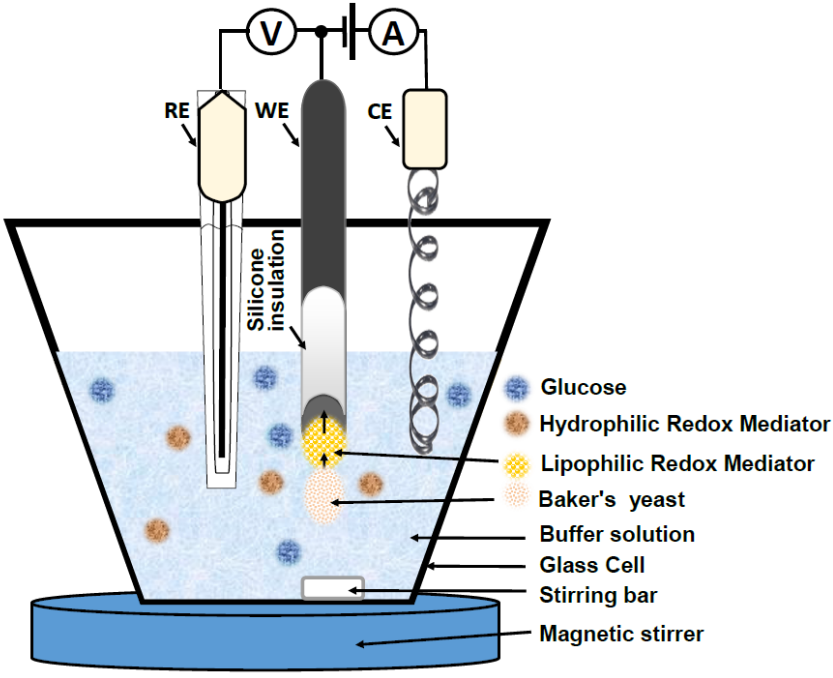

Fig. 2.2. Three-electrode electrochemical cell: graphite electrode as a working electrode (WE); platinum electrode as a counter electrode (CE); Ag/AgCl/KCl (3M) electrode as a reference electrode (RE)

Borosilicate glass titration vessel (height 80 mm, outer diameter 78 mm, volume 70 mL) was chosen for the electrochemical cell. The graphite electrode was connected to the electrochemical set up as a working electrode, the platinum electrode (tip made of Pt wire, the shaft from glass, measuring range from –2000 to

2000 mV, pH range from 0 to 14) – as a counter electrode and Ag/AgCl/KCl (3M) electrode (variable bridge electrolyte type, ground-joint diaphragm, 3 M KCl, the shaft from glass) – as a reference electrode. The electrochemical cell was placed in a Faraday cage with an earth terminal (Autolab, Utrecht, Netherlands).

Cyclic voltammogram (CV) was chosen as the basic electrochemical test for materials. The current is recorded by sweeping the potential back and forth (from positive to negative and negative to positive) between the chosen limits. The information obtained from the CV can be used to learn about the electrochemical behaviour of the material. The graphical CV analysis gives the redox peaks, which are reduction and oxidation peaks of the material, predicting the capacitive behaviour of the electrode. Hence, the potential can be found at which the material is oxidised and reduced. All CVs in the research were recorded at the potential sweep rate of 0.1 V/s in the range from -0.6 V to +0.8 V. The five CV cycles were performed, and the settled data from the last one was plotted. In all cases, when the concentration of any additional compound was changed, it was done sequentially by adding this compound to the same measurement cell. All CV measurements were repeated five times, and the average was calculated.

2.6.1. Electrochemical Measurements with 9,10-Phenanthrenequinone

MFC's generated power result was studied using a two-electrode-based electrochemical cell, with an anode based on PQ/yeast-modified graphite electrode and a cathode based on a bare graphite electrode (Fig. 2.3). A polycarbonate membrane with a 3 μm pore size was used to cover the anode surface. During current measurements of MFC, the external resistances (of 0.01 kΩ; 0.1 kΩ; 0.42 kΩ; 0.9 kΩ; 5 kΩ; 12 kΩ; 50 kΩ; 100 kΩ; 400 kΩ; 800 kΩ; 1100 kΩ; 1500 kΩ; 2100 kΩ; 2600 kΩ) were plugged into an external electrical circuit to imitate external load and to assess power density of designed MFC anode (Equation (2.5)). All experiments were performed at room temperature while stirring in the phosphate-acetate buffer, pH 6.8, under aerobic conditions.

2.6.2. Electrochemical Measurements with Menadione

A two-electrode-based electrochemical cell was used to study the MFC performance (Fig. 2.3). An MD/yeast-modified graphite electrode was used as the anode, and a bare graphite electrode was used as the cathode. A track-etched polycarbonate membrane with a 3 μm pore size was used to cover the anode surface. During voltage measurements of the MFC, the external resistances (of 0.01 kΩ, 0.1 kΩ, 0.42 kΩ, 0.9 kΩ, 5 kΩ, 12 kΩ, 50 kΩ, 100 kΩ, 470 kΩ, 1100 kΩ, 2100

kΩ, and 2600 kΩ) were plugged into an external electrical circuit to imitate the load and to assess the power density of the designed MFC anode (Equation (2.5)).

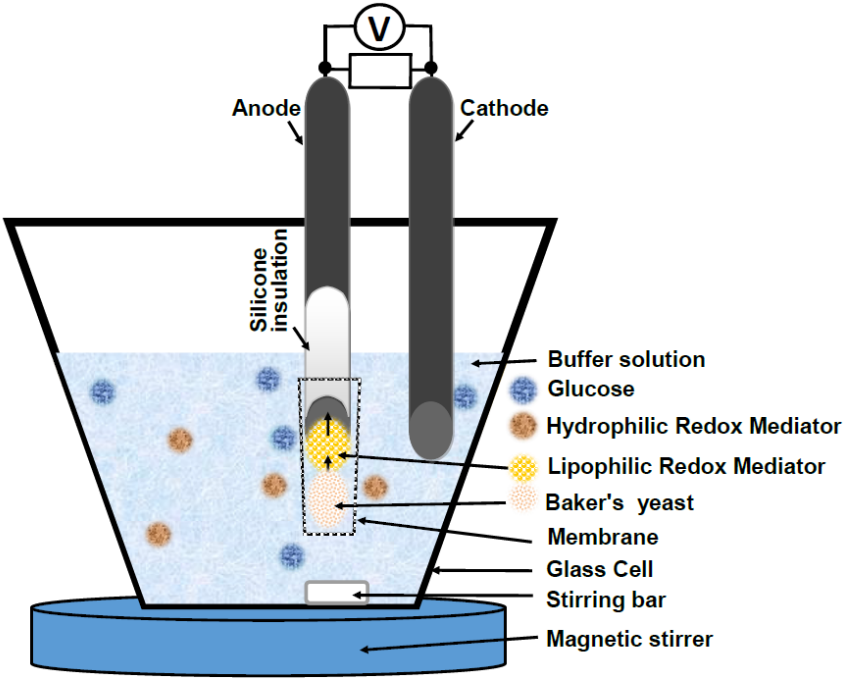

Fig. 2.3. Two-electrode electrochemical cell: an MD/yeast-modified or PQ/yeast-modified graphite electrode as the anode; a bare graphite electrode as the cathode

2.6.3. Electrochemical Measurements with Multi-Walled Carbon Nanotubes

Two graphite electrodes with different materials immobilised on the electrode surface were used in the MFC (Fig. 2.4): one only with PQ and the second with PQ and MW-CNTs. The MFC was made from two electrodes: one differently modified graphite as the anode and another – platinum electrode as the cathode. They were placed in a phosphate–acetate buffer solution with 70 mM of glucose, 10 mM $K_3[Fe(CN)_6]$, and 0.3 mg/mL yeast. During voltage measurements, the external resistances were plugged into the external electrical circuit to imitate the external load and assess the complete MFC's power output. Electrochemical impedance representing the resistivity of the layers formed at the anode surface was registered at a frequency range from 50 kHz to 10 mHz, amplitude 10 mV.

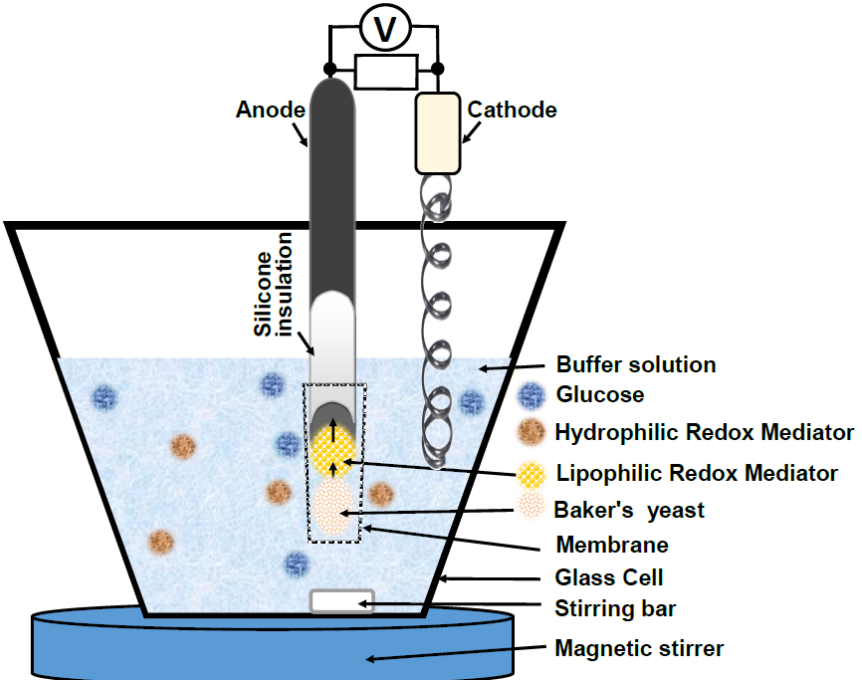

Fig. 2.4. Two electrodes electrochemical cell: a PQ/yeast-modified or a PQ/MW-CNTs-modified or a graphite electrode as the anode; a platinum electrode as the cathode

2.7. Characterisation of Nanoparticles

2.7.1. Scanning Electron Microscopy (SEM)

For SEM, the samples with the carbon nanotubes were dispersed in ethanol using an ultrasound bath; the clumps were disintegrated, and a suspension drop was put on the carbon conductive tab and dried. Before measurements, the surface of MW-CNTs was coated with a layer of Au by evaporation in a vacuum using a QUORUM Q150RES device (Quorum Technologies Ltd., Laughton, UK). Afterwards, such samples were assayed by the scanning electron microscope JSM-7600F from JEOL (Tokyo, Japan). SEM images of MW-CNTs were obtained at various magnifications to determine the shape of the carbon MW-CNTs.

2.7.2. X-ray Diffraction Analysis (XRD)

The phase composition of the MW-CNTs was clarified by X-ray diffraction patterns of the samples with the MW-CNTs were recorded with a DRON 6 diffractometer Cu Kα radiation (Joint Stock Company "Bourevestnik", Saint Petersburg, Russia) ($\lambda = 1.54178$ Å) at a scanning speed of 0.05° scan/min from $2\theta = 10–70°$. The analysis of experimental XRD spectra of MW-CNTs was performed using the Crystallografica software (X-ray line profile fitting program XFIT by A. A. Coelho and R. W. Cheary, Sydney, Australia, 2007).

2.7.3. Raman Spectroscopy Measurements

MW-NCT samples for Raman spectroscopy measurements were prepared on a clean slide glass. The Raman spectra were measured using a confocal Raman spectroscopy system (NTEGRA Spectra, NT-MDT) with a 532 nm wavelength laser. The laser beam power was 0.17 mW. Raman spectra were collected with an integration time of 10 s. The analysis of the shape of different modes and their intensity ratio confirms the material (MW-CNTs) and shows no radial breathing mode bands.

2.7.4. Yeast Cell Viability Assays

Cells count. The samples of the yeast cells with and without MW-CNTs suspension were centrifuged, and then the supernatants were decanted. The remaining pellet was resuspended with BS, pH 7.4. Cell preparations were stained with methylene blue solution and analysed by light microscope 1 h after the incubation with the dyes. Light microscope Olympus CX41 from Olympus (Tokyo, Japan) was used for optical image acquisition.

Fluorescence microscopy. After cultivating the yeast cells with or without MW-CNT suspension, the cells were collected by centrifugation, washed twice, and resuspended in BS. Cell suspensions were transferred to the tubes and stained with PI. A fluorescence microscope Nikon Eclipse Ci-L from Nikon Instruments Inc. (New York, NY, US) was used for the optical image acquisition.

Assessment of a temporal change in the yeast population size. The yeast *Saccharomyces cerevisiae* cells were inoculated in the presence of MW-CNT suspension, which contained 2 μg/mL, 50 μg/mL or 100 μg/mL MW-CNTs. In the control sample used as a reference, MW-CNTs were absent. The population size of yeast cells was monitored on a liquid YPG medium by measuring the light absorbance of the samples using YPG medium with the cells using a spectrophotometer Genesys 10S UV-VIS from Thermo Fisher Scientific (Vilnius, Lithuania). The inoculated incubation medium was kept for 24 h. The initial OD of the

culture at 600 nm wavelength was 0.1 ± 0.01, which corresponds to 1–2 × 106 of CFU/mL.

The evaluation of the mathematical data model developed by Juska (Juška, 2011) was used for calculations (Equation (2.1))

$$\begin{cases} \frac{dx}{dt} = \alpha x z \, exp\left(\varsigma(z^3 - 1)\right) \\ \frac{dz}{dt} = -\mu x \end{cases}. \tag{2.1}$$

Here x is the population size; α is the relative growth rate; z is the function of the resources used to produce the energy; and μ is the close death rate.

2.8. Methodology for Improving the Accuracy of Electromagnetic Actuator-Based Atomic Force Microscope Operation

2.8.1. Scanning Experiments

Before creating the dynamic model, the experiments with different loads for the cantilever and different scanning speeds should be used to check the model's adequacy. First, contact mode AFM in the air was applied with a rectangular cross-section, silicon nitride cantilever, type CONTR (Resonance Frequency 13 kHz, Force Constant 0.2 N/m, tip radius of curvature of less than 8 nm) from *Nano-World Services*, GmbH (Erlangen, Germany). Then, two types of samples were scanned: the rectangular cross-section silicon calibration grid with a height of 100 nm (10 μm period) obtained from *NanoWorld Services*, GmbH (Erlangen, Germany), and the rectangular cross-section Poly (methyl methacrylate) (PMMA) with a height of 800 nm (50 μm period).

2.8.2. Simulation

The AFM modelling was performed using the *Matlab/Simulink/Simscape* software. Simscape allows the rapid creation of models of physical systems within the Simulink environment. *Simscape* does not require building equations and makes them internally from structural components and their relations. Our model was built according to the general dynamics equation (Equation (2.6)). The model of the system linear part and the model of the contact between the tip and the surface were made using *Matlab/Simscape*, nonlinear stiffness and damping coefficients and feedback control were realised in *Matlab/Simulink*. A simplified block diagram of the *Simulink/Simscape* model is shown in Fig. 2.5.

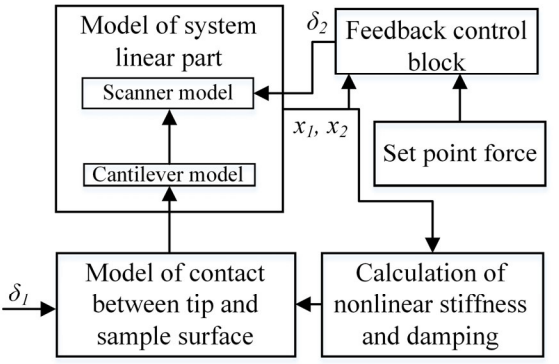

Fig 2.5. Simplified block diagram of the *Simulink/Simscape* model (Morkvenaite-Vilkonciene et al., 2019b)*

The model can be divided into five main blocks. The linear part of the model includes physical models of a scanner and cantilever. The input for the model is a profile of the sample, which is described by the coordinate δ_1. The feedback control block describes the AFM control system, which considers the setpoint force between the cantilever's tip and the sample's surface, and evaluates the error signal from the positions of the cantilever (x_1) scanner (x_2) and generates a corresponding control signal (δ_2). Stiffness and damping coefficients were calculated using Equations (2.9) and (2.10), considering certain moments of the time in a separate block. Defined stiffness is transferred to the model contact block at a certain time moment, which provides time-dependent resulting force F(t) to the linear part of the system.

2.8.3. Relative Error Calculation

The relative error of displacement x_1 (Fig. 2.6) for all data was calculated by the equation:

$$\Delta x_1 = \frac{|x_1 - max(|x_1^*|,|x_1^{**}|)|}{x_1} \cdot 100\% \,. \tag{2.2}$$

Here, x_1 — the real profile height; x_1^* — the observed profile height.

*The reference is given in the list of publications by the author on the topic of the dissertation.

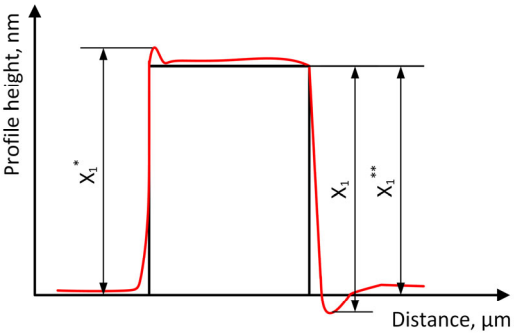

Fig. 2.6. Real and observed profiles from topography (Morkvenaite-Vilkonciene et al., 2019b) *

2.9. Calculations

2.9.1. Electrochemical Measurements Were Evaluated using Hill's Function

$$J = \frac{C^n}{k^n + C^n}\,. \tag{2.3}$$

Here, J is the current density; C is the concentration of selected substrate (glucose, MD, or FCN); k is the half-maximal concentration constant; and n is the Hill coefficient.

The modified Hill's function was used for the evaluation of time-dependent experiments:

$$J = \frac{t^n}{k^n + t^n}\,. \tag{2.4}$$

Here: J is the current density, t is the reaction time, k is the half-maximal concentration constant, and n is the Hill coefficient.

2.9.2. Electrical Power Density Calculation

Electrical power density calculation:

$$P = \left(\frac{U^2}{R}\right)/S\,. \tag{2.5}$$

*The reference is given in the list of publications by the author on the topic of the dissertation.

Here, P is power in watts; R is resistance in Ohms; U is voltage in volts (DC); and S is the total surface area of the electrode in squared meters.

2.9.3. Model of the Mechanical Part of the Scanner and Cantilever

A dynamic model of the mechanical part of the scanner and cantilever is shown in Fig. 2.7. Only vertical movements of mass centres of the cantilever and scanner are considered. The topography of the scanned surface kinematically excites the entire model through the coordinate δ_1, the deflection of cantilever δ_2, obtained from feedback control, excites only the scanner model. The reaction sensitivity and reaction delay of the control system depends on elements k_v and h_v, which are stiffness and damping of control latency, respectively. Mechanical scanner properties are described by its mass ms, stiffness k_s and damping h_s. The cantilever is modelled as a mechanical one degree of freedom (DOF) system with the mass m_c, stiffness k_c and damping h_c (Sitti and Hashimoto, 2000; Potekin et al., 2017). A general mechanical equation could represent the whole model:

$$[m]\{\ddot{x}\} + [h]\{\dot{x}\} + [k]\{x\} = \{F(t)\}\,. \tag{2.6}$$

Here, [m], [h], [k] – matrices of mass; damping; stiffness, correspondingly; $\{\ddot{x}\}, \{\dot{x}\}, \{x\}$ – the vector of independent coordinate and its derivatives; {F(t)} – the time-dependent load vector transferred from kinematical excitation (active coordinates δ_1, δ_2).

Tip–sample interaction in the model is expressed by the nonlinear spring and damper system (Stan et al., 2012), the stiffness k_k(D) and damping coefficient h_k(D) (Fig. 2.7) of which depends on Van der Waals force, described as (Butt et al., 2005):

$$\mathrm{D} = \sqrt{\frac{AR}{6F}}\,. \tag{2.7}$$

Here, D – the distance between the tip and the sample surface; A – Hamaker constant; R – the radius of the tip; F – the value of Van der Waals force at a certain moment of the time.

The stiffness of the contact between the surface and the tip is calculated as a ratio of force and distance:

$$k_k(\mathrm{D}) = \frac{F}{D}\,. \tag{2.8}$$

From Equations (2.7) and (2.8), the stiffness of the contact between the surface and the tip in the model was expressed as:

$$k_k(\mathrm{D}) = \frac{AR}{6D^3}\,. \tag{2.9}$$

The damping of the contact between the surface and the tip h_k is described using a case of the Rayleigh damping model, in which damping is proportional to stiffness (Jehel et al., 2014):

$$h_k(\mathrm{D}) = \lambda\, k_k(\mathrm{D})\,. \tag{2.10}$$

Here, λ is the stiffness proportional to the Rayleigh damping coefficient.

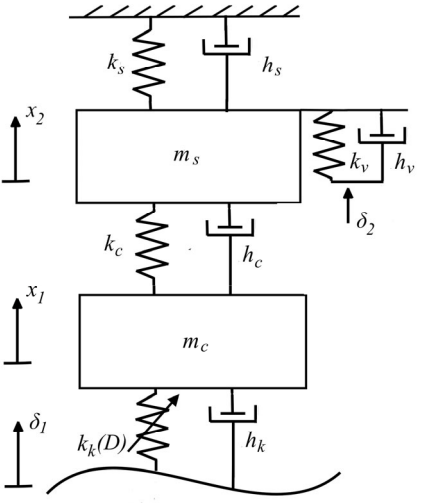

Fig 2.7. The dynamic model of the mechanical part of the scanner and cantilever. m_s – the mass of the scanner; k_s – the stiffness of the scanner; h_s – the damping coefficient of the scanner; mc – the mass of the cantilever; k_c – the stiffness of the cantilever; h_c – the damping coefficient of the cantilever; δ_1 – the coordinate, which describes excitation effect created by sample surface topography; δ_2 – the coordinate which represents the displacement of the scanner, caused by a control signal from feedback loop (Fig. 2.3); k_k – the stiffness of the contact between the surface and the tip (Equation (2.8)); h_k – the damping coefficient of the contact between the surface and the tip (Equation (2.9)); kv – the stiffness of control latency DOF; h_v – the damping coefficient of control latency DOF; x_1 – the coordinate of the cantilever's mass centre; x_2 – the coordinate of the scanner's mass centre (Morkvenaite-Vilkonciene et al., 2019b)*

*The reference is given in the list of publications by the author on the topic of the dissertation.

2.10. Conclusions of Chapter 2

This chapter presents all the information about the materials used for the investigations and describes the chosen methods. First, the methods are presented for a graphite electrode, yeast cells and MW-CNT suspension preparation. Then, separate descriptions are given for viability studies of different yeast cells using redox mediators (MD and PQ) and nanotubes. It also provides information on electrochemical measurement methods using different materials. A separate section is devoted to describing the methods for the characterisation of nanoparticles: SEM, XRD, Raman Spectroscopy Measurements. A detailed description is offered of the methodology for improving the accuracy of the electromagnetic actuator-based atomic force microscope operation. It includes information about managing the force microscope, scanning experiments, simulation and relative error calculation. The chapter closes with calculations.

The chapter led to the following conclusions:

1. Accurate graphite area is ensured by special preparation of graphite electrode for measurements.
2. The optical density results of the yeast cell modified by MD, PQ and MW-CNTs show the viability assays of the yeast cell.
3. Electrochemical measurements with different redox mediators and MW-CNTs are performed to obtain the current results for the first step of the experiments in a three-electrode electrochemical cell. The power density result is received in a two-electrode electrochemical cell while connecting the external resistances.
4. Characterisation of nanoparticles should be done by performing SEM, XRD and Raman spectroscopy measurements.
5. Methodology for improving the accuracy of electromagnetic actuator-based atomic force microscope operation is prepared after the scanning experiments, simulation and relative error calculation is done.

3

Investigation of Applying Yeast *Saccharomyces cerevisiae* in Biofuel Cells

Electrochemical studies were performed to modify the anode of an MFC by using yeast and different electron transport mediators: PQ, MD, MW-CNTs.

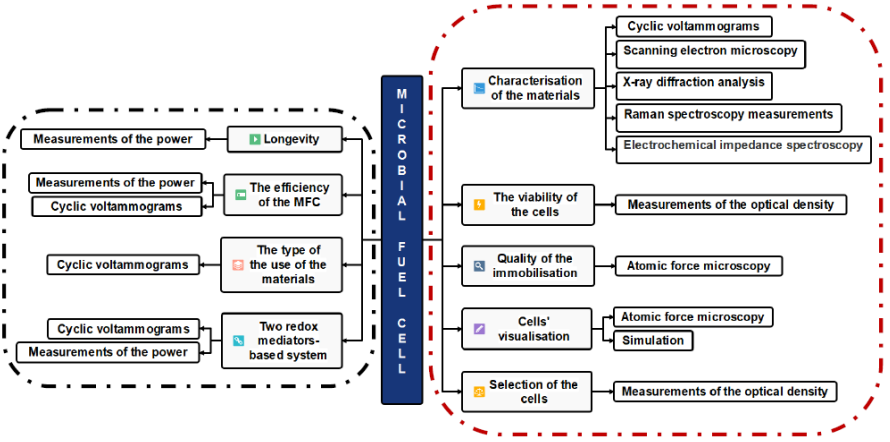

Fig. 3.1. Scheme of the research methods and the examined parameters

A research plan was carried out to implement the tasks set in the dissertation (Fig. 3.1). The research scheme consists of two parts: the first with the analysis of all the materials and cells (the red frame), and the second with the examination of the developed biofuel element parameters (the black frame). The first level of the scheme presents the research task, and the second level is the method. The research methods for materials and cells are included in the first part: the determination of the mechanical cell properties, the selection of suitable cells, the concentration of the used materials, the viability of the cells and the quality of the immobilisation. The methods for the MFC research are included in the second part: ways for incorporating the materials, analyses of the two redox mediators-based system, and the efficiency and longevity of the MFC.

Seven scientific articles by the author have been published on this chapter topics (Morkvenaite-Vilkonciene et al., 2019, 2019b, Bruzaite et al., 2020a, Rozene et al., 2020, 2021a, 2021b, 2022).

3.1. Simulation of the Contact Mode of an Atomic Force Microscope

3.1.1. Influence of the Scanning Speed

Knowing the absolute error at the required scanning speed enables determining the structure's shape more accurately.

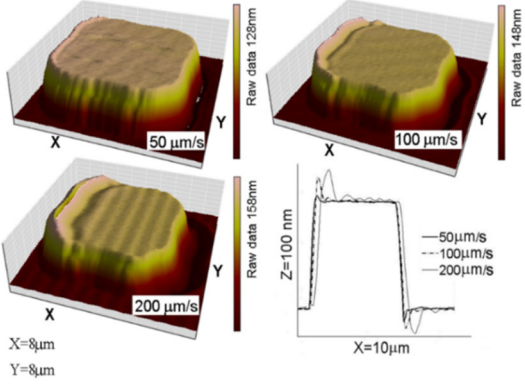

Fig. 3.2. Measurements of the calibration grid using different scanning speeds (Morkvenaite-Vilkonciene et al., 2019b)*

*The reference is given in the list of publications by the author on the topic of the dissertation.

The relationship between the scanning speed and the error from the ideal surface profile is shown in Fig. 3.2. The calibration grid was measured at different scanning speeds with a 20 nN setpoint force. As expected, the best picture quality was observed at the lowest scanning speed of 50 µm/s. However, the same structure horizontal dimensions in the x-axis were observed scanning at all scanning speeds.

The silicon calibration grid surface profile was scanned at different scanning speeds and two different surface-tip interaction forces. The scan with a 10 nN interaction force is shown in Fig. 3.3a. The higher scanning velocity determines the higher distortion in the picture. At a low scanning speed (1.5 s per line), the structure's height corresponds to that given by the manufacturer (100 nm) and is flat on the top and bottom of the structure. At higher scanning speeds, the picture contains dynamic artefacts: there are overshooting errors at the top and bottom of the structure, resulting in the incorrect estimation that the height of the structure is higher than 100 nm.

Equation (2.2) was used to evaluate the error, where "real profile height" (x_1) was profile height, determined at the lowest scanning speed and marked by an arrow a and arrow b for the upper surface structure and bottom surface structure, respectively (Fig. 3.3). A comparison of errors is shown in Fig. 3.3b. At the bottom, the error (arrow b) is much higher: at 100 µm/s (0.2 s per line), the scanning speed Δx_1 is 50 %, while the error at the upper surface structure (arrow a) is 6.8 %.

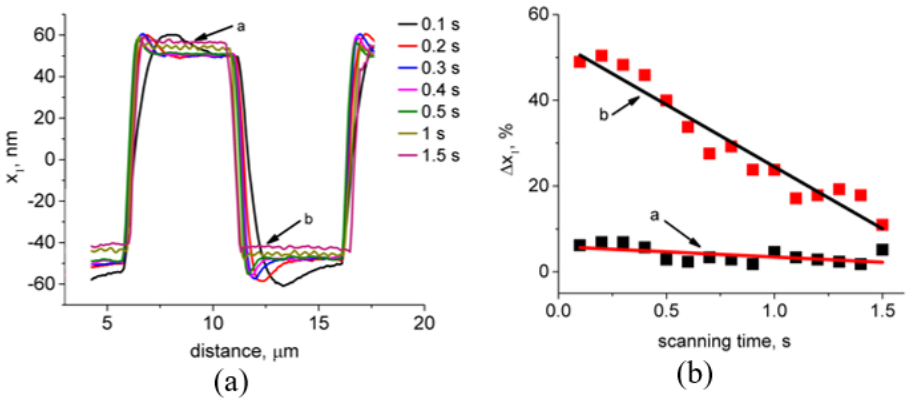

Fig. 3.3. Scanning results: (a) silicon calibration grid surface profile scanned at various velocities with a 10 nN force applied to the cantilever; (b) relative error from the upper (arrow a) and the lower (arrow b) surface structure (Morkvenaite-Vilkonciene et al., 2019b)*

*The reference is given in the list of publications by the author on the topic of the dissertation.

Δx_1 dependence on scanning time is linear and increases together with scanning speed: at 10 nN, the bottom error changes from 11 % to 50 % (Fig. 3.3b), while at 20 nN, the bottom error changes from 3 % to 47 % (Fig. 3.4b). Thus, it can be concluded that the scanning speed has a more significant influence on the picture resolution when the force is lower.

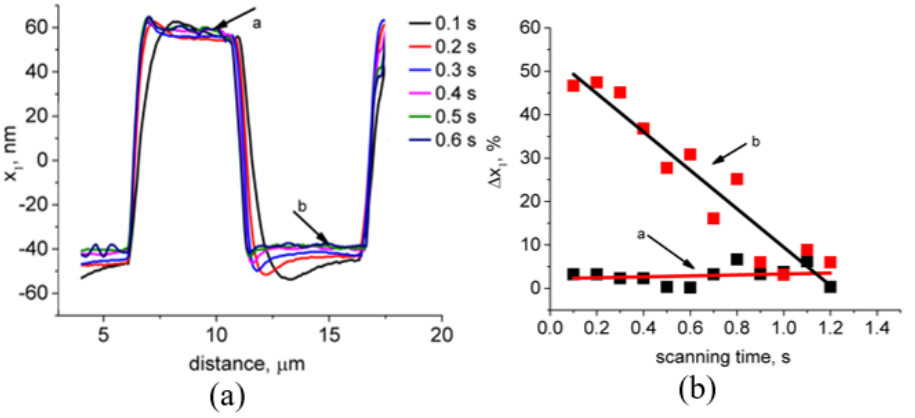

Fig. 3.4. Scanning results: (a) silicon calibration grid surface profile scanned at different scanning speeds with a 20 nN force applied to the cantilever; (b) relative error from the upper and lower surface structure (Morkvenaite-Vilkonciene et al., 2019b)*

Another set of experiments was performed by scanning the PMMA surface, which is softer (Young's modulus $1 \cdot 10^6$ Pa), compared to silicon (Young's modulus $165 \cdot 10^9$ Pa) (Fig. 3.5). The PMMA surface structure period is 50 μm, and the height is 800 μm. The change in picture resolution obtained from the PMMA scanning was at both 10 nN (Fig. 3.5) and 20 nN (Fig. 3.6) interaction forces. In this case, a higher error was observed: from 11 % to 111 % at the bottom surface structure (Fig. 3.5b) and from 5 % to 60 % at the upper surface structure (Fig. 3.5b). In addition, it was observed that high scanning speeds lead to the loss of the tip contact with the surface, and at 750 μm/s (0.1 s per line), the tip does not follow the surface at all. Therefore, the error, calculated at a 20 nN interaction force, is deficient; practically, only scanning at the highest scanning speeds of 375 μm/s (0.2 s per line) and 750 μm/s (0.1 s per line) has an effect on the picture resolution and can be distinguished from other curves (Fig. 3.6).

*The reference is given in the list of publications by the author on the topic of the dissertation.

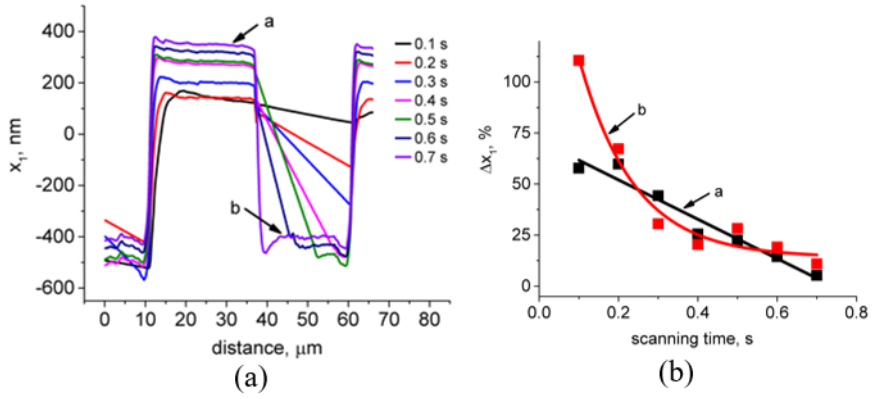

Fig. 3.5. Scanning results: (a) PMMA surface profile scanned at different scanning speeds with a 10 nN force applied to the cantilever; (b) error from the upper and lower surface structure (Morkvenaite-Vilkonciene et al., 2019b)*

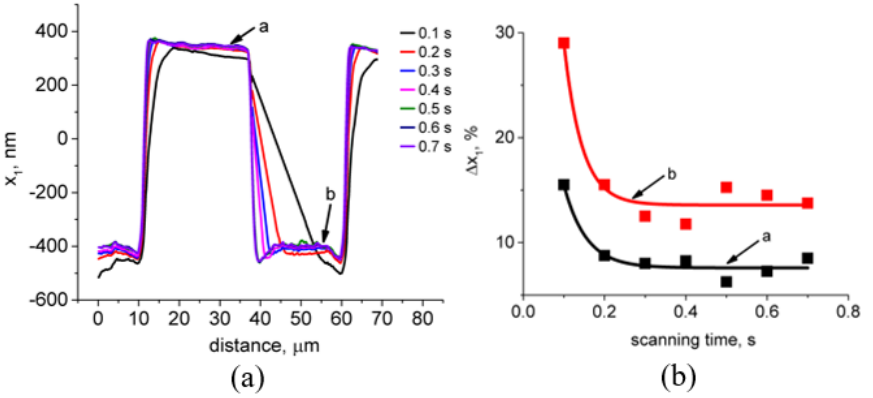

Fig. 3.6. Scanning results: (a) PMMA surface profile scanned at different scanning speeds with a 20 nN force applied to the cantilever; (b) relative error from the upper and lower surface structure (Morkvenaite-Vilkonciene et al., 2019b)*

All the measurements using various setpoint forces and performed at different velocities show the actual surface image errors. A decrease in the interaction

*The reference is given in the list of publications by the author on the topic of the dissertation.

force results in false information, which is an excellent example of how two essential parameters affect the quality of registered pictures. At the high scanning speed of 750 µm/s and a low setpoint force (10 nN), the valley at x-coordinate 50–60 µm is no longer represented in the picture. At this point, the influence of surface material on picture quality remains unclear. It can be assumed that softer material (lower elasticity modulus) causes a part of the tip to be absorbed, i.e., the surface interaction energy, which results in overshooting and vibrations to the cantilever if the structure is made of harder material with a higher elasticity modulus. This hypothesis, however, needs to be proved.

3.1.2. Influence of the Tip Radius

The influence of the surface effect caused forces, which are observed when the tip interacts with the PMMA surface (Figs. 3.5a and 3.6a).

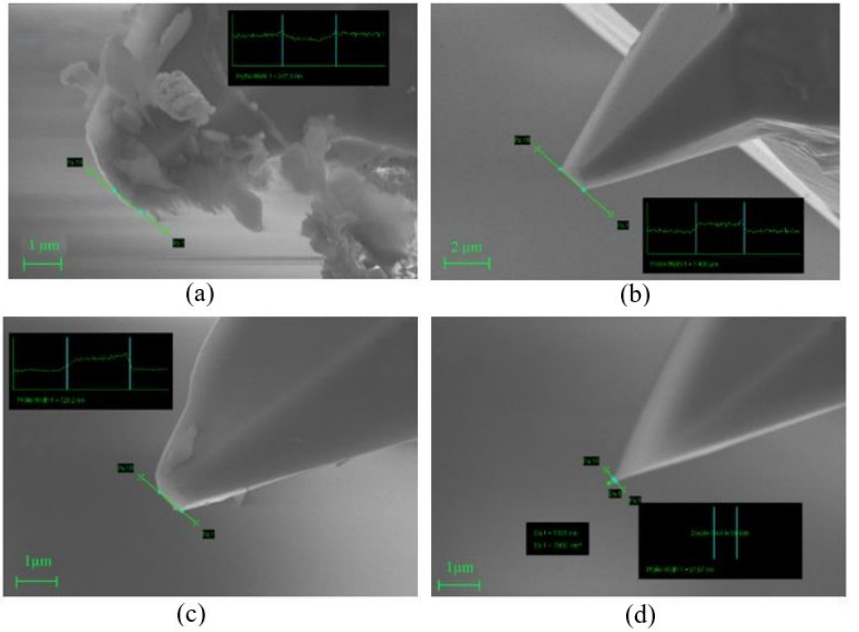

Fig. 3.7. SEM images of AFM tips, which were used for experiments, with the radii of (a) 1745 nm; (b) 1406 nm; (c) 728 nm; (d) 53 nm (Morkvenaite-Vilkonciene et al., 2019b)*

*The reference is given in the list of publications by the author on the topic of the dissertation.

These forces can distort the image when high scanning speeds are applied. The adhesion force depends on the interaction between both surfaces (the tip and the sample) and is higher if the contact area increases. The contact area depends only on the tip radius, which becomes the most critical factor in evaluating the adhesion force. The tip radii before scanning were assessed by SEM. The tip of the highest radius is shown in Fig. 3.7a. Also, the tip is not clean, and this example is interesting for evaluating the contamination influence. The tips shown in SEM pictures (Figs. 3.7a, 3.7b, 3.7c, 3.7d) were used for further experiments.

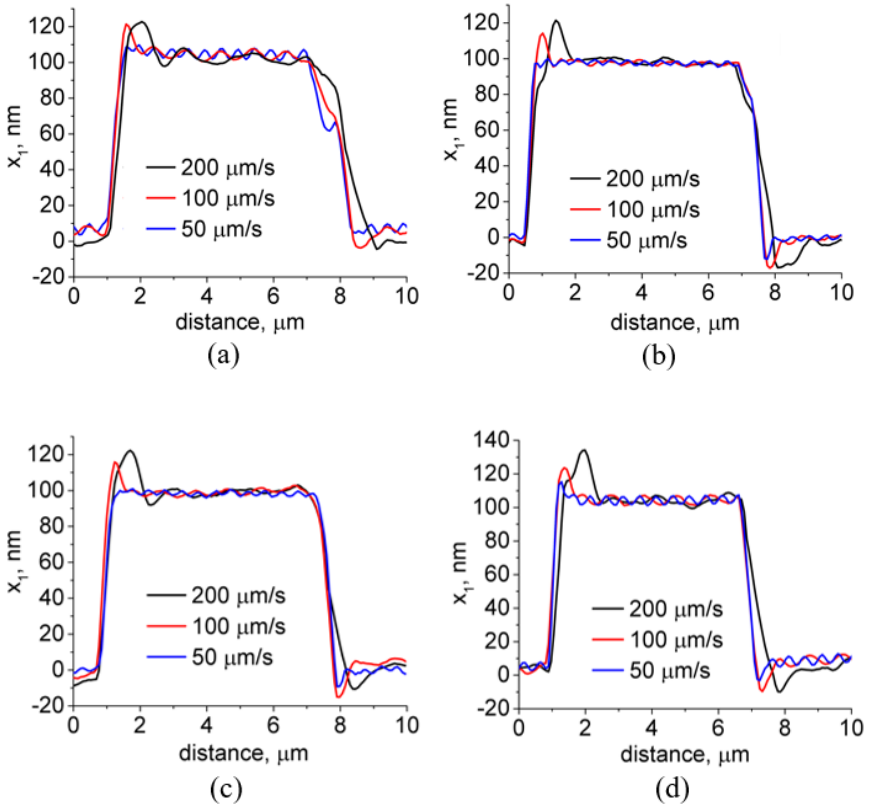

Fig. 3.8. Scan of the silicon calibration grid at different scanning speeds using: (a) the 1745 nm radius tip; (b) the 1406 nm radius tip; (c) the 728 nm radius tip; and (d) the 53 nm radius tip (Morkvenaite-Vilkonciene et al., 2019b)*

*The reference is given in the list of publications by the author on the topic of the dissertation.

Cantilevers with different tip geometries were used to scan the silicon calibration grid at different scanning speeds (Fig. 3.8). The 1745 nm radius tip with high contamination (Fig. 3.7a) gives adhesion-induced artefacts observed in the image at a distance from 7 μm to 8 μm (Fig. 3.8a). The tip with the 1406 nm radius (Fig. 3.7b) generates the same artefact, but the error is lower than in the previous case (Fig. 3.8b). The 728 nm radius tip (Figs. 3.7c and 3.8c) provides a scanning result similar to that registered by the 53 nm radius tip (Figs. 3.7d and 3.8d). However, at a high scanning speed, the structure's height was higher when scanning was performed with the tip of a lower radius.

3.1.3. Results from the Model: Parameters Applied for the Modelling

Fig. 2.4 shows a model of the AFM system with the electromechanical actuator, cantilever and interaction forces. Rectangular pulses simulate the ideal surface profile and are described as a timed input function.

Table 3.1. Values used in the model (Morkvenaite-Vilkonciene et al., 2019b)*

Parameters	Symbols	Values
Density of the cantilever material	ρ	3180 kg/m^3
Mass of the cantilever $m = \rho V$	m_c	$1.431 \cdot 10^{-10}$ kg
Stiffness of the cantilever	k_c	0.2 N/m
Damping of the cantilever	h_c	$4.32 \cdot 10^{-5}$ N/m·s^{-1}
Mass of the scanner	m_s	35 g
Stiffness of the scanner	k_s	185 N/m
Damping of the scanner	h_s	81 N/m·s^{-1}
Stiffness of the control latency DOF	k_v	37 000 N/m
Damping of the control latency DOF	h_v	300 N/m·s^{-1}
Damping of the contact between the surface and the tip	h_k	
In contact with silicon		0.8 N/m·s^{-1}
In contact with PMMA		1 N/m·s^{-1}
Young's module of silicon	E_s	$165 \cdot 10^9$ Pa
Young's module of PMMA		$1 \cdot 10^6$ Pa
Poisson's ratio of silicon	P	0.22
Poisson's ratio of PMMA		0.51

*The reference is given in the list of publications by the author on the topic of the dissertation.

Coefficients for the cantilever's geometry (cantilever thickness, length, and width) were taken from the data declared by the manufacturer. All parameters used for modelling are provided in Table 3.1.

Model adequacy was checked by comparing the simulated data with experimental registered by the scanning silicon and PMMA surfaces (Fig. 3.9). In the model, the effect of the surface material is evaluated using Equation (2.6). In an actual scanning experiment, the influence of the surface material on the registered result is based on the interaction between the tip and the surface, which is nonlinear and depends on the distance between both objects. The model evaluated the energy loss by the damping constant, which was chosen according to the best fit with experimental data. The determined damping and stiffness coefficients were different for different evaluated materials (Table 3.1).

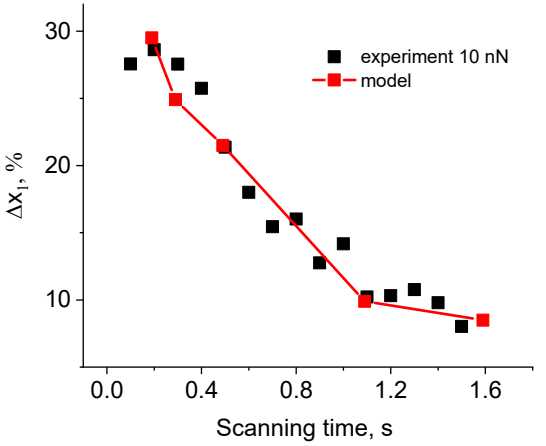

Fig. 3.9. Comparison of AFM experimental data with data obtained using the developed model. The scanning speed 100 µm/s, the setpoint force is 10 nN, the surface material is silicon (Morkvenaite-Vilkonciene et al., 2019b)*

3.1.4. Modelling Results

A silicon calibration grid scan was simulated by applying different scanning speeds (Fig. 3.10a). The dependence of the relative error on the scanning speed is nonlinear and depends on the tip quality and sharpness, e.g., using the tip of 10 nm radius, the relative error is 21 %, while the tip of 1000 nm radius generates the relative error of 29 % when the same 200 µm/s scanning speed is applied.

The resulting relative errors, which were calculated when different surface materials were used for modelling, are provided in Fig. 3.10b. The highest error

*The reference is given in the list of publications by the author on the topic of the dissertation.

was calculated for the silicon surface, compared to that calculated for "softer" materials, e.g., for silicon surface, the error is 21%, for glass – 18%, and PMMA – 10% at the same 200 µm/s scanning speed.

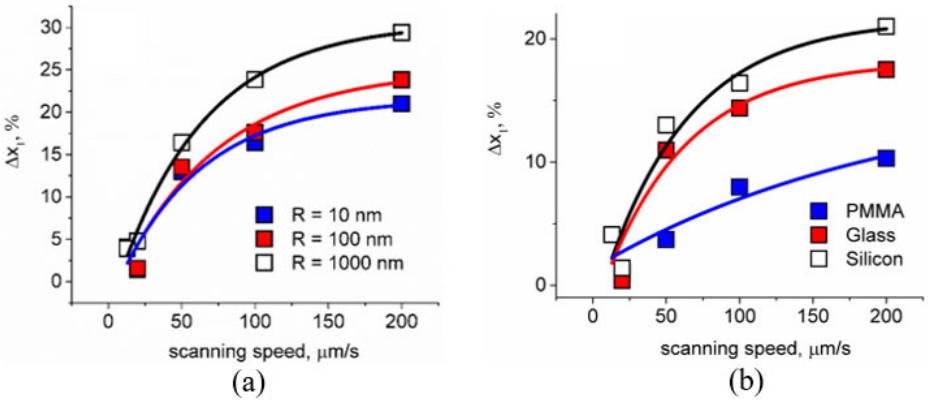

Fig. 3.10. Simulation results: (a) results calculated using the model for different tip geometries and the same 200 µm/s scanning speed modelled with the silicon calibration grid structure in the model input; (b) results from the model using different surface materials modelled for the 10 nm radius tip (Morkvenaite-Vilkonciene et al., 2019b)*

3.2. Electrochemical Studies of a Yeast-Modified Biofuel Cell

3.2.1. Application of 9,10-Phenanthrenequinone

3.2.1.1. Assessment of Yeast Cell Viability

The growth of yeast cells was evaluated by determining the cell suspension optical density at 600 nm. Optical density measurements for baker's yeast and yeast *Saccharomyces cerevisiae* cells grown in the liquid YPG medium with or without PQ solution are presented in Fig. 3.11. The results showed that the quantity growth of yeast *Saccharomyces cerevisiae* cells increased with increasing temperature, but an increase in temperature had a negative effect on the growth of baker's yeast. It depends on the species and strains of yeast cells. The growth of baker's yeast in liquid YPG at 22.5 °C temperature is faster (Control II, Fig. 3.11b) than at 30 °C

*The reference is given in the list of publications by the author on the topic of the dissertation.

temperature. The temperature significantly affects the permeability of the phospholipid membrane (Salvadó et al., 2011, Lip et al., 2020). These experiments illustrate that the most optimal temperature for the growth of yeast *Saccharomyces cerevisiae* 21PMR (MAT leu2 ura3-52) cells is 30 °C (Control I, Fig. 3.11a).

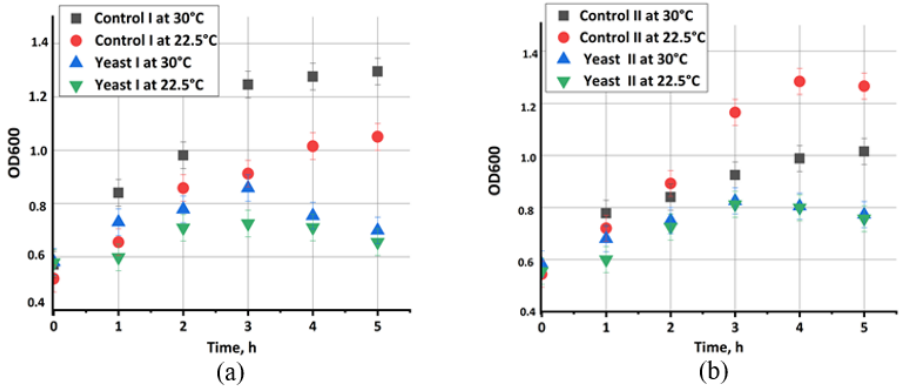

Fig. 3.11. Variation of the optical density at 600 nm (OD600) during the determination of growth efficiency of yeast cells. (a) The comparison of growth efficiency: (i) Yeast I – *Saccharomyces cerevisiae* with 3.75 mM PQ; Control I – *Saccharomyces cerevisiae* in the liquid YPG; (b) The comparison of growth efficiency: (ii) Yeast II – baker's yeast with 3.75 mM PQ; Control II – baker's yeast in the liquid YPG (Rozene et al., 2021a)*

A significant increase in the optical density is observed during the cell growth phase, lasting up to the 3rd hour of incubation (Fig. 3.11). Hence, after 3 h of yeast cell cultivation, the optical density was lower in the yeast *Saccharomyces cerevisiae* aliquot containing 3.75 mM of PQ solution (0.75±0.05) (Fig. 3.11a) than in the baker's yeast aliquot containing 3.75 mM of PQ solution (0.81±0.05) (Fig. 3.11b). However, when both *Saccharomyces cerevisiae* yeast strains were cultivated with the 3.75 mM solution of PQ at 22.5C, the optical density changed differently for both strains (Fig. 3.11). The decrease in the optical density of the yeast cell suspension showed that PQ in the aliquot solution and incubation at higher temperatures inhibited the proliferation of yeast cells (Scott et al., 2007; Brousse et al., 2018).

The exposure of baker's yeast to PQ significantly decreased the yeast cell viability at lower incubation temperatures (Fig. 3.11b). But the growth curves of both yeast aliquots showed that baker's yeasts are more resistant to dissolved PQ than *Saccharomyces cerevisiae* yeast cells. It is known that PQ can cause oxidative stress in cells by generating ROS. ROS cause DNA damage resulting in gene

*The reference is given in the list of publications by the author on the topic of the dissertation.

mutation (Rodriguez et al., 2008). Therefore, dissolved PQ's antimicrobial activity was investigated against (ii) baker's yeast and (i) *Saccharomyces cerevisiae* yeast cells using the agar well diffusion assay.

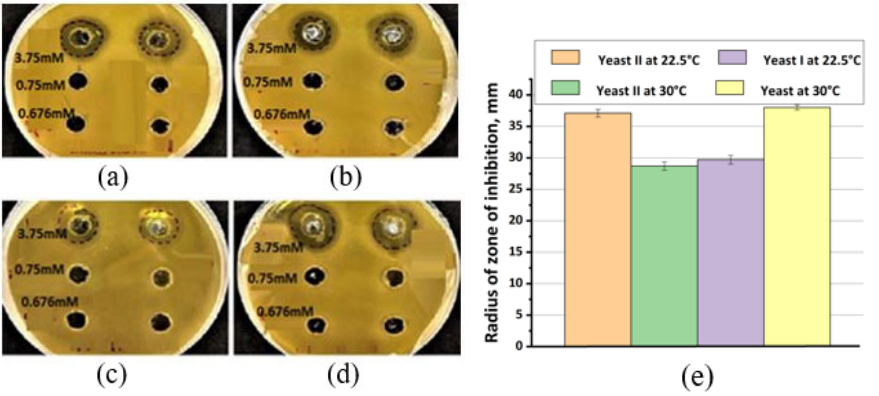

Fig. 3.12. Antimicrobial activity of the PQ solution at different concentrations evaluated by the agar well diffusion method against yeast cells: (a) Yeast II (baker's yeast) at 22.5 °C; (b) Yeast II (baker's yeast) at 30 °C; (c) Yeast I (*Saccharomyces cerevisiae*) at 22.5 °C; (d) Yeast I (*Saccharomyces cerevisiae*) at 30 °C; (e) the histogram presents the radius of the inhibition zone at the 3.75 mM concentration of PQ in the solution (Rozene et al., 2021a)*

Fig. 3.12 illustrates the radius of the inhibition zone of the yeast cells cultivated at 22.5 °C and 30 °C temperatures. Antimicrobial activity was not observed for 0.676 mM and 0.75 mM concentrations of PQ solutions (Figs. 3.12a, 3.12b, 3.12c, 3.12d). In the solution containing 3.75 mM of PQ, some inhibition zones were recorded, indicating some antimicrobial activity dependent on the type of yeast cells and cultivation temperature. The results of antimicrobial activity of PQ solution are shown in Fig. 3.12e. The radius of inhibition zones for baker's yeast cells and yeast *Saccharomyces cerevisiae* cells was determined as 37.1±0.61 mm (at 22.5 °C), 28.7±0.69 mm (at 30 °C), 29.7±0.67 mm (at 22.5 °C), 30±0.4 mm (at 30 °C), respectively. Considering the evolution, the radius of the inhibition zone was used as the characteristic of antimicrobial activity, which indicated that baker's yeast cells were more resistant to the antimicrobial activity of dissolved PQ. For this reason, baker's yeast cells were selected for further development of MFCs.

*The reference is given in the list of publications by the author on the topic of the dissertation.

3.2.1.2. Influence of Different Potassium Ferricyanide Concentrations on the Charge Transfer Rate from Yeast

CVs were recorded at different PQ concentrations in buffer solution (Fig. 3.13).

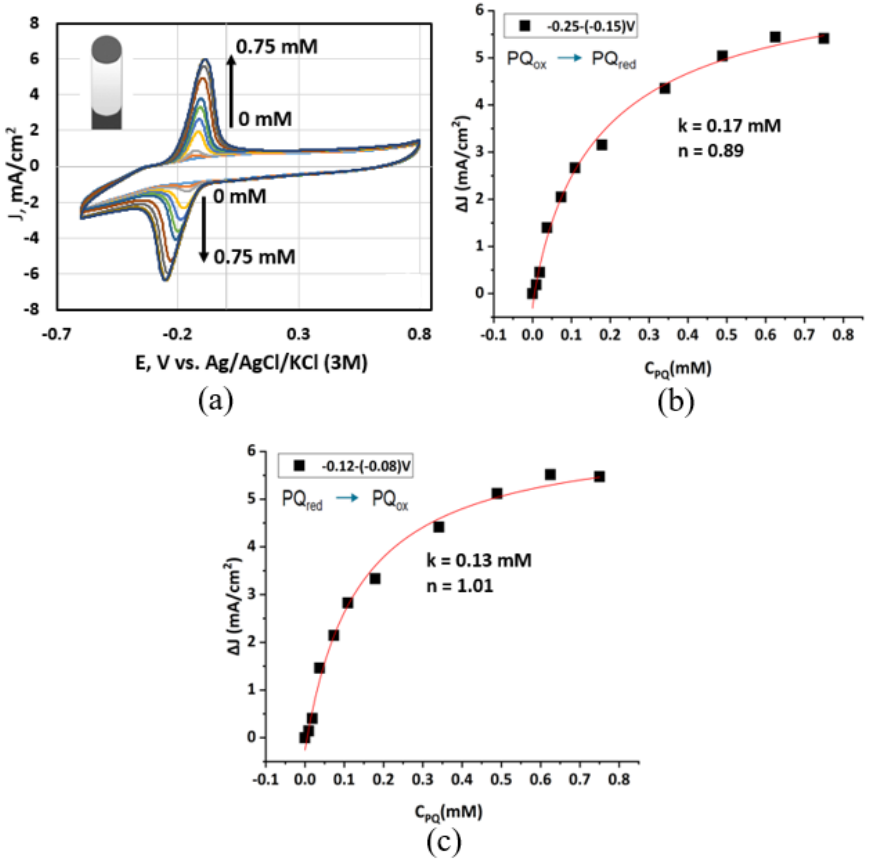

Fig. 3.13. Measuring results: (a) CVs registered using a non-modified graphite electrode at different PQ concentrations in the buffer solution. The scan rate of 0.1 V/s and the potential step of 0.01 V was applied. The peak currents, which were determined from voltammograms vs PQ concentration (Fig. 3.13a), were fitted using the Hill's function (Equation (2.3)): (b) reduction peak potentials in the range from –0.25 to –0.15 V vs used PQ concentration; (c) oxidation peak potentials in the range from –0.12 to –0.08 V vs used PQ concentration. Measurements were performed in a three-electrode-based electrochemical cell (Rozene et al., 2021a)*

*The reference is given in the list of publications by the author on the topic of the dissertation.

When PQ concentration increased, the current density values at both the cathodic (PQ reduction, at an interval from -0.25 V to -0.15 V) and anodic (PQ oxidation, at an interval from -0.12 V to -0.08 V) peaks increased accordingly. When the concentration of PQ increased from 0 to 0.75 mM, then the current density changed from -1 to -6.5 mA/cm^2 while measured at -0.25 V potential, and when the concentration of PQ increased from 0 to 0.75 mM, then the current density increased from 0.5 to 6 mA/cm^2 while measured at -0.1 V potential.

The current, observed at the peaks of CVs, was plotted as dependent on PQ concentration (Fig. 3.13b, 3.13c). Results were assessed using Hill's function by fitting to experimentally determined measurement results (Equation (2.3)). At the reduction reaction peak (Fig. 3.13b), the Hill's coefficient n is lower than 1, which corresponds to negative cooperativity of substrate binding, i.e., if the concentration of PQ increases, then the affinity of other PQ molecules decreases. The constant k, which indicates the concentration at which half of the maximal current is observed, calculated for oxidation current registered as the maximum oxidation peak is equal to 0.17 mM, and it is higher than the constant k (of 0.13 mM) determined for the establishment of the reduction peak in CV. Hill's coefficient n, which was determined at the oxidation reaction peak, is greater than 1, which corresponds to the positive cooperativity, i.e., if PQ concentration increases, then the efficiency of charge transfer by PQ molecules also increases (Fig. 3.13c). However, the evaluation of the type of cooperativity is questionable because the value of n is close to 1 in both cases; hence, in this case, the distinct difference between negative and positive cooperativity cannot be determined.

3.2.1.3. Influence of Different Dissolved PQ Concentration on the Charge Transfer Rate from Yeast at Constant Potassium Ferricyanide Concentration

The effect of PQ concentration on charge transfer from yeast-modified graphite electrode was investigated during further experiments. The CVs of the yeast-modified graphite electrode (Fig 3.14a, left corner) were registered after the addition of corresponding PQ concentrations in the presence of constant concentrations of both the second redox mediator (FCN) and glucose in the buffer solution (Fig. 3.14a). The current density increased more significantly when the PQ concentration reached 0.098 mM at –0.15 V and –0.35 V potentials. However, the overall current density remained unchanged. Only the oxidation peak maximum shifted from +0.37 to +0.4 V for registered at higher potential and from 0.12 to 0 V for oxidation peak registered at lover potential due to the presence of ferricyanide.

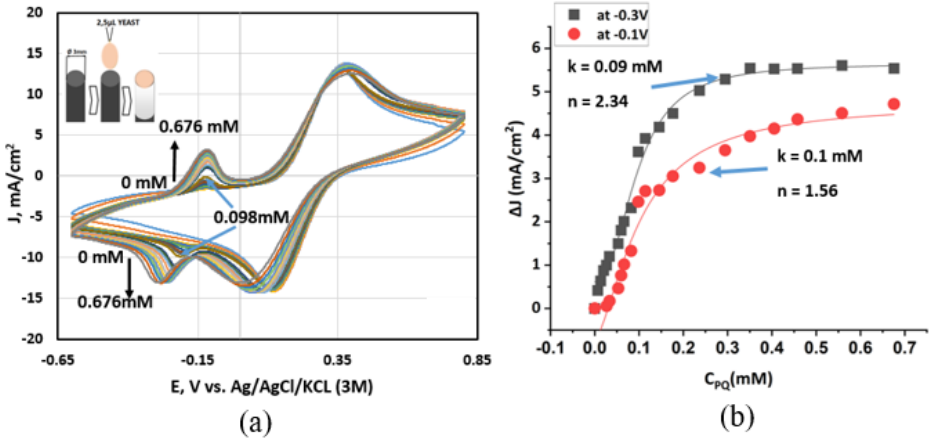

Fig. 3.14. Measuring results: (a) CVs of yeast-modified graphite electrode at different PQ concentrations. Measurements were performed in a buffer solution with the FCN 37 mM and glucose 32 mM; (b) fittings of the peak current from voltammograms (Fig. 3.14a) recorded using yeast-modified graphite electrode, results are fitted using Hill's function (Equation (2.3)). Measurements were performed in a three-electrodes electrochemical cell (Rozene et al., 2021a)*

The current peaks from voltammograms were plotted as PQ concentration dependencies and evaluated by fitting with Hill's function (Equation (2.3)) (Fig. 3.14b). At both -0.3 V and -0.1 V potentials, the Hill coefficient n is higher than 1 (n = 2.34; n = 1.56, respectively), which means that positive cooperativity is observed in both cases, but at -0.1 V potential, the current value became lower by 0.5 times. This effect can be attributed to the fact that PQ_{ox} is consumed in yeast and involved in intracellular enzymatic reactions. The constant k, which indicates the concentration at which half the maximal current is registered, is equal (k = 0.1 mM) at both potentials.

3.2.1.4. Evaluation of the 9,10-Phenanthrenequinone/Yeast-Modified Graphite Electrode at Different Potassium Ferricyanide Concentrations

The efficiency of the system based on two redox mediators was evaluated using the PQ/yeast-modified graphite electrode. One redox mediator (FCN) was hydro-

*The reference is given in the list of publications by the author on the topic of the dissertation.

philic, and another redox mediator (PQ) was lipophilic, so the yeast cell membrane absorbed it. Experiments demonstrate that this system efficiently transfers electrons from yeast cells to the anode. CVs (Fig. 3.15a) illustrate yeast's redox activity and electron transfer efficiency from yeast cells to the electrode. The system based on two redox mediators first adsorbed PQ and then immobilised yeast layers on the graphite electrode (graphite/PQ/yeast electrode). Next, the graphite/PQ/yeast electrode was incubated in an electrolyte containing glucose and FCN. The oxidised form of PQ diffuses through the yeast cell's wall and membrane and participates in the redox reactions inside the cell. Then, the reduced form of PQ diffuses back towards an external solution and passes the electrons to the oxidiser – $[Fe(CN)_6]^{3-}$. Then formed reduced form ($[Fe(CN)_6]^{4-}$) is re-oxidised back into $[Fe(CN)_6]^{3-}$ at the anode at +0.35 V potential. The yeast consumes glucose during metabolic processes and other chemical reactions inside the cell.

The graphite/PQ/yeast electrode (Fig. 3.15a, upper-left corner) was connected as a working electrode in the three-electrode-based electrochemical cell. CVs were recorded in the presence and absence of glucose (Fig. 3.15a). In addition, the steady-state voltammograms were evaluated. CVs observed in a buffer solution with and without glucose are similar. The PQ oxidation-reduction peaks were obtained because the PQ was immobilised directly on the electrode. However, the charge transfer from cells was not observed. Therefore, a second redox mediator – FCN – was applied to facilitate the charge transfer from cells, and then the anodic current significantly increased, as was initially expected. Equilibration of steady-state current took approx. 20 min.

After adding FCN into the solution, the maximum increment in the current density was observed at 0.15 V and 0.35 V potentials, which are the reduction and oxidation potentials of FCN, respectively. Also, the current density increased in time: from 0.5 mM/cm^2 (at the start of the measurement) to 8 mM/cm^2 (at 20th min of the measurement) at 0.15 V potential; and from -0.5 mM/cm^2 (at the start of the measurement) to 7 mM/cm^2 (at 20 min) at 0.25 V potential. This shows that the system based on two redox mediators is operating efficiently, and this system can be used in the design of yeast-based MFCs.

To determine the dependency of yeast-generated current density on time, the peak current from time-dependent voltammograms (data not shown) was plotted as a time-dependence and evaluated by fitting with results that were calculated using Hill's function (Equation (2.4), Fig. 3.15b). The Hill coefficient n is higher than one ($n = 2.58$), and it indicates positive cooperativity. The constant k, which indicates the concentration at which half of the maximal current is registered, is equal to 2.7 mM, which is rather similar to that observed when the yeast-modified electrode was evaluated in PQ containing solution ($k = 2.34$).

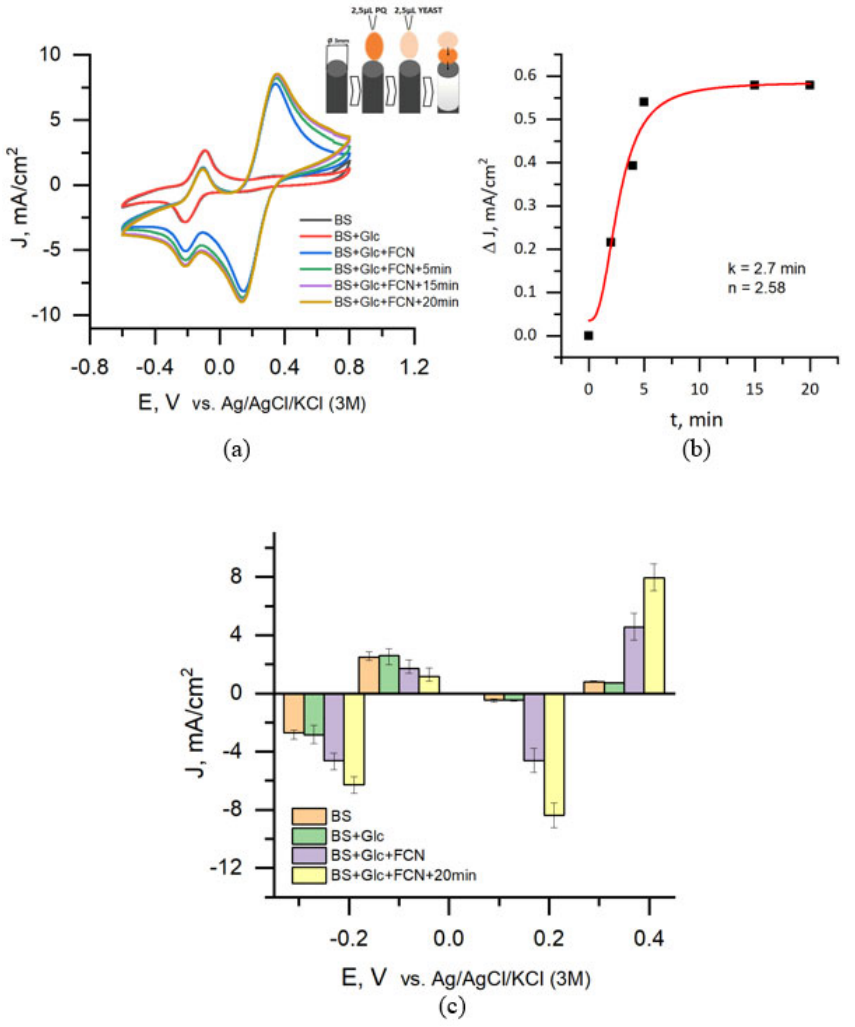

Fig. 3.15. Measuring results: (a) CVs of the graphite electrode with immobilised PQ and yeast cells registered in BS in the presence and absence of glucose (Glc) and FCN; (b) current density *vs* time dependence fitting of results gathered from the voltammograms recorded at 0.4 V using graphite electrode with immobilised PQ and the yeast cell in BS with 46.5 mM glucose and 11.6 mM FCN, with Hill's function (Equation (2.4)); (c) data from replicated experiments with PQ and yeast-modified electrode. Measurements were performed in a three-electrodes electrochemical cell (Rozene et al., 2021a)*

*The reference is given in the list of publications by the author on the topic of the dissertation.

The diagram of experiments using a PQ-modified graphite electrode shows the change of current density at the different stages of the process: before and after adding an additional portion of redox mediator into the solution and the stabilisation of current density (Fig. 3.15c).

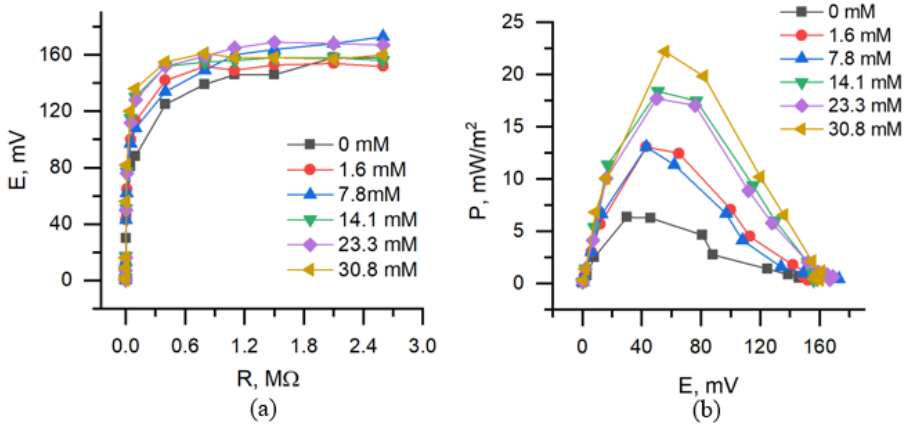

Fig. 3.16. Measuring results: (a) potential dependence on applied external load; (b) calculated power density dependence on the generated potential in a single-compartment-based MFC, which consisted of (i) graphite/PQ/yeast modified anode and (ii) bare graphite cathode immersed in the phosphate-acetate buffer solution containing 23 mM of FCN and different concentrations of glucose: 0 mM (1), 1.6 mM (2), 7.8 mM (3), 14.1 mM (4), 23.3 mM (5) and 30.8 mM (6). All measurements were performed in a two-electrode electrochemical cell (Rozene et al., 2021a)*

The current density before and after glucose addition is similar at –0.25V and –0.1V potentials and similar at 0.15V and 0.35V potentials. FCN provides almost the same current density value at all potentials, except for –0.1 V. This potential is related to the reduction of PQ_{ox} in yeast; hence, PQ_{ox} is consumed, and the concentration of this PQ form becomes lower. At potentials, –0.25; 0.15; 0.35 V positive and negative values of current densities increased over the time when FCN was added.

To assess the MFC performance, a two-electrode-based electrochemical cell was applied, with (i) anode based on PQ and yeast modified graphite electrode and (ii) cathode based on bare graphite electrode (Fig. 3.16). It was determined that MFC, in which the anode was modified by PQ and yeast, generated 173 mV potential in the presence of 7.8 mM glucose at the load of 2.6 MΩ, which resulted

*The reference is given in the list of publications by the author on the topic of the dissertation.

in 0.407 mW/m^2 power (Fig. 3.16a). Maximal open circuit potential was 178 mV at 7.8 mM of glucose and 23 mM of FCN.

Maximal calculated power was 22.2 mW/m^2 at 56 mV (Fig. 3.16b). This fact reveals that PQ has a good potential to be applied as a redox mediator in the design of MFCs.

3.2.2. Application of Menadione

3.2.2.1. Assessment of the Yeast Cell Viability

In viability studies, it is crucial to determine the critical time after which a cell number change during cultivation is observed. Therefore, the growth of yeast cells was assessed by measuring the optical density of the cells' suspension at 600 nm. Measurements of the optical density of baker's yeast and *Saccharomyces cerevisiae* yeast cells grown in the liquid YPG medium with or without MD solution are shown in Fig. 3.17.

This research cultured different yeast cell species and determined that the optical density of the cells' suspension increased with increasing temperature and by prolonging the time of cultivation. The optimal temperature for *Saccharomyces cerevisiae* 21PMR (MAT leu2 ura3-52) yeast strain grows at 30 °C temperature (Fig. 3.17a, control I). However, the *Saccharomyces cerevisiae* baker's yeast strain cells (Fig. 3.17b, control II) multiplied more slowly; it depends on the species of yeast cells. When yeast cells were cultivated with 3.75 mM of MD, optical density changed differently for both species. OD slightly decreased after 4 h and 26 h cultivation of *Saccharomyces cerevisiae* 21PMR (MAT leu2 ura3-52) yeast strain (Fig. 3.17a, yeast I). However, the baker's yeast cells increased after cultivation of 4 h and 26 h (Fig. 3.17b, yeast II). The viability decreased for both species of yeast cells. This result may indicate cell death due to adverse growing conditions, which was due to the toxic effect of MD (Castro et al., 2008; Lushchak et al., 2009). The growth curves of both yeast aliquots showed that *Saccharomyces cerevisiae* baker's yeast strain is more resistant to dissolved MD than *Saccharomyces cerevisiae* 21PMR (MAT leu2 ura3-52) yeast strain cells.

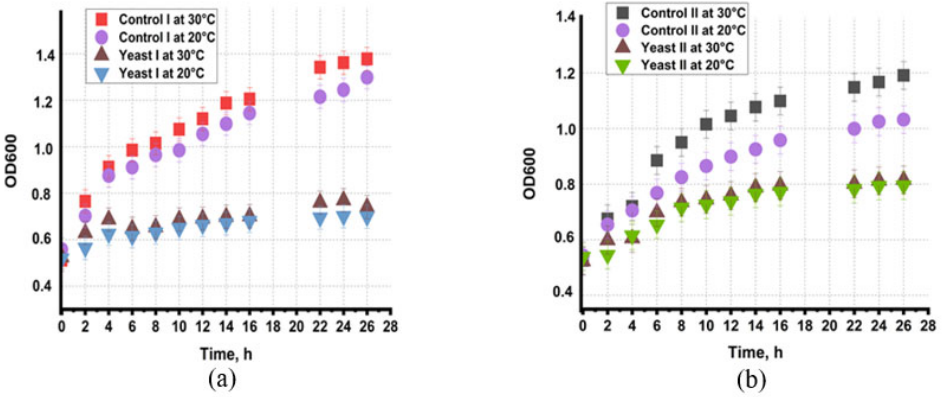

Fig. 3.17. Variation of the optical density (OD) during the determination of growth curves of yeast: (a) a comparison of growth curves: (i) yeast I – *Saccharomyces cerevisiae* 21PMR (MAT leu2 ura3-52) yeast strain with 3.75 mM menadione (MD); control I – *Saccharomyces cerevisiae* 21PMR (MAT leu2 ura3-52) yeast strain cells in the liquid YPG agar medium; (b) a comparison of growth curves: (ii) yeast II – *Saccharomyces cerevisiae* baker's yeast strain cells with 3.75 mM MD; control II – *Saccharomyces cerevisiae* baker's yeast strain cells in the liquid YPG agar medium (Rozene et al., 2021b)*

The influence of 3.75 mM MD solution on yeasts' viability was investigated against (i) *Saccharomyces cerevisiae* 21PMR (MAT leu2 ura3-52) yeast strain cells and (ii) *Saccharomyces cerevisiae* baker's yeast strain cells. Fig. 3.18 represents the radius of the inhibition zone of both yeast cells cultivated at 20 °C and 30 °C (Fig. 3.18a, 3.18b). In the solution containing 3.75 mM of MD, inhibition zones were recorded, which indicated antimicrobial activity dependent on the species of the yeast cell and the temperature of cultivation. The results of the antimicrobial activity of the MD solution are shown in Fig. 3.18c. The radius of zones of inhibition for *Saccharomyces cerevisiae* 21PMR (MAT leu2 ura3-52) yeast strain cells and *Saccharomyces cerevisiae* baker's yeast strain cells was determined as 27.9 ± 0.6 mm (at 30 °C) and 24.7 ± 0.7 mm (at 20 °C) and 25.0 ± 0.6 mm (at 30 °C) and 23.1 ± 0.7 mm (at 20 °C), respectively. Considering that the radius of the inhibition zone was the measure of antimicrobial activity, baker's yeast cells were more resistant to dissolved MD. For this reason, baker's yeast cells were selected for further development of MFCs.

*The reference is given in the list of publications by the author on the topic of the dissertation.

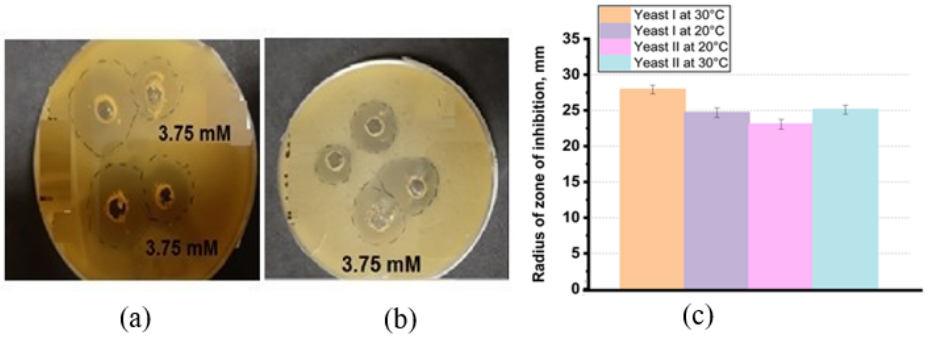

Fig. 3.18. Antimicrobial activity of the MD solution evaluated by the agar well diffusion method against yeast cells: (a) yeast I ((i) *Saccharomyces cerevisiae* 21PMR (MAT leu2 ura3-52) yeast strain) at 30 °C); (b) yeast II ((ii) *Saccharomyces cerevisiae* baker's yeast strain) at 30 °C; (c) the histogram presents the radius of the inhibition zone at 3.75 mM concentration of MD in the solution (Rozene et al., 2021b)*

3.2.2.2. Evaluation of the Menadione-Modified Graphite Electrode

CVs were recorded while yeast solution concentration was being incrementally increased in the same electrochemical cell.

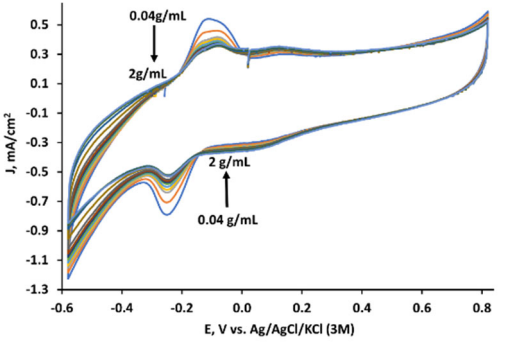

Fig. 3.19. CVs recorded with the MD-modified anode at different yeast concentrations in the phosphate–acetate buffer solution. The scan rate was 0.1 V/s (Rozene et al., 2021b)*

*The reference is given in the list of publications by the author on the topic of the dissertation.

In this experiment, only MD was immobilised on the anode. The concentration of yeast solution was sequentially increased in the same measurement cell with the phosphate–acetate buffer solution to 2 g/mL (Fig. 3.19). The current density decreased from 0.55 to 0.4 mA/cm^2 at -0.15 V and from –0.8 to –0.52 mA/cm^2 at –0.25 V potentials, while the yeast concentration increased from 0.04 to 2 g/mL.

3.2.2.3. Evaluation of the Yeast-Modified Graphite Electrode at Different Menadione Concentrations

The CVs of the yeast-modified graphite electrode were recorded with the FCN and the glucose in the phosphate-acetate buffer solution with different menadione concentrations (Fig. 3.20a). The current density increased evenly in the range from 0.0 mM to 0.066 mM.

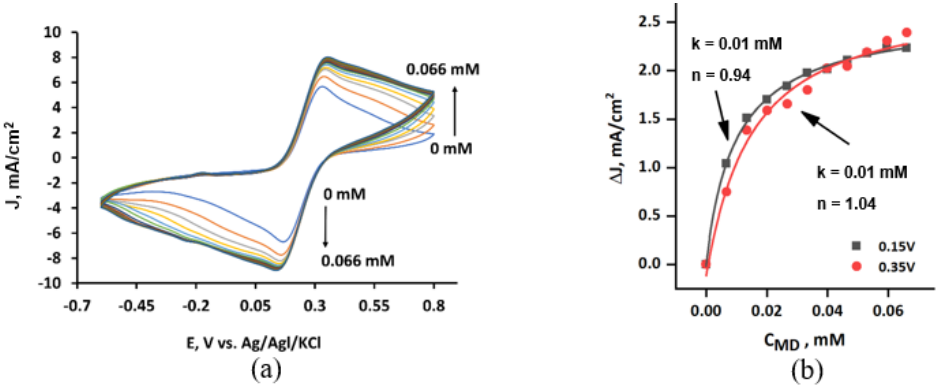

Fig. 3.20. Measuring results: (a) CVs registered by the yeast-modified graphite electrode at different MD concentrations. Measurements were performed in the phosphate–acetate buffer solution with the 37 mM FCN and 31 mM glucose. A scan rate of 0.1 V/s and a potential step of 0.01 V was applied; (b) reduction peak potentials at 0.15 V and 0.35 V vs used MD concentration recorded using the yeast-modified graphite electrode (results were fitted using Hill's function (Equation (2.3)). Measurements were performed in a three-electrode-based electrochemical cell (Rozene et al., 2021b)*

The current peaks from the voltammogram were plotted as current density vs MD concentration dependence and evaluated by fitting Hill's equation (Equation (2.3)) (Fig. 3.20b). At the 0.15 V potential, the Hill coefficient n was less than one (n = 0.94). This means negative cooperativity for substrate binding, i.e., if the concentration of MD increases, then the affinity of other MD molecules decreases.

*The reference is given in the list of publications by the author on the topic of the dissertation.

At the 0.35 V potential, n was higher than one (n = 1.04), and this indicated positive cooperativity, i.e., if MD concentration increases, then the efficiency of charge transfer by MD molecules also increases. The half-maximal concentration constant k was low (k = 0.01 mM) at both potentials, which made the reaction rate speedy.

3.2.2.4. Evaluation of the Yeast and Menadione-Modified Graphite Electrode at Different Menadione Concentrations

The graphite electrode modified with MD and yeast was used as a working electrode in the electrochemical cell, and CVs were recorded with and without glucose (Fig. 3.21a).

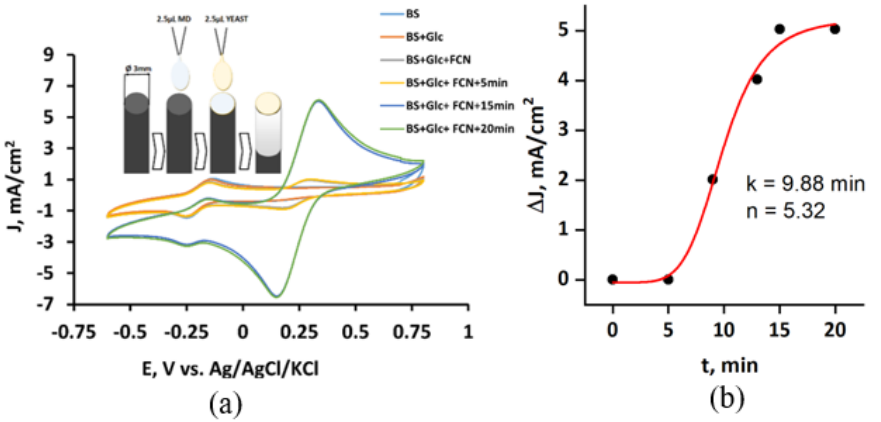

Fig. 3.21. Measuring results: (a) CVs of graphite electrode with immobilised MD and yeast cells registered in the phosphate–acetate buffer solution (BS) with the presence and absence of Glc and FCN; (b) reduction peak current density at 0.4 V vs used MD concentration recorded using an immobilised MD-and yeast-modified graphite electrode (results were fitted using Hill's function (Eq. (2.4)). Measurements were performed in a three-electrode-based electrochemical cell in the phosphate–acetate buffer solution with 23 mM glucose and 23 mM FCN (Rozene et al., 2021b)*

CVs observed in the phosphate–acetate buffer solution with and without glucose were similar. In addition, the MD oxidation-reduction peaks were obtained since MD was immobilised on the electrode (Fig. 3.21a, upper-left corner). The second redox mediator, FCN, to achieve a higher electrochemical signal and to

*The reference is given in the list of publications by the author on the topic of the dissertation.

transfer charge from yeast to the electrode was used. It lasted 15 min to achieve steady-state conditions for yeast.

Peaks from time-dependent CVs (not shown) were plotted as time dependence and evaluated by fitting Hill's function (Eq. (2.4)) (Fig. 3.21b). The Hill coefficient (n) was higher than one (n = 5.32), which meant positive cooperativity. However, the half-maximal concentration constant k was high (k = 9.88), so the reactions were slow. Compared to the only yeast-modified electrode, the Hill coefficient range became five times higher (from n = 0.94 and 1.04 measured with the yeast-modified electrode (Fig. 3.20b) to n = 5.32 obtained with the yeast-and MD-modified electrode). Additionally, compared to the only yeast-modified electrode, the range of the half-maximal concentration constant k became 1000 times higher (from k = 0.01 mM measured with the yeast-modified electrode (Fig. 3.20b) to k = 9.88 obtained with the yeast-and MD-modified electrode).

The comparison of the data from all experiments demonstrated that the MFC would generate the highest current at 0.15 V and 0.35 V (the oxidation and reduction potentials of FCN, respectively). The most significant change in current was seen when the second redox mediator was added to the solution. The toxic effects of MD on yeast were absent. Therefore, both of them are suitable for the design of MFCs.

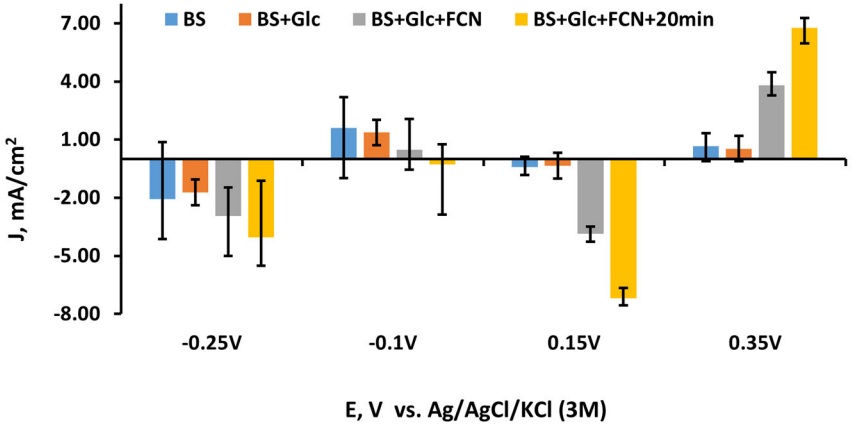

Fig. 3.22. Data from replicated experiments with the MD and yeast-modified electrode (Rozene et al., 2021b)*

The diagram of experiments using the MD-modified graphite electrode shows the change in the current density at different stages of the process: before

*The reference is given in the list of publications by the author on the topic of the dissertation.

and after adding new material to the solution and after the stability in the current density was reached (Fig. 3.22). The current density after adding glucose was lower at –0.1 V potentials but similar at 0.15 V and 0.35 V potentials. A rather significant difference was observed between negative and positive potentials. FCN provided almost the same current density value at all potentials, except for -0.1 V. At potentials –0.25, 0.15, and 0.35 V, positive and negative values of current densities increased over time, but at the –0.1 V potential, the current density value decreased when FCN was added.

3.2.2.5. Performance of the Microbial Fuel Cell

To assess the MFC performance, a two-electrode-based electrochemical cell was used with the MD-and yeast-modified graphite electrode used as the anode and a bare graphite electrode as the cathode. It was determined that MFC, in which the anode was modified by MD and yeast, generated 58 mV potential in the absence of glucose at an external load of 2.6 MΩ and resulted in 0.0046 mW/m^2 of power (Fig. 3.23a). The maximal open circuit potential was 62 mV at 23 mM FCN and the absence of glucose. The maximal calculated power was 0.408 mW/m^2 at 24 mV (Fig. 3.23b).

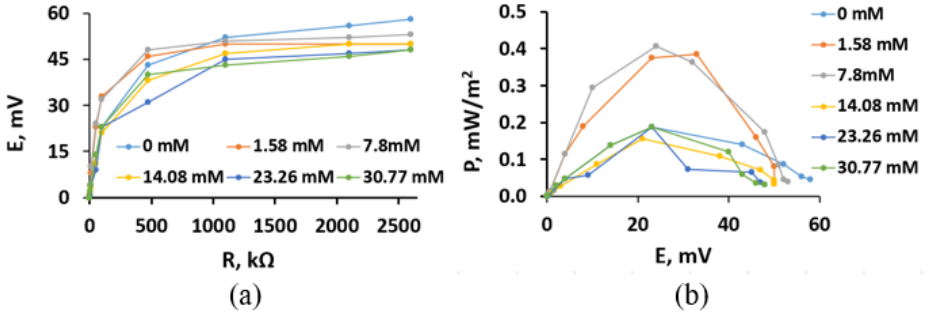

Fig. 3.23. Measuring results: (a) potential dependence on applied load; (b) calculated power density dependence on the generated potential in a single-compartment-based MFC, which consisted of an MD- and yeast-modified anode and a bare graphite cathode immersed in the phosphate–acetate buffer solution containing 23 mM of FCN and variable concentrations of glucose: 0 mM, 1.58 mM, 7.8 mM, 14.08 mM, 23.26 mM, and 30.77 mM (Rozene et al., 2021b)*

In previous research, the performance of MFC based on baker's yeast and a PQ-modified anode was evaluated (Rozene et al., 2021a)*. This MFC generated

*The reference is given in the list of publications by the author on the topic of the dissertation.

22.2 mW/m^2 of power at 56 mV in the presence of 30 mM glucose. The maximal open circuit potential was 178 mV at 7.8 mM of glucose and 23 mM FCN and PQ. Therefore, it can be concluded that menadione, as well as PQ, can be used in MFCs as redox mediators. However, PQ has a better ability to cross the yeast cell membrane and, thus, a PQ-based MFC result in a higher power than an MD-based MFC.

3.2.3. Application of Carbon Nanotubes

3.2.3.1. Analysis of the Structure of Multi-Walled Carbon Nanotubes

The samples were scanned using the scanning electron microscope to determine the shape and size of the MW-CNTs used in the present thesis. The form of the carbon MW-CNTs was determined by means of the data analysis of SEM measurements. The diameter of MW-CNTs was 10–25 nm, and the length was several micrometres (Fig. 3.24).

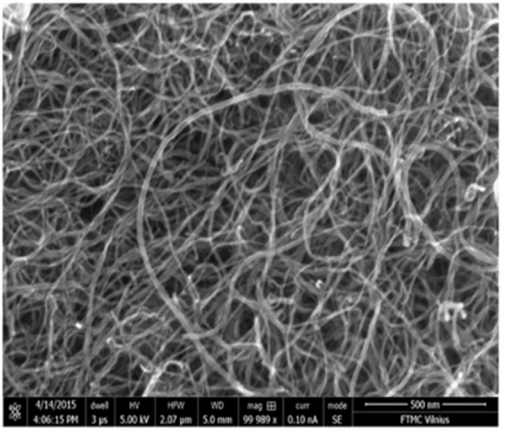

Fig. 3.24. SEM image of carbon nanotube-based nanostructure (Bruzaite et al., 2020a)

The phase composition of the MW-CNTs was obtained by X-ray diffraction analysis. Three peaks of MW-CNTs (2θ = 25.4°; 43.1°; 54°) are present in XRD registered patterns (Fig. 3.25)

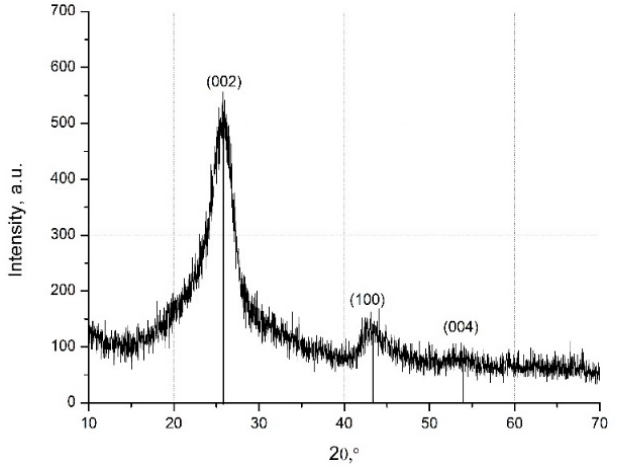

Fig. 3.25. X-ray spectra of the MW-CNTs (Bruzaite et al., 2020a)*

The peaks at the angle (*2θ*) of 43.1 °and 54 ° were associated with the (100), (004) diffractions of the hexagonal graphite structure (Safarova et al., 2007). The most significant diffraction peak at the angle (*2θ*) of 25.4° suggests the typical structure of the multi-layer nanotubes (Zhu et al., 2008; Saleh et al., 2011).

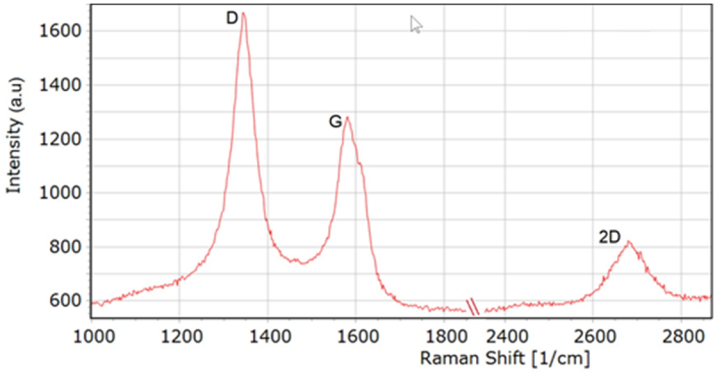

Fig. 3.26. Raman spectra of MW-CNTs used in the experiment (Bruzaite et al., 2020a)*

Fig. 3.26 presents a Raman spectrum of the MW-CNTs used in the experiment. The occurrence of the following bands characterises a range of MW-CNTs: 1345 cm^{-1} (D band corresponding to the degree of nanotube structural disorder),

*The reference is given in the list of publications by the author on the topic of the dissertation.

1579 cm^{-1} (G band corresponding to the degree of nanotube graphitisation) and 2683 cm^{-1} (2D band corresponding to stresses). The analysis of the shape of D and G modes and their ID/IG intensity ratio confirmed that it was MW-CNTs. Besides, no presence of RBM (Radial Breathing Mode) bands was observed in the investigations performed, confirming the use of MW-CNTs.

3.2.3.2. Evaluation of Toxicity of Multi-Walled Carbon Nanotubes on Yeast Cells

Initially, the possible effect of the carbon nanotube suspension of various concentrations on the yeast cells was determined by evaluating their viability using light and fluorescence microscopes. No difference was noticed between the incubation of either MW-CNT-treated or MW-CNT-untreated (for 24 h) yeast cells. Further, the viability of yeast cells was investigated in more detail. The cells were stained with methylene blue, and dead and living cells were counted using a light microscope after 1, 2, 3, 20, 22, 24 h from the moment of inoculation. The counts of treated and untreated cells were compared. The dead yeast cells were dyed blue, as shown in Fig. 3.27a.

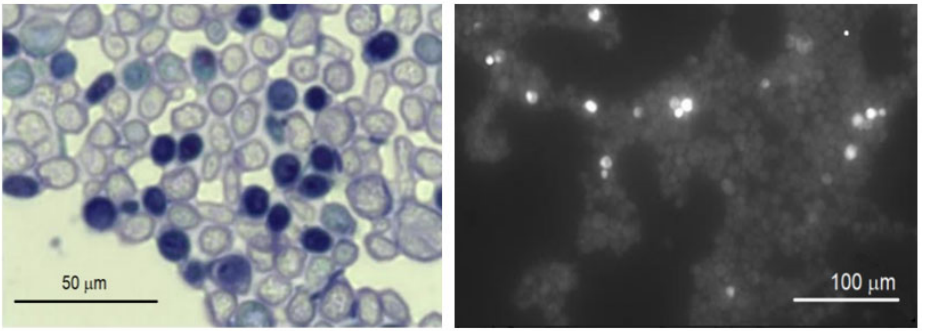

Fig. 3.27. Images of the yeast *Saccharomyces cerevisiae* cells in a field stained with: (a) methylene blue (bright cells, living; dark, dead) and (b) PI (bright, dead; dark, living) (Bruzaite et al., 2020a)*

The cells were also stained with PI, counted, and compared as previously described using the fluorescence microscope. The results of the staining are presented in Fig. 3.27b. The results of the counts (the ratio of numbers of dead and living cells) are presented in Fig. 3.28.

*The reference is given in the list of publications by the author on the topic of the dissertation.

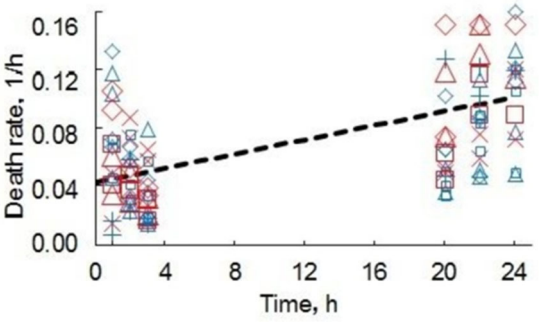

Fig. 3.28. Relative death of the yeast cells. Blue symbols correspond to cell staining with methylene blue and monitoring by optical microscopy, the red, to PI and the fluorescence microscope. The number of cells without MW-CNTs x or + and with MW-CNTs squares, triangles, and rhombuses (Bruzaite et al., 2020a)*

Finally, a possible effect of the MW-CNTs on the development of the yeast population was investigated. The yeast culture was incubated in the liquid nutritional medium YPG and various concentrations of the carbon nanotubes. The size of the population was estimated spectroscopically. The absorption of the cellular suspension was measured at approx. 600 nm wavelength, both in the control samples (the cells grown in the absence of carbon nanotubes) as well as in the samples with the nanotubes.

Over 24 h, the yeast population is assumed to grow first and then decline (Juška, 2011; Zhu et al., 2016). However, the experiment does not show this effect (Fig. 3.29). The size of the population was modelled by Equation (2.3) (Juška, 2011; Zhu et al., 2016). The model fitted well for MW-CNTs-free medium (Fig. 3.29a) and those containing 2 μg/mL MW-CNTs (Fig. 3.29b). For 50 μg/mL MW-CNTs (Fig. 3.29c) and 100 μg/mL MW-CNTs (Fig. 3.29d), the increase in optical density was observed after 16–24 h. Also, the behaviour of yeast cells treated with solutions containing different concentrations of MW-CNTs was different: in the case when yeasts were treated with solutions containing 0 and 2 μg/mL of MW-CNTs, the experimental results followed the model curve for the treatment of yeast cells by 50 μg/mL and 100 μg/mL of MW-CNTs containing solutions, from the third-hour results did not change significantly.

*The reference is given in the list of publications by the author on the topic of the dissertation.

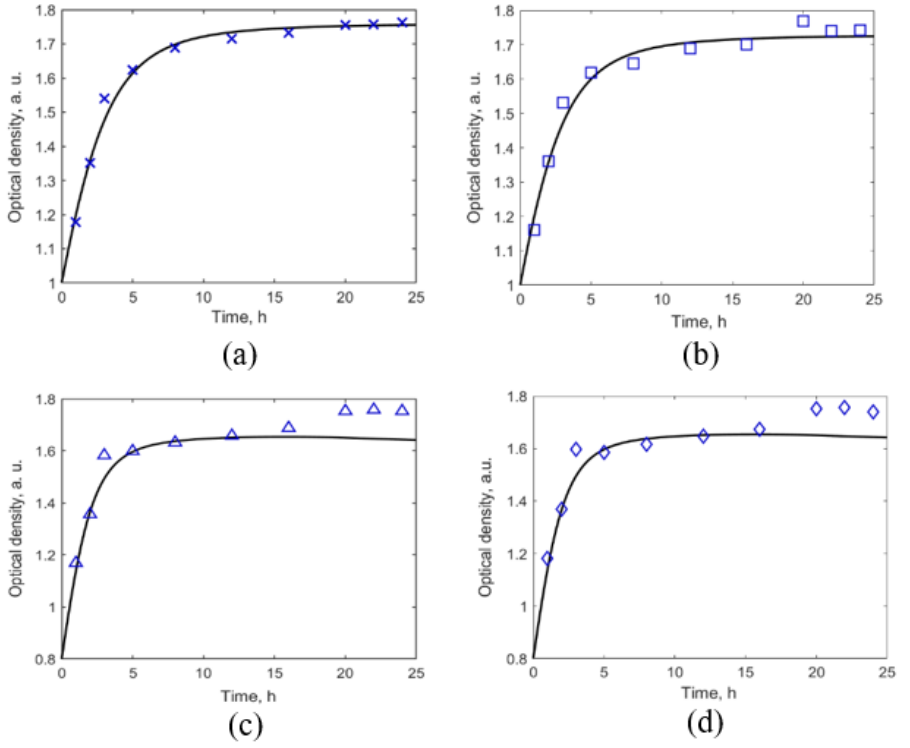

Fig. 3.29. Dependence of optical density on time at different MW-CNTs concentrations: (a) without MW-CNTs; (b) 2 µg/mL MW-CNTs; (c) 50 µg/mL MW-CNTs; and (d) 100 µg/mL MW-CNTs (Bruzaite et al., 2020a)*

Moreover, steady-state conditions were achieved at a higher optical density of 1.7 for yeast cells treated with 0 and 2 µg/mL of MW-CNTs, while for the other two MW-CNTs concentrations, steady-state conditions were obtained at an optical density of 1.6. Compared to other concentrations, relative growth and death rates calculated by the model were two times higher in the case of treatment by 50 µg/mL and 100 µg/mL MW-CNTs (Table 3.2). This suggests some effect of the MW-CNTs on the development of the yeast cell population.

*The reference is given in the list of publications by the author on the topic of the dissertation.

Table 3.2. Parameters of the model (Bruzaite et al., 2020a)*

Concentration	Relative Growth Rate (α), h^{-1}	Relative Death Rate (μ), h^{-1}	Consumption of Non-Saccharide Resources (ζ)	Initial Population Size x(0) #
Unaffected cells	0.215	0.0207	5	1
2 µg/mL MW-CNTs	0.219	0.022	5	1
50 µg/mL MW-CNTs	0.46	0.041	4.8	0.8
100 µg/mL MW-CNTs	0.46	0.041	4.8	0.8

z(0) = 1 was used in all simulations.

To analyse the data in more detail, the same data as optical density vs MW-CNTs dependencies (Fig. 3.30) was plotted.

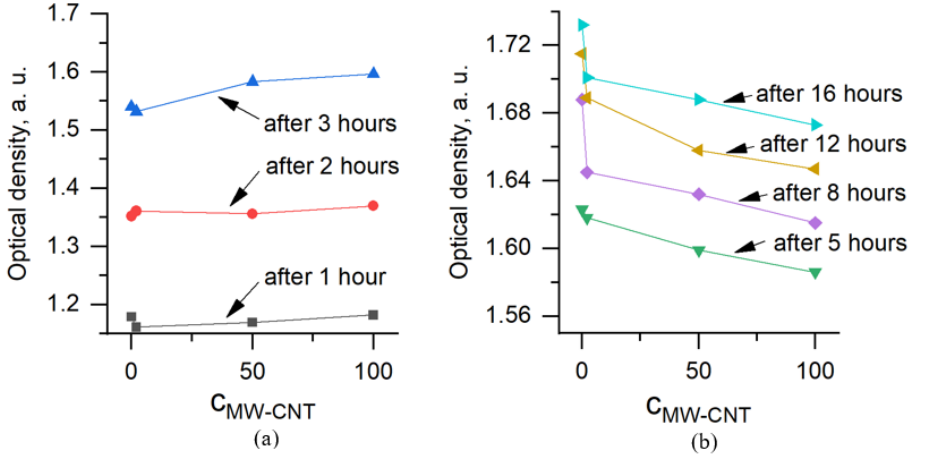

Fig 3.30. Dependence of optical density on MW-CNTs concentration at different times (a) 1–3 h; and (b) 5–16 h (Bruzaite et al., 2020a)*

Data of experiments performed at 1–3 h (Fig. 3.30a) were plotted separately after 5–16 h (Fig. 3.30b) to show a different MW-CNT effect on yeast cells. It was obtained that at the very beginning of the treatment, within 1 to 3 h, MW-CNTs did not affect yeast cells or the effect was very small. The optical density increased with increasing MW-CNTs concentration. Measurement after 5 h

* The reference is given in the list of publications by the author on the topic of the dissertation.

showed a decrease in optical density, revealing the toxic impact of MW-CNTs. However, the optical density at 0 μg/mL and 2 μg/mL MW-CNTs was practically the same; hence, the toxic effect after 5 h was observed at higher MW-CNTs concentrations. The highest difference at 0 μg/mL and 2 μg/mL MW-CNTs was seen after 8 h of the experiment. This may be a critical time at which the reaction of yeast to the MW-CNTs becomes sufficiently high to be registered. Data from the entire measurement period reveal the toxic effect of MW-CNTs (Fig. 3.30b), while the dependence of optical density on time (Fig. 3.29) did not show this effect. Measurements of optical density performed at 20, 22, and 24 h did not show reliable dependencies, and they are not shown here. These time points are also not according to the model (Fig. 3.29), especially at the higher MW-CNTs concentrations.

The investigation of the interaction of MW-CNTs with the yeast *Saccharomyces cerevisiae* cells was done using integrated AFM and confocal Raman spectroscopy (Spectra, NT-MDT).

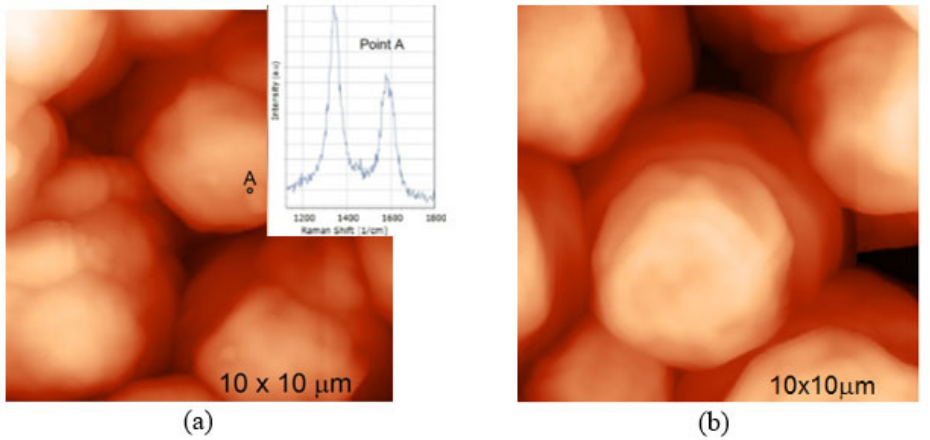

Fig. 3.31. AFM image of yeast cells: (a) AFM image of yeast cells and Raman spectra of MW-CNTs at the point of MW-CNTs at the point A (insert), (b) AFM image of yeast cells without MW-CNTs (Bruzaite et al., 2020a)*

The AFM image of the yeast cells is presented in Fig. 3.31b, and confocal Raman spectra collected from the selected points on the cell surface are presented in the insert of Fig. 3.31a. The Raman spectra of biological components from the yeast cell surface were subtracted as background during the Raman spectra measurement. The collected MW-CNTs Raman spectra from the cells surface confirm the MW-CNT interaction with the yeast cells.

3.2.3.3. Electrochemical Analysis and Biofuel Cell Development

This research used the two-redox mediators-based system. One redox mediator PQ was used to modify the graphite electrode, and another one – $K_3[Fe(CN)_6]$ – was added to the solution. PQ can cross the cell's membrane and achieve redox centres of enzymes located in the cytoplasm of cells. $K_3[Fe(CN)_6]$ takes electrons from PQ and passes them to the electrode. The CVs using PQ were registered, and PQ/MW-CNT modified graphite electrode (Fig. 3.32). Four peaks were observed in both CVs, PQ oxidation/reduction peaks (two on the left) and $[Fe(CN)_6]^{3-/4-}$ oxidation/reduction peaks. The comparison of the measurement using PQ and PQ/MW-CNT graphite electrodes demonstrates that using MW-CNTs allows the increase in the current for both PQ and $[Fe(CN)_6]^{3-/4-}$ oxidation/reduction processes.

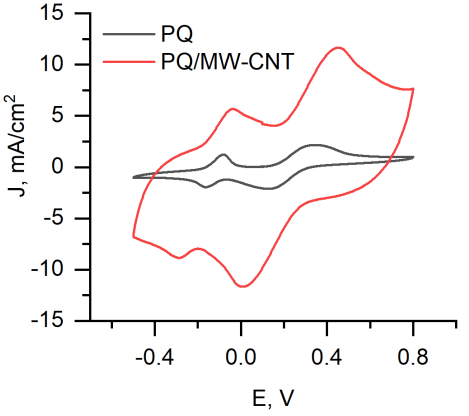

Fig. 3.32. CVs of PQ and PQ/MW-CNT modified MFC anode (graphite electrode), immersed in a phosphate buffer solution with 10 mM $K_3[Fe(CN)_6]$, 70 mM glucose, and 3 mg/mL yeast cells (Bruzaite et al., 2020a)*

Electrochemical impedance spectroscopy-based measurements represent the resistivity of the layers formed at the anode surface (Fig. 3.33). In the case when a PQ-modified anode was used, charge transfer resistance was much higher compared to MFC based on the PQ/MW-CNT electrode. This effect was well observed in both Nyquist (Fig. 3.33a) and Bode plots (Fig. 3.33b).

*The reference is given in the list of publications by the author on the topic of the dissertation.

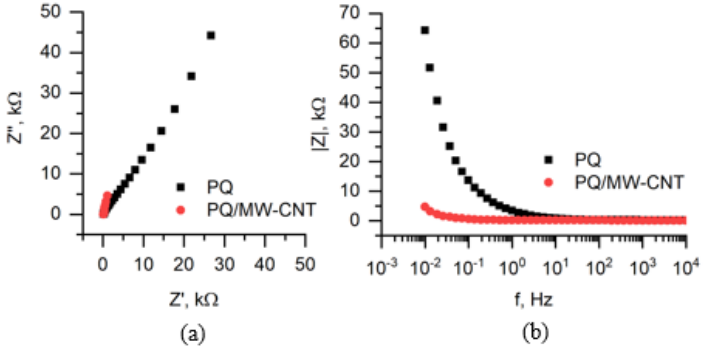

Fig. 3.33. Electrochemical impedance spectroscopy-based measurements: (a) Nyquist plot and (b) Bode plot. Measurements conditions are the same as in Fig. 3.32 (Bruzaite et al., 2020a)*

During measurements of the MFC performance, the two-electrode-based electrochemical cell was used, with one PQ or PQ/MW-CNT modified graphite-based electrode and another platinum-based electrode (Fig. 3.33).

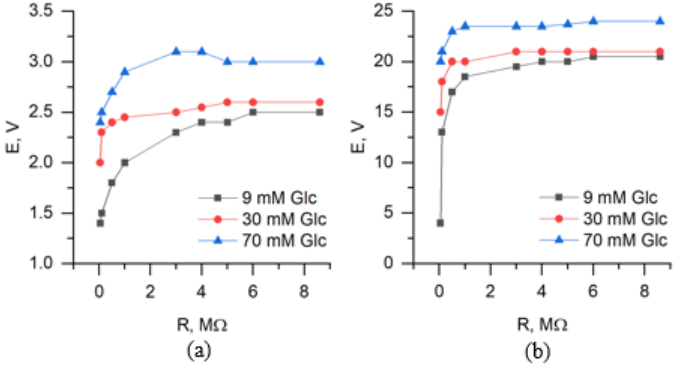

Fig. 3.34. Generated potential dependence on applied load, using (a) PQ- and (b) PQ/MW-CNT-modified graphite electrode as an anode (Bruzaite et al., 2020a)*

It was determined that MFC, in which PQ/MW-CNT modified electrode was applied, generated eight times higher potential at the load of 8.6 MΩ, and 70 mM glucose concentration: the potential, measured with PQ-modified electrode, was

*The reference is given in the list of publications by the author on the topic of the dissertation.

3 mV while using PQ/MW-CNT electrode, the 24-mV potential was observed (Fig. 3.34a).

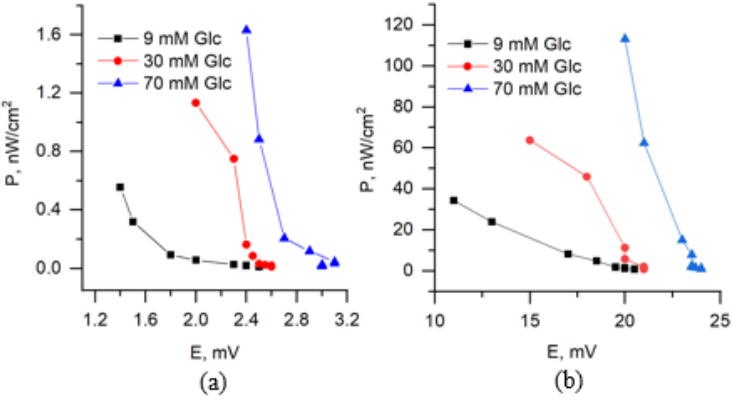

Fig. 3.35. Generated power dependence on potential, (a) PQ- and (b)PQ/MW-CNT-modified graphite electrode as an anode (Bruzaite et al., 2020a)*

At the same conditions, calculated maximal power for PQ/MW-CNT-electrode was 113 nW/cm2, while for PQ-electrode, maximal power was just 1.63 nW/cm2, i.e., for PQ/MW-CNT power was 69 times higher (Fig. 3.35). Therefore, it can be concluded that MW-CNTs have an excellent potential to be used in MFCs.

3.3. Conclusions of Chapter 3

The presented experimental research pursued the following objectives: 1) to create a simulation of an atomic force microscope and the investigation of the results from the model; 2) to explore electrochemical studies of a yeast-modified MFC with the application of PQ; 3) to investigate electrochemical studies of a yeast-modified MFC with the application of MD; 4) to explore the performance of the MFC with the application of MW-CNTs, and 5) to assess the yeast cell viability.

The following conclusions can be drawn based on the experimental study:

1. Experiments conducted at different scanning speeds, two different materials (silicon and PMMA), and two setpoint forces (10 nN and 20 nN) showed that the scanning speed has a more significant influence on picture resolution when the force is lower, and the material is of the lower

*The reference is given in the list of publications by the author on the topic of the dissertation.

Young's modulus. Also, the tip radius over 728 nm induces significant errors when vertical topography is evaluated.

2. The dependence of scanning speed on calculated errors has a nonlinear behaviour in accordance with experimental data: the highest error was found at a "hard" surface (silicon), using a higher radius tip of 1000 nm at the highest scanning speed of 200 μm/s.
3. The maximal calculated power of the designed baker's yeast-based MFC anode, which was modified by adsorbed PQ, was 22.2 mW/m^2, and this power output was registered at 56 mV. At the same time, the cell generated 178 mV open circuit potential in the presence of 7.8 mM glucose and 23 mM FCN.
4. The maximal calculated power of the designed baker's yeast-based MFC anode was 0.408 mW/m^2, and this power output was registered at 24 mV. Simultaneously, the cell generated a 62-mV open circuit potential in the presence of 23 mM FCN and the absence of glucose and immobilised MD.
5. The lowest investigated concentration (2 μg/mL) of MW-CNTs and at rather short-lasting exposure of MW-CNTs do not significantly affect the viability and other properties of yeast cells.
6. A plot of optical density vs incubation time dependencies shows some differences between low (0 and 2 μg/mL) and high (50 and 100 μg/mL) MW-CNTs concentrations as the steady-state conditions were observed faster for high MW-CNTs concentrations. Also, calculated relative growth and relative death rates show the difference between results registered after the incubation in low and high MW-CNTs concentrations containing solutions: both rates were two times higher for higher concentrations of MW-CNTs.
7. The results obtained from electrochemical measurements state that MW-CNTs are excellent candidates for the development of MFCs because the application of MW-CNTs in the anode increased generated power by 69 times with the result of 113 nW/cm^2 and generated voltage by eight times with the result of 24 mV.
8. Compared to *Saccharomyces cerevisiae* cells, the baker's yeast is more resistant to PQ at 30 °C. This research showed that baker's yeast cells compared to *Saccharomyces cerevisiae* cells are more resistant to MD exposure at a 30 °C temperature of cultivation.

General Conclusions

The present study aims to contribute to developing MFCs with the anode based on yeast, quinones and MW-CNTs. Based on the literature review and experimental data results, the following conclusions can be drawn:

1. The methodology for better visualization, viability and electrochemical properties of living cells, based on measurements of generated electric current density, cell stiffness and optical density, has been developed after selecting the optimal concentration of substances used and evaluating different cells' immobilization effects and cell viability. However, in the future, it is recommended to focus on studies of the influence created using the electroporation method to modify cells with the presented redox mediators and MW-CNTs.
2. A dynamic model of the atomic force microscope has been developed to select the input parameters for an individual experiment, taking into account the needle geometry and the sample's material. The adequacy of the model was assessed by comparing the results of the modelling and experimentation. The difference between the model and experimental results in scanning a sample shall not exceed 3% (at a scan rate of 100 μm/s and a needle pressure of 10 nN). In the future, the focus should be placed on simulating other AFM scanning modes, refining the model by introducing more degrees of freedom and parameters, monitoring cantilever

rotation displacement and automation the dynamic model itself using machine learning to accelerate model results.

3. According to the developed methodology, the influence of lipophilic redox mediators or (and) multi-walled carbon nanotubes on cell viability and electrical activity was found to have the highest current density in PQ (10,000 mA/m^2), and cell viability is equally affected by all materials (OD 0.81 ± 0.05). Therefore, in the future, it is possible to examine the possibilities of applying other materials that have shown the best results in further electrochemical research, using them according to the methodology presented in the dissertation and combination with the redox mediators presented in the thesis.
4. The study of the developed biofuel cell has shown that the power of the biofuel cell generated by applying different redox mediators can be increased more than 50 times. However, looking to the future, it is necessary to consider the amount of power that can be received while using minimally toxic substances. It is also possible to focus on electrodes' material replacement to improve the resulting power result and stable longevity.

Future investigations in this area should be related to developing a strategy of how MW-CNTs could be inserted within the yeast cell wall and membrane to apply such modified cells in the design of microbial fuel cells. Also, the development of the cathode is more suitable for *Saccharomyces cerevisiae*-based MFC with PQ, MD and MW-CNTs. The developed atomic force microscope model should also be more widely used to study yeast and other cells.

References

Andriukonis, E., Stirke, A., Garbaras, A., Mikoliunaite, L., Ramanaviciene, A., Remeikis, V. Thornton, B. & Ramanavicius, A. (2018). Yeast-assisted synthesis of polypyrrole: Quantification and influence on the mechanical properties of the cell wall. *Colloids and Surfaces B: Biointerfaces*, *164*, 224–231.

Apetrei, R. M., Carac, G., Bahrim, G., Ramanaviciene, A., & Ramanavicius, A. (2018). Modification of Aspergillus niger by conducting polymer, Polypyrrole, and the evaluation of electrochemical properties of modified cells. *Bioelectrochemistry*, *121*, 46–55. https://doi.org/10.1016/j.bioelechem.2018.01.001

Apetrei, R. M., Carac, G., Ramanaviciene, A., Bahrim, G., Tanase, C., & Ramanavicius, A. (2019). Cell-assisted synthesis of conducting polymer – polypyrrole – for the improvement of electric charge transfer through fungal cell wall. *Colloids and Surfaces B: Biointerfaces*, *175*(December 2018), 671–679. https://doi.org/10.1016/j.colsurfb.2018.12.024

Babanova, S., Hubenova, Y., & Mitov, M. (2011). Influence of artificial mediators on yeast-based fuel cell performance. *Journal of Bioscience and Bioengineering*. https://doi.org/10.1016/j.jbiosc.2011.06.008

Baronian, K. H. R. (2004). The use of yeast and moulds as sensing elements in biosensors. *Biosensors and Bioelectronics*, *19*(9), 953–962.

Binnig, G, Gerber, C., Stoll, E., Albrecht, T. R., & Quate, C. F. (1987). Atomic resolution with atomic force microscope. *EPL (Europhysics Letters)*, *3*(12), 1281.

Binnig, Gerd, Quate, C. F., & Gerber, C. (1986). Atomic force microscope. *Physical Review Letters*, *56*(9), 930.

Bolton, J. L., Trush, M. A., Penning, T. M., Dryhurst, G., & Monks, T. J. (2000, March). Role of quinones in toxicology. *Chemical Research in Toxicology*, Vol. 13, pp. 135–160. https://doi.org/10.1021/tx9902082

Brousse, T., Cougnon, C., & Bélanger, D. (2018, May). Grafting of quinones on carbons as active electrode materials in electrochemical capacitors. *Journal of the Brazilian Chemical Society*, Vol. 29, pp. 989–997. https://doi.org/10.21577/0103-5053.20180015

Brunmark, A., & Cadenas, E. (1989). Redox and addition chemistry of quinoid compounds and its biological implications. *Free Radical Biology & Medicine*, *7*(4), 435–477. https://doi.org/10.1016/0891-5849(89)90126-3

Bučinskas, V., Dzedzickis, A., Šešok, N., Šutinys, E., & Iljin, I. (2016). Research of modified mechanical sensor of atomic force microscope. In *Dynamical Systems: Theoretical and Experimental Analysis* (pp. 39–48). Springer.

Bučinskas, V., Dzedzickis, A., Šutinys, E., Šešok, N., & Iljin, I. (2016). Experimental research of improved sensor of atomic force microscope. *International Conference on Systems, Control and Information Technologies 2016*, 601–609. Springer.

Butt, H.-J., Cappella, B., & Kappl, M. (2005). Force measurements with the atomic force microscope: Technique, interpretation and applications. *Surface Science Reports*, *59*(1–6), 1–152.

Castro, F. A. V., Mariani, D., Panek, A. D., Eleutherio, E. C. A., & Pereira, M. D. (2008). Cytotoxicity Mechanism of Two Naphthoquinones (Menadione and Plumbagin) in Saccharomyces cerevisiae. *PLoS ONE*, *3*(12), e3999. https://doi.org/10.1371/journal.pone.0003999

Chandrasekhar, P. (2018). Electro-Optic and Optical Devices. In *Conducting Polymers, Fundamentals and Applications*. https://doi.org/10.1007/978-3-319-69378-1_41

Cheng, C., Müller, K. H., Koziol, K. K. K., Skepper, J. N., Midgley, P. A., Welland, M. E., & Porter, A. E. (2009). Toxicity and imaging of multi-walled carbon nanotubes in human macrophage cells. *Biomaterials*, *30*(25), 4152–4160. https://doi.org/10.1016/j.biomaterials.2009.04.019

Christwardana, M., Frattini, D., Accardo, G., Yoon, S. P., & Kwon, Y. (2018a). Effects of methylene blue and methyl red mediators on performance of yeast based microbial fuel cells adopting polyethylenimine coated carbon felt as anode. *Journal of Power Sources*, *396*(June), 1–11. https://doi.org/10.1016/j.jpowsour.2018.06.005

Christwardana, M., Frattini, D., Accardo, G., Yoon, S. P., & Kwon, Y. (2018b). Optimization of glucose concentration and glucose/yeast ratio in yeast microbial fuel cell using response surface methodology approach. *Journal of Power Sources*, *402*, 402–412.

Dai, G., Wolff, H., Pohlenz, F., Danzebrink, H.-U., & Wilkening, G. (2006). Atomic force probe for sidewall scanning of nano-and microstructures. *Applied Physics Letters*, *88*(17), 171908.

Davis, F., & Higson, S. P. J. (2007). Biofuel cells-Recent advances and applications. *Biosensors and Bioelectronics*. https://doi.org/10.1016/j.bios.2006.04.029

Dzedzickis, A., Bucinskas, V., Viržonis, D., Sesok, N., Ulcinas, A., Iljin, I., … Morkvenaite-Vilkonciene, I. (2018). Modification of the AFM sensor by a precisely regulated air stream to increase imaging speed and accuracy in the contact mode. *Sensors*, *18*(8), 2694.

Francis, A. P., & Devasena, T. (2018, March). Toxicity of carbon nanotubes: A review. *Toxicology and Industrial Health*, Vol. 34, pp. 200–210. https://doi.org/10.1177/0748233717747472

Frederix, P. L. T. M., Bosshart, P. D., & Engel, A. (2009). Atomic force microscopy of biological membranes. *Biophysical Journal*, *96*(2), 329–338.

Genys, P., Aksun, E., Tereshchenko, A., Valiūnienė, A., Ramanaviciene, A., & Ramanavicius, A. (2019). Electrochemical deposition and investigation of poly-9,10-phenanthrenequinone layer. *Nanomaterials*, *9*(5). https://doi.org/10.3390/nano9050702

German, N., Ramanavicius, A., Voronovic, J., & Ramanaviciene, A. (2012). Glucose biosensor based on glucose oxidase and gold nanoparticles of different sizes covered by polypyrrole layer. *Colloids and Surfaces A: Physicochemical and Engineering Aspects*, *413*, 224–230. https://doi.org/10.1016/j.colsurfa.2012.02.012

Ghafari, P., St-Denis, C. H., Power, M. E., Jin, X., Tsou, V., Mandal, H. S., … Tang, X. (2008). Impact of carbon nanotubes on the ingestion and digestion of bacteria by ciliated protozoa. *Nature Nanotechnology*, *3*(6), 347–351. https://doi.org/10.1038/nnano.2008.109

Gunawardena, A., Fernando, S., & To, F. (2008). Performance of a yeast-mediated biological fuel cell. *International Journal of Molecular Sciences*, *9*(10), 1893–1907. https://doi.org/10.3390/ijms9101893

Handy, R. D., Von Der Kammer, F., Lead, J. R., Hassellöv, M., Owen, R., & Crane, M. (2008, May). The ecotoxicology and chemistry of manufactured nanoparticles. *Ecotoxicology*, Vol. 17, pp. 287–314. https://doi.org/10.1007/s10646-008-0199-8

Hao Yu, E., & Scott, K. (2010). Enzymatic Biofuel Cells—Fabrication of Enzyme Electrodes. *Energies*, *3*(1), 23–42. https://doi.org/10.3390/en3010023

Hossain, M. S., Tryk, D., & Yeager, E. (1989). The electrochemistry of graphite and modified graphite surfaces: the reduction of O2. *Electrochimica Acta*, *34*(12), 1733–1737. https://doi.org/10.1016/0013-4686(89)85057-1

Howald, L. E. (2003, February 25). *Multiaxis actuator and measuring head, especially for a scanning probe microscope*. Google Patents.

Hubenova, Y. V, Rashkov, R. S., Buchvarov, V. D., Arnaudova, M. H., Babanova, S. M., & Mitov, M. Y. (2010). Improvement of yeast− biofuel cell output by electrode modifications. *Industrial & Engineering Chemistry Research*, *50*(2), 557–564.

Hubenova, Y., & Mitov, M. (2015). Extracellular electron transfer in yeast-based biofuel cells: A review. *Bioelectrochemistry*, *106*, 177–185. https://doi.org/10.1016/j.bioelechem.2015.04.001

Hurley, D. C. (2010). Measuring mechanical properties on the nanoscale with contact resonance force microscopy methods. In *Scanning Probe Microscopy of Functional Materials* (pp. 95–124). Springer.

Hutter, J. L., & Bechhoefer, J. (1993). Calibration of atomic-force microscope tips. *Review of Scientific Instruments*, *64*(7), 1868–1873.

Ishioka, T., Uchida, T., & Teramae, N. (2001). Analysis of the redox reaction of 9,10-phenanthrenequinone on a gold electrode surface by cyclic voltammetry and time-resolved Fourier transform surface-enhanced Raman scattering spectroscopy. *Analytica Chimica Acta*, *449*(1–2), 253–260. https://doi.org/10.1016/S0003-2670(01)01352-6

Janickis, V., Petrašauskienė, N., Žalenkienė, S., Morkvėnaitė-Vilkončienė, I., & Ramanavičcius, A. (2018). Morphology of CdSe-based coatings formed on polyamide substrate. *Journal of Nanoscience and Nanotechnology*, *18*(1), 604–613.

Jehel, P., Léger, P., & Ibrahimbegovic, A. (2014). Initial versus tangent stiffness-based Rayleigh damping in inelastic time history seismic analyses. *Earthquake Engineering & Structural Dynamics*, *43*(3), 467–484.

Jiang, H., Yang, L., Deng, W., Tan, Y., & Xie, Q. (2017). Macroporous graphitic carbon foam decorated with polydopamine as a high-performance anode for microbial fuel cell. *Journal of Power Sources*, *363*, 27–33. https://doi.org/10.1016/j.jpowsour.2017.07.064

Jones, D. M., Smith, J. R., Huck, W. T. S., & Alexander, C. (2002). Variable adhesion of micropatterned thermoresponsive polymer brushes: AFM investigations of poly (N-isopropylacrylamide) brushes prepared by surface-initiated polymerizations. *Advanced Materials*, *14*(16), 1130–1134.

Juška, A. (2011). Minimal models of growth and decline of microbial populations. *Journal of Theoretical Biology*, *269*(1), 195–200. https://doi.org/10.1016/j.jtbi.2010.10.030

Khedmati, M., Kim, Y.-R., Turner, J. A., Alanazi, H., & Nguyen, C. (2018). An integrated microstructural-nanomechanical-chemical approach to examine material-specific characteristics of cementitious interphase regions. *Materials Characterization*, *138*, 154–164.

Kisieliute, A., Popov, A., Apetrei, R.-M., Cârâc, G., Morkvenaite-Vilkonciene, I., Ramanaviciene, A., & Ramanavicius, A. (2019). Towards microbial biofuel cells: Improvement of charge transfer by self-modification of microoganisms with conducting polymer – Polypyrrole. *Chemical Engineering Journal*, *356*, 1014–1021. https://doi.org/10.1016/J.CEJ.2018.09.026

Kisin, E. R., Murray, A. R., Keane, M. J., Shi, X. C., Schwegler-Berry, D., Gorelik, O., … Shvedova, A. A. (2007). Single-walled carbon nanotubes: Geno- and cytotoxic effects in lung fibroblast V79 cells. *Journal of Toxicology and Environmental Health - Part A: Current Issues*, *70*(24), 2071–2079. https://doi.org/10.1080/15287390701601251

Kocun, M., Labuda, A., Gannepalli, A., & Proksch, R. (2015). Contact resonance atomic force microscopy imaging in air and water using photothermal excitation. *Review of Scientific Instruments*, *86*(8), 83706.

Krikstolaityte, V., Oztekin, Y., Kuliesius, J., Ramanaviciene, A., Yazicigil, Z., Ersoz, M., Ramanavicius, A. (2013). Biofuel cell based on anode and cathode modified by glucose oxidase. *Electroanalysis*, *25*(12), 2677–2683. https://doi.org/10.1002/elan.201300482

Kumagai, Y., Koide, S., Taguchi, K., Endo, A., Nakai, Y., Yoshikawa, T., & Shimojo, N. (2002). Oxidation of proximal protein sulfhydryls by phenanthraquinone, a component of diesel exhaust particles. *Chemical Research in Toxicology*, *15*(4), 483–489. https://doi.org/10.1021/tx0100993

Lai, C.-Y., Perri, S., Santos, S., Garcia, R., & Chiesa, M. (2016). Rapid quantitative chemical mapping of surfaces with sub-2 nm resolution. *Nanoscale*, *8*(18), 9688–9694.

Le Comte, A., Chhin, D., Gagnon, A., Retoux, R., Brousse, T., & Bélanger, D. (2015). Spontaneous grafting of 9,10-phenanthrenequinone on porous carbon as an active electrode material in an electrochemical capacitor in an alkaline electrolyte. *Journal of Materials Chemistry A*, *3*(11), 6146–6156. https://doi.org/10.1039/c4ta05536e

Liao, Z. H., Sun, J. Z., Sun, D. Z., Si, R. W., & Yong, Y. C. (2015). Enhancement of power production with tartaric acid doped polyaniline nanowire network modified anode in microbial fuel cells. *Bioresource Technology*, *192*, 831–834. https://doi.org/10.1016/j.biortech.2015.05.105

Lip, K. Y. F., García-Ríos, E., Costa, C. E., Guillamón, J. M., Domingues, L., Teixeira, J., & van Gulik, W. M. (2020). Selection and subsequent physiological characterization of industrial Saccharomyces cerevisiae strains during continuous growth at sub- and-supra optimal temperatures. *Biotechnology Reports*, *26*. https://doi.org/10.1016/j.btre.2020.e00462

Liu, J., Notbohm, J. K., Carpick, R. W., & Turner, K. T. (2010). Method for characterizing nanoscale wear of atomic force microscope tips. *ACS Nano*, *4*(7), 3763–3772.

Liu, Xiang, Zhao, X., Yu, Y. Y., Wang, Y. Z., Shi, Y. T., Cheng, Q. W., … Yong, Y. C. (2017). Facile fabrication of conductive polyaniline nanoflower modified electrode and its application for microbial energy harvesting. *Electrochimica Acta*, *255*, 41–47. https://doi.org/10.1016/j.electacta.2017.09.153

Liu, Xing, Wu, W., & Gu, Z. (2015). Poly (3,4-ethylenedioxythiophene) promotes direct electron transfer at the interface between Shewanella loihica and the anode in a microbial fuel cell. *Journal of Power Sources*, *277*, 110–115. https://doi.org/10.1016/j.jpowsour.2014.11.129

Liu, Y., Zhang, J., Cheng, Y., & Jiang, S. P. (2018). *Effect of Carbon Nanotubes on Direct Electron Transfer and Electrocatalytic Activity of Immobilized Glucose Oxidase*. https://doi.org/10.1021/acsomega.7b01633

Lushchak, O. V., Bayliak, M. M., Korobova, O. V., Levine, R. L., & Lushchak, V. I. (2009). Buffer modulation of menadione-induced oxidative stress in Saccharomyces

cerevisiae. *Redox Report*, *14*(5), 214–220. https://doi.org/10.1179/135100009X12525712409454

Marinello, F., Schiavuta, P., Carmignato, S., & Savio, E. (2010). Critical factors in quantitative atomic force acoustic microscopy. *CIRP Journal of Manufacturing Science and Technology*, *3*(1), 49–54.

Markiewicz, P., & Goh, M. C. (1995). Atomic force microscope tip deconvolution using calibration arrays. *Review of Scientific Instruments*, *66*(5), 3186–3190.

Mehdinia, A., Ziaei, E., & Jabbari, A. (2014). Facile microwave-assisted synthesized reduced graphene oxide / tin oxide nanocomposite and using as anode material of microbial fuel cell to improve power generation. *International Journal of Hydrogen Energy*, *39*(20), 10724–10730. https://doi.org/10.1016/j.ijhydene.2014.05.008

Min, B., Cheng, S., & Logan, B. E. (2005). Electricity generation using membrane and salt bridge microbial fuel cells. *Water Research*, *39*(9), 1675–1686.

Mohanta, D., Patnaik, S., Sood, S., & Das, N. (2019, October). Carbon nanotubes: Evaluation of toxicity at biointerfaces. *Journal of Pharmaceutical Analysis*, Vol. 9, pp. 293–300. https://doi.org/10.1016/j.jpha.2019.04.003

Monks, T. J., & Lau, S. S. (1992). Toxicology of quinone-thioethers. *Critical Reviews in Toxicology*, *22*(5–6), 243–270. https://doi.org/10.3109/10408449209146309

Morkvenaite-Vilkonciene, I., Ramanaviciene, A., & Ramanavicius, A. (2016). 9,10-Phenanthrenequinone as a redox mediator for the imaging of yeast cells by scanning electrochemical microscopy. *Sensors and Actuators, B: Chemical*, *228*. https://doi.org/10.1016/j.snb.2015.12.102

Morkvenaite-Vilkončiene, I., Ramanavičiene, A., & Ramanavičius, A. (2013). Atomic force microscopy as a tool for the investigation of living cells. *Medicina (Lithuania)*, *49*(4), 155–164.

Morkvenaite-Vilkonciene, Inga, Ramanaviciene, A., & Ramanavicius, A. (2016). 9,10-Phenanthrenequinone as a redox mediator for the imaging of yeast cells by scanning electrochemical microscopy. *Sensors and Actuators, B: Chemical*, *228*, 200–206. https://doi.org/10.1016/j.snb.2015.12.102

Nievergelt, A. P., Andany, S. H., Adams, J. D., Hannebelle, M. T., & Fantner, G. E. (2017). Components for high-speed atomic force microscopy optimized for low phase-lag. *IEEE/ASME International Conference on Advanced Intelligent Mechatronics, AIM*, 731–736. https://doi.org/10.1109/AIM.2017.8014104

O'Brien, P. J. (1991). Molecular mechanisms of quinone cytotoxicity. *Chemico-Biological Interactions*, Vol. 80, pp. 1–41. https://doi.org/10.1016/0009-2797(91)90029-7

Oztekin, Y., Ramanaviciene, A., Yazicigil, Z., Solak, A. O., & Ramanavicius, A. (2011). Direct electron transfer from glucose oxidase immobilized on polyphenanthroline-modified glassy carbon electrode. *Biosensors & Bioelectronics*, *26*(5), 2541–2546. https://doi.org/DOI 10.1016/j.bios.2010.11.001

Pandey, P., Shinde, V. N., Deopurkar, R. L., Kale, S. P., Patil, S. A., & Pant, D. (2016, April). Recent advances in the use of different substrates in microbial fuel cells toward wastewater treatment and simultaneous energy recovery. *Applied Energy*, Vol. 168, pp. 706–723. https://doi.org/10.1016/j.apenergy.2016.01.056

Petroniene, J., Morkvenaite-Vilkonciene, I., Miksiunas, R., Bironaite, D., Ramanaviciene, A., Rucinskas, K., … Ramanavicius, A. (2020). Scanning electrochemical microscopy for the investigation of redox potential of human myocardium-derived mesenchymal stem cells grown at 2D and 3D conditions. *Electrochimica Acta*, *360*. https://doi.org/10.1016/j.electacta.2020.136956

Petroniene, J., Morkvenaite-Vilkonciene, I., Miksiunas, R., Bironaite, D., Ramanaviciene, A., Mikoliunaite, L., … Ramanavicius, A. (2020). Evaluation of redox activity of human myocardium-derived mesenchymal stem cells by scanning electrochemical microscopy. *Electroanalysis*, elan.201900723. https://doi.org/10.1002/elan.201900723

Potekin, R., Dharmasena, S., McFarland, D. M., Bergman, L. A., Vakakis, A. F., & Cho, H. (2017). Cantilever dynamics in higher-harmonic atomic force microscopy for enhanced material characterization. *International Journal of Solids and Structures*, *110*, 332–339.

Qiao, Y., Bao, S.-J., Ming Li, C., Cui, X.-Q., Lu, Z.-S., & Guo, J. (2008). *Nanostructured Polyaniline/Titanium Dioxide Composite Anode for Microbial Fuel Cells*. https://doi.org/10.1021/nn700102s

Qiao, Y., Li, C. M., Bao, S. J., & Bao, Q. L. (2007). Carbon nanotube/polyaniline composite as anode material for microbial fuel cells. *Journal of Power Sources*. https://doi.org/10.1016/j.jpowsour.2007.03.048

Qiao, Y., Li, M., Bao, S., & Hong, Y. (2008). *Direct electrochemistry and electrocatalytic mechanism of evolved Escherichia coli cells in microbial fuel cells w*. (11), 1290–1292. https://doi.org/10.1039/b719955d

Quan, X., Sun, B., & Xu, H. (2015). Anode decoration with biogenic Pd nanoparticles improved power generation in microbial fuel cells. *Electrochimica Acta*, *182*, 815–820.

Raghavulu, S. V., Goud, R. K., Sarma, P. N., & Mohan, S. V. (2011). Saccharomyces cerevisiae as anodic biocatalyst for power generation in biofuel cell: Influence of redox condition and substrate load. *Bioresource Technology*, *102*(3), 2751–2757. https://doi.org/10.1016/j.biortech.2010.11.048

Rahimnejad, M., Adhami, A., Darvari, S., Zirepour, A., & Oh, S. E. (2015a). Microbial fuel cell as new technol ogy for bioelectricity generation: A review. *Alexandria Engineering Journal*, *54*(3), 745–756. https://doi.org/10.1016/j.aej.2015.03.031

Rahimnejad, M., Adhami, A., Darvari, S., Zirepour, A., & Oh, S. E. (2015b). Microbial fuel cell as new technology for bioelectricity generation: A review. *Alexandria Engineering Journal*, *54*(3), 745–756. https://doi.org/10.1016/j.aej.2015.03.031

Rahimnejad, M., Ghoreyshi, A. A., Najafpour, G., & Jafary, T. (2011). Power generation from organic substrate in batch and continuous flow microbial fuel cell operations. *Applied Energy*. https://doi.org/10.1016/j.apenergy.2011.04.017

Ramanavicius, A., Morkvenaite-Vilkonciene, I., Kisieliute, A., Petroniene, J., & Ramanaviciene, A. (2017). Scanning electrochemical microscopy based evaluation of influence of pH on bioelectrochemical activity of yeast cells − Saccharomyces cerevisiae. *Colloids and Surfaces B: Biointerfaces*, *149*, 1–6. https://doi.org/10.1016/j.colsurfb.2016.09.039

Ramanavicius, A, & Ramanaviciene, A. (2009). Hemoproteins in Design of Biofuel Cells. *Fuel Cells*, *9*(1), 25–36. https://doi.org/10.1002/fuce.200800052

Ramanavicius, Arunas, Andriukonis, E., Stirke, A., Mikoliunaite, L., Balevicius, Z., & Ramanaviciene, A. (2016). Synthesis of polypyrrole within the cell wall of yeast by redox-cycling of [Fe(CN)6]3−/[Fe(CN)6]4−. *Enzyme and Microbial Technology*, *83*, 40–47. https://doi.org/10.1016/j.enzmictec.2015.11.009

Ramanavicius, Arunas, Kausaite-Minkstimiene, A., Morkvenaite-Vilkonciene, I., Genys, P., Mikhailova, R., Semashko, T., … Ramanaviciene, A. (2015). Biofuel cell based on glucose oxidase from Penicillium funiculosum 46.1 and horseradish peroxidase. *Chemical Engineering Journal*, *264*, 165–173. https://doi.org/10.1016/j.cej.2014.11.011

Ramanavicius, Arunas, Kausaite, A., & Ramanaviciene, A. (2005). Biofuel cell based on direct bioelectrocatalysis. *Biosensors and Bioelectronics*, *20*(10 SPEC. ISS.), 1962–1967. https://doi.org/10.1016/j.bios.2004.08.032

Ramanavicius, Arunas, Kausaite, A., & Ramanaviciene, A. (2008). Enzymatic biofuel cell based on anode and cathode powered by ethanol. *Biosensors and Bioelectronics*, *24*(4), 761–766. https://doi.org/10.1016/j.bios.2008.06.048

Rodriguez, C. E., Shinyashiki, M., Froines, J., Yu, R. C., Fukuto, J. M., & Cho, A. K. (2004). An examination of quinone toxicity using the yeast Saccharomyces cerevisiae model system. *Toxicology*. https://doi.org/10.1016/j.tox.2004.04.016

Rodriguez, C. E., Sobol, Z., & Schiestl, R. H. (2008). 9, 10-Phenanthrenequinone induces DNA deletions and forward mutations via oxidative mechanisms in the yeast Saccharomyces cerevisiae. *Toxicology in Vitro*, *22*(2), 296–300.

Rossi, R., Cavina, M., & Setti, L. (2016). Characterization of electron transfer mechanism in mediated microbial fuel cell by entrapped electron mediator in saccharomyces cerevisiae. *Chemical Engineering Transactions*, *49*, 559–564.

Ruzgas, T., Larpant, N., Shafaat, A., & Sotres, J. (2019). *Wireless, Battery-Less Biosensors Based on Direct Electron Transfer Reactions*. https://doi.org/10.1002/celc.201901015

Safarova, K., Drovak, A., & Kubinek, R. (2007). Usage of AFM, SEM and TEM for the research of carbon nanotubes. *Modern Research and Educational Topics in Microscopy*, 513–519.

Saleh, T. A., Gondal, M. A., Drmosh, Q. A., Yamani, Z. H., & AL-yamani, A. (2011). Enhancement in photocatalytic activity for acetaldehyde removal by embedding ZnO nano particles on multiwall carbon nanotubes. *Chemical Engineering Journal*, *166*(1), 407–412. https://doi.org/10.1016/j.cej.2010.10.070

Salvadó, Z., Arroyo-López, F. N., Guillamón, J. M., Salazar, G., Querol, A., & Barrio, E. (2011). Temperature adaptation markedly determines evolution within the genus Saccharomyces. *Applied and Environmental Microbiology*, *77*(7), 2292–2302.

Santos, S., Barcons, V., Christenson, H. K., Font, J., & Thomson, N. H. (2011). *The Intrinsic Resolution Limit in the Atomic Force Microscope: Implications for Heights*.

Schaetzle, O., Barrière, F., & Baronian, K. (2008). Bacteria and yeasts as catalysts in microbial fuel cells: electron transfer from micro-organisms to electrodes for green electricity. *Energy & Environmental Science*, *1*(6), 607–620.

Schillers, H., Rianna, C., Schäpe, J., Luque, T., Doschke, H., Wälte, M., … Bobrowska, J. (2017). Standardized nanomechanical atomic force microscopy procedure (SNAP) for measuring soft and biological samples. *Scientific Reports*, *7*(1), 1–9.

Scott, K., Rimbu, G. A., Katuri, K. P., Prasad, K. K., & Head, I. M. (2007). Application of modified carbon anodes in microbial fuel cells. *Process Safety and Environmental Protection*. https://doi.org/10.1205/psep07018

Sedin, D. L., & Rowlen, K. L. (2001). Influence of tip size on AFM roughness measurements. *Applied Surface Science*, *182*(1–2), 40–48.

Sekrecka-Belniak, A., & Toczyłowska-Mamińska, R. (2018). Fungi-based microbial fuel cells. *Energies*, *11*(10), 2827.

Shaik, N. H., Reifenberger, R. G., & Raman, A. (2016). Enhancing the optical lever sensitivity of microcantilevers for dynamic atomic force microscopy via integrated low frequency paddles. *Nanotechnology*, *27*(19), 195502.

Sharma, Y., & Li, B. (2010). The variation of power generation with organic substrates in single-chamber microbial fuel cells (SCMFCs). *Bioresource Technology*. https://doi.org/10.1016/j.biortech.2009.10.040

Sitti, M., & Hashimoto, H. (2000). Controlled pushing of nanoparticles: modeling and experiments. *IEEE/ASME Transactions on Mechatronics*, *5*(2), 199–211.

Slate, A. J., Whitehead, K. A., Brownson, D. A. C., & Banks, C. E. (2019, March). Microbial fuel cells: An overview of current technology. *Renewable and Sustainable Energy Reviews*, Vol. 101, pp. 60–81. https://doi.org/10.1016/j.rser.2018.09.044

Stan, G., King, S. W., & Cook, R. F. (2012). Nanoscale mapping of contact stiffness and damping by contact resonance atomic force microscopy. *Nanotechnology*, *23*(21), 215703.

Stirke, A., Apetrei, R. M., Kirsnyte, M., Dedelaite, L., Bondarenka, V., Jasulaitiene, V., … Ramanavicius, A. (2016). Synthesis of polypyrrole microspheres by Streptomyces spp. *Polymer*, *84*, 99–106. https://doi.org/10.1016/j.polymer.2015.12.029

Sumisha, A., & Haribabu, K. (2018). Modification of graphite felt using nano polypyrrole and polythiophene for microbial fuel cell applications-a comparative study. *International Journal of Hydrogen Energy*, *43*(6), 3308–3316. https://doi.org/10.1016/j.ijhydene.2017.12.175

Sun, D. Z., Yu, Y. Y., Xie, R. R., Zhang, C. L., Yang, Y., Zhai, D. D., … Yong, Y. C. (2017). In-situ growth of graphene/polyaniline for synergistic improvement of extracellular electron transfer in bioelectrochemical systems. *Biosensors and Bioelectronics*, *87*, 195–202. https://doi.org/10.1016/j.bios.2016.08.037

Taatjes, D. J., Quinn, A. S., Lewis, M. R., & Bovill, E. G. (1999). Quality assessment of atomic force microscopy probes by scanning electron microscopy: correlation of tip structure with rendered images. *Microscopy Research and Technique*, *44*(5), 312–326.

The OD600 Basics | Best OD600 Tool To Generate Microbial Growth Curves. (n.d.). Retrieved March 11, 2022, from https://www.implen.de/od600-diluphotometer/od600/

Tranchida, D., Piccarolo, S., & Deblieck, R. A. C. (2006). Some experimental issues of AFM tip blind estimation: the effect of noise and resolution. *Measurement Science and Technology*, *17*(10), 2630.

Wade, L. A., Shapiro, I. R., Ma, Z., Quake, S. R., & Collier, C. P. (2004). Correlating AFM probe morphology to image resolution for single-wall carbon nanotube tips. *Nano Letters*, *4*(4), 725–731.

Walker, A. L., & Walker Jr, C. W. (2006). Biological fuel cell and an application as a reserve power source. *Journal of Power Sources*, *160*(1), 123–129.

Wang, Q. Q., Wu, X. Y., Yu, Y. Y., Sun, D. Z., Jia, H. H., & Yong, Y. C. (2017). Facile in-situ fabrication of graphene/riboflavin electrode for microbial fuel cells. *Electrochimica Acta*, *232*, 439–444. https://doi.org/10.1016/j.electacta.2017.03.008

Wang, Y., Li, B., Zeng, L., Cui, D., Xiang, X., & Li, W. (2013). Polyaniline / mesoporous tungsten trioxide composite as anode electrocatalyst for high-performance microbial fuel cells. *Biosensors and Bioelectronic*, *41*, 582–588. https://doi.org/10.1016/j.bios.2012.09.054

Yablon, D. G., Gannepalli, A., Proksch, R., Killgore, J., Hurley, D. C., Grabowski, J., & Tsou, A. H. (2012). Quantitative viscoelastic mapping of polyolefin blends with contact resonance atomic force microscopy. *Macromolecules*, *45*(10), 4363–4370.

Yamashoji, S. (2016). Different characteristics between menadione and menadione sodium bisulfite as redox mediator in yeast cell suspension. *Biochemistry and Biophysics Reports*. https://doi.org/10.1016/j.bbrep.2016.03.007

Yang, C.-W., Hwang, S., Chen, Y. F., Chang, C. S., & Tsai, D. P. (2007). Imaging of soft matter with tapping-mode atomic force microscopy and non-contact-mode atomic force microscopy. *Nanotechnology*, *18*(8), 84009.

Yang, X., Ma, X., Wang, K., Wu, D., Lei, Z., & Feng, C. (2016). Eighteen-month assessment of 3D graphene oxide aerogel-modified 3D graphite fiber brush electrode as a high-performance microbial fuel cell anode. *Electrochimica Acta*, *210*, 846–853. https://doi.org/10.1016/j.electacta.2016.05.215

Yuan, X., Zhang, X., Sun, L., Wei, Y., & Wei, X. (2019, April). Cellular Toxicity and Immunological Effects of Carbon-based Nanomaterials. *Particle and Fibre Toxicology*, Vol. 16. https://doi.org/10.1186/s12989-019-0299-z

Zamaleeva, A. I., Sharipova, I. R., Porfireva, A. V., Evtugyn, G. A., & Fakhrullin, R. F. (2010). Polyelectrolyte-Mediated Assembly of Multiwalled Carbon Nanotubes on Living Yeast Cells. *Langmuir*, *26*(4), 2671–2679. https://doi.org/Doi 10.1021/La902937s

Zhao, J., Zhang, N., Prestwich, G. D., & Wen, X. (2008). Recruitment of endogenous stem cells for tissue repair. *Macromolecular Bioscience*, *8*(9), 836–842.

Zhou, S., Lin, M., Zhuang, Z., Liu, P., & Chen, Z. (2019). Biosynthetic graphene enhanced extracellular electron transfer for high performance anode in microbial fuel cell. *Chemosphere*, *232*, 396–402. https://doi.org/10.1016/j.chemosphere.2019.05.191

Zhu, S., Zhu, B., Huang, A., Hu, Y., Wang, G., & Ling, F. (2016). Toxicological effects of multi-walled carbon nanotubes on Saccharomyces cerevisiae: The uptake kinetics and mechanisms and the toxic responses. *Journal of Hazardous Materials*, *318*, 650–662. https://doi.org/10.1016/j.jhazmat.2016.07.049

Zhu, Z. Z., Wang, Z., & Li, H. L. (2008). Functional multi-walled carbon nanotube/polyaniline composite films as supports of platinum for formic acid electrooxidation. *Applied Surface Science*, *254*(10), 2934–2940. https://doi.org/10.1016/j.apsusc.2007.10.033

Zou, L., Lu, Z., Huang, Y., Long, Z. er, & Qiao, Y. (2017). Nanoporous Mo2C functionalized 3D carbon architecture anode for boosting flavins mediated interfacial bioelectrocatalysis in microbial fuel cells. *Journal of Power Sources*, *359*, 549–555. https://doi.org/10.1016/j.jpowsour.2017.05.101

List of Scientific Publications by the Author on the Topic of the Dissertation

Papers in the Reviewed Scientific Journals

Rožėnė, J.; Morkvėnaitė-Vilkončienė, I.; Bružaitė, I.; Zinovičius, A.; Ramanavičius, A. Baker's yeast-based microbial fuel cell mediated by 2-methyl-1,4-naphthoquinone // *Membranes: Special issue: Membranes for electrochemical devices*. Basel: MDPI. ISSN 2077-0375. 2021, vol. 11, iss. 3, art. no. 182, p. 1–10.

https://doi.org/10.3390/membranes11030182.

Rožėnė, J.; Morkvėnaitė-Vilkončienė, I.; Bružaitė, I.; Dzedzickis, A.; Ramanavičius, A. Yeast-based microbial biofuel cell mediated by 9,10-phenantrenequinone // *Electrochimica acta*. Oxford: Pergamon-Elsevier Science Ltd. ISSN 0013-4686. eISSN 1873-3859. 2021, vol. 373, art. no. 137918, p. 1–10.

https://doi.org/10.1016/j.electacta.2021.137918.

Bružaitė, I.; Rožėnė, J.; Morkvėnaitė-Vilkončienė, I.; Ramanavičius, A. Towards microorganism-based biofuel cells: the viability of Saccharomyces cerevisiae modified by multiwalled carbon nanotubes // *Nanomaterials*. Basel: MDPI. ISSN 2079-4991. eISSN 2079-4991. 2020, vol. 10, iss. 5, art. no. 954, p. [1–14]. https://doi.org/10.3390/nano10050954.

Morkvėnaitė-Vilkončienė, I.; Viržonis, D.; Dzedzickis, A.; Bučinskas, V.; Rožėnė, J.; Vilkončius, R.; Vaičiulis, D.; Ramanavičienė, A.; Ramanavičius, A. The improvement of the accuracy of electromagnetic actuator based atomic force microscope operating in contact mode and the development of a new methodology for the estimation of control parameters and the achievement of superior image quality // *Sensors and actuators A: Physical*. Amsterdam: Elsevier. ISSN 0924-4247. 2019, Vol. 287, p. 168–176. https://doi.org/10.1016/j.sna.2019.01.015.

Rožėnė, J.; Blaževič, K.; Zinovičius, A.; Šataitė, V.-G.; Morkvėnaitė-Vilkončienė, I. Quinones-mediated microbial biofuel cell based on Baker's yeast //*Automation 2021. Recent achievements in automation, robotics and measurement techniques*, 23-24 September 2021, Warsaw, Poland: conference proceedings. Cham: Springer, 2021. ISBN 9783030748920.eISBN 9783030748937. p. 431–441. (Advances in intelligent systems and computing, ISSN2194-5357, eISSN 2194-5365; vol. 1390).

https://doi.org/10.1007/978-3-031-03502-9_21.

Rožėnė, J.; Zinovičius, A.; Kačinskaitė, B.; Bučinskas, V.; Ramanavičius, A.; Morkvėnaitė-Vilkončienė, I. Microbial fuel cell-based toxicity sensor // *Automation 2020: Towards industry of the future*. Cham: Springer, 2020. ISBN 9783030409708. eISBN 9783030409715. p. 379–388. https://doi.org/10.1007/978-3-030-40971-5_35.

Morkvėnaitė-Vilkončienė, I.; Vilkončius, R.; Rožėnė, J.; Zinovičius, A.; Balitskyi, O.; Ramanavičienė, .; Ramanavičius, A.; Dzedzickis, A.; Bučinskas, V. Method for living cell mechanical properties evaluation from force-indentation curves // *Automation 2019. Progress in automation, robotics and measurement techniques*, 27–29 March 2019, Warsaw, Poland: conference proceedings. Cham: Springer, 2020. ISBN 9783030132729. eISBN 9783030132736. p. 657-663. https://doi.org/10.1007/978-3-030-13273-6-61.

Summary in Lithuanian

Įvadas

Problemos formulavimas

Pastaraisiais metais sparčiai augant energijos išteklių poreikiui ir stebint aplinkos užterštumo problemą atsigręžiama į alternatyviuosius energijos šaltinius. Vienas iš jų, pastarąjį pusšimtį metų aktyviai nagrinėjamas mokslininkų, – biokuro elementai, kuriuose naudojami mikroorganizmai cheminių redukcijos ir oksidacijos reakcijų metu dalyvauja bioenergijos gavybos procese. Tačiau tik visai neseniai biokuro elementai pradėti vertinti kaip alternatyvusis energijos šaltinis, ypač sprendžiant nuotekų valymo energijos sunaudojimo problemą. Maisto ir gėrimų pramonėje nuotekoms valyti pasitelkiami biokuro elementai, kurių sugeneruojama galia išaugo nuo 50 iki 2000 $\mu W/cm^2$.

Pagrindiniu ir daug lemiančiu aspektu naudojant biokuro elementą tampa elektrodų savybės. Jiems turi būti parenkama medžiaga, kurios aukštas biologinis suderinamumas. Pasirinkus elektrodus taip pat būtina pasirinkti katalizatorių: tai gali būti fermentai, bakterijos ar mikroorganizmai.

Biokuro elementuose naudojant elektronų pernašos tarpininkus svarbu atsižvelgti į jų savybes: elektrocheminis aktyvumas; netoksiškumas mikroorganizmams; lengvas prasiskverbimas pro ląstelės membraną; tinkamas redokso potencialas tarpininkaujamam elektronų perdavimui; tirpus ir chemiškai stabilus anolite; greita oksidacijos proceso kinetika ties elektrodo paviršiumi. Taip pat siekiant užtikrinti tinkamą elektronų pernašą iš ląstelių į elektrodą, dažniausiai taikoma dviejų mediatorių sistema.

Taigi pagrindinė problema, kurią vis dar stengiamasi išspręsti, tai sudėtingas reikiamų medžiagų ir jų taikymo būdo parinkimas siekiant pagerinti elektros krūvio pernašą iš ląstelės į anodą alternatyvios energijos šaltinyje.

Darbo aktualumas

Sparčiai daugėjant tyrimų, kuriuose nagrinėjamas biokuro elementų veikimas ir jų pritaikymo galimybės, išaiškėja, jog žemas jų efektyvumas vis dar išlieka svarbia problema. Siekiant padidinti efektyvumo rodiklius tenka išspręsti nemažai naujų mokslinių uždavinių.

Mielių *Saccharomyces cerevisiae* taikymo biokuro elementuose tyrimas atskleidžia elektronų pernašos tarpininko imobilizavimo galimybes, naujų medžiagų pritaikyto biokuro elementuose efektyvumą bei tyrimams naudojamo atominių jėgų mikroskopo parametrų parinkimo galimybes.

Tyrimo objektas

Disertacinių tyrimų objektas yra biokuro elementas ir jo efektyvumo valdymas.

Darbo tikslas

Disertacijos tikslas yra sukurti ir ištirti biokuro elementą modifikuojant jo anodinę dalį ir kaip katalizatorių naudojant mieles.

Darbo uždaviniai

Darbo tikslui pasiekti buvo sprendžiami šie *uždaviniai*:

1. Sukurti ir įvertinti biokuro elementuose naudojamų gyvų ląstelių gyvybingumo, elektrocheminių savybių ir pagerinto vizualizavimo nustatymo metodiką.
2. Sukurti dinaminį modelį siekiant nustatyti parametrus, tinkamus biokuro elementuose naudojamoms gyvoms ląstelėms vizualizuoti atominės jėgos mikroskopo kantaktiniu režimu.
3. Įvertinti lipofilinių elektronų pernašos tarpininkų ir (arba) daugiasienių anglies nanovamzdelių poveikį mielių, naudojamų biokuro elementuose, gyvybingumui, elektrocheminiam aktyvumui.
4. Nustatyti sukurto biokuro elemento efektyvumą anodinėje dalyje naudojant daugiasieniais anglies nanovamzdeliais modifikuotas arba nemodifikuotas mieles bei dviejų elektronų pernašos tarpininkų sistemą.

Tyrimų metodika

Darbe pirmiausia atlikti teoriniai analizės tyrimai siekiant išsiaiškinti pirminius tyrimams naudingus duomenis ir rasti nagrinėjamos problematikos sprendimo būdus, kurie buvo nagrinėti ankstesniuose tyrimuose. Taip pat duomenys buvo apdoroti juos klasifikuojant ir apibendrinant. Toliau buvo pradėti eksperimentiniai tyrimai, kai *Saccharomyces cerevisiae* mielės buvo modifikuotos chinonais ir (arba) daugiasieniais anglies nanovamzdeliais. Mielių gyvybingumas buvo įvertintas optiniu mikroskopu. Elektrocheminės savybės

buvo tiriamos ciklinės voltamperometrijos metodu. Lokalios elektrocheminės savybės buvo tiriamos skenuojančiu elektrocheminiu mikroskopu (SECM), o ląstelių vizualizacija atlikta atominių jėgų mikroskopijos metodu. Biokuro elementų tyrimai buvo atliekami esant skirtingoms apkrovos varžoms, matuojant įtampą ir skaičiuojant generuojamą galią. Užbaigiant darbą visi gauti duomenys buvo analizuojami ir pateikiamos išvados bei rekomendacijos.

Darbo mokslinis naujumas

Rengiant disertaciją buvo gauti šie medžiagų inžinerijos mokslui nauji rezultatai:

1. Sukurtas atominių jėgų mikroskopo dinaminis modelis, tinkamas skenavimo optimizavimui, atsižvelgiant į matavimo adatos geometriją ir mėginio medžiagą.
2. Pirmą kartą įvertintos 9,10-fenantrenchinono taikymo biokuro elementuose, kaip katalizatorių naudojančiuose *Saccharomyces cerevisiae* mielių ląsteles, galimybės ir aprašyti krūvio perdavimo tarp gyvų mielių ląstelių ir elektrodo aspektai.
3. Pirmą kartą įvertintas 2-metil-1,4-naftochinono poveikis *Saccharomyces cerevisiae* mielių ląstelių gyvybingumui ir galimybė naudoti šią medžiagą kaip elektronų pernašos tarpininką biokuro elementuose.
4. Pirmą kartą ištirta daugiasienių anglies nanovamzdelių įtaka *Saccharomyces cerevisiae* mielių ląstelėms bei jų pritaikomumas biokuro elementuose.

Darbo rezultatų praktinė reikšmė

Gauti tyrimų rezultatai praplečia biokuro elementų tyrimų ir panaudojimo galimybes. Be to, gauti rezultatai įgalina naujus tyrimo metodus. Taikant sukurtą atominių jėgų mikroskopijos modelį ir parenkant skenavimo parametrus galima nustatyti vaizdo kokybę prieš matavimą, jei žinoma paviršiaus medžiaga ir struktūra. AFM operatorius gali lengvai įvesti modelio paviršiaus struktūros parametrus, pasirinkti optimaliausią nuskaitymo greitį ir patikimiausią sąveikos jėgą. Be to, AFM nustatytus rezultatus galima palyginti su teoriniais, apskaičiuotais siūlomu modeliu.

Taip pat pasitelkus pasirinktų ir pritaikytų tyrimuose elektronų pernašos tarpininkų taikymo biokuro elementuose būdus galima gauti didesnio efektyvumo biokuro elementus.

Ginamieji teiginiai

1. Biokuro elementų tyrimams naudojant sukurtą dinaminį modelį, galima parinkti įvesties parametrus matavimui atominės jėgos mikroskopu siekiant pagerinti gyvų ląstelių vizualizavimą.
2. Daugiasieniais anglies nanovamzdeliais ir chinonais modifikuotos mielės naudojamos kuriant biokuro elementus – pagerina elektros krūvio perdavimą tarp mielių ir anodo.
3. Dviejų elektronų perdavimo tarpininkų sistema yra tinkama krūviui biokuro elementuose, kai anodas modifikuojamas 9,10-fenantrenchinonu arba 2-metil-1,4-naftochinonu.

4. Chinonų arba daugiasienių anglies nanovamzdelių koncentracija, naudojama mielių modifikacijai biokuro elementuose, turėtų būti parenkama pagal mielių gyvybingumo ir elektrocheminio aktyvumo tyrimų rezultatų duomenis.

Darbo rezultatų aprobavimas

Disertacijos tema yra atspausdinti septyni moksliniai straipsniai.

Disertacijoje atliktų tyrimų rezultatai buvo paskelbti vienuolikoje tarptautinių mokslinių konferencijų Lietuvoje ir užsienyje:

- Tarptautinėje konferencijoje „The 16th International Conference „Mechatronic Systems and Materials“ (MSM 2021)“ 2021 m. Vilniuje, Lietuvoje.
- Tarptautinėje konferencijoje „Advanced materials and technologies: 23rd international conference-school“ 2021 m. Palangoje, Lietuvoje.
- Tarptautinėje konferencijoje „2021 IEEE Open Conference of Electrical, Electronic and Information Sciences (eStream)“ 2021 m. Vilniuje, Lietuvoje.
- Tarptautinėje konferencijoje „Automation 2021. Recent achievements in automation, robotics and measurementtechniques“ 2021 m. Varšuvoje, Lenkijoje.
- Tarptautinėje konferencijoje „14th international scientific conference „The vital nature sign“ 2020 m. Kaune, Lietuvoje.
- Tarptautinėje konferencijoje „Advanced materials and technologies: 22nd international conference-school“ 2020 m. Palangoje, Lietuvoje.
- Tarptautinėje konferencijoje „Automation 2020. Towards industry of the future“ 2020 m. Varšuvoje, Lenkijoje.
- Tarptautinėje konferencijoje „Open readings 2019: 62nd international conference for students of physics and natural sciences“ 2019 m. Vilniuje, Lietuvoje.
- Tarptautinėje konferencijoje „Fizinių ir technologijos mokslų tarpdalykiniai tyrimai: 9-oji jaunųjų mokslininkų konferencija“ 2019 m. Vilniuje, Lietuvoje.
- Tarptautinėje konferencijoje „The immunosensors based on scanning electrochemical microscopy // 10th International workshop on SECM and related techniques“ 2019 m. Paryžiuje, Prancūzijoje.
- Tarptautinėje konferencijoje „Automation 2019. Progress in automation, robotics and measurement techniques“ 2019 m. Varšuvoje, Lenkijoje.

Disertacijos struktūra

Disertaciją sudaro trys pagrindiniai skyriai.

Pirmajame skyriuje pateikiama visų biokuro elementams reikalingų komponentų apžvalga ir analizė. Pradžioje buvo aptariami per pastaruosius kelerius metus kurti ir tirti biokuro elementai ir jų tipai. Taip pat aprašyti biokuro elementų tyrimams pasirinkti elektronų pernašos tarpininkai: 9,10-fenantrenchinonas; 2-metil-1,4-naftochinonas; anglies nanovamzdeliai. Taip pat buvo įtraukta *Saccharomyces cerevisiae* mielių ląstelių analizė. Galiausiai buvo pristatytas atominės jėgos mikroskopijos taikymas gyvų ląstelių tyrimuose.

Antrajame skyriuje apžvelgiamas medžiagų paruošimas ir visi tyrimui taikomi metodai. Aprašomas grafito elektrodų, mielių ląstelių ir daugiasienių anglies nanovamzdelių suspensijos paruošimas. Taip pat aprašomas mielių ląstelių paruošimas eksperimentams su skirtingais elektronų pernašos tarpininkais ir daugiasieniais anglies nanovamzdeliais. Galiausiai dalį skyriaus sudaro nanodalelių elektrocheminių matavimų ir charakteristikų aprašymas.

Trečiajame skyriuje pateikiami mielių *Saccharomyces cerevisiae* taikymo biokuro elementuose eksperimentinių tyrimų rezultatai. Remiantis 2 skyriuje aptartais metodais mielėmis modifikuoto biokuro elemento modeliavimo ir elektrocheminių tyrimų rezultatai pateikiami trečiajame skyriuje.

Bendrosios išvados ir rekomendacijos tolesniems tyrimams apibendrina šį darbą. Pabaigoje pateikiamas platus literatūros sąrašas ir 4 autoriaus publikacijų disertacijos tema sąrašas.

Darbą sudaro įvadas, trys pagrindiniai skyriai, bendrosios išvados, literatūros sąrašas, autoriaus publikacijų disertacijos tema sąrašas. Disertacijos apimtis (be priedų) – 101 puslapis, 43 iliustracijos ir 3 lentelės.

1. Biokuro elementų apžvalga ir analizė

Pirmajame disertacijos skyriuje atlikta literatūros šaltinių disertacijos tematika apžvalga, kurioje pateikiama visų biokuro elementams reikalingų komponentų analizė. Pirmiausia bendrai atsižvelgiama į tipinius biokuro elementus kaip energijos šaltinius galinčius gyvuose organizmuose vykstančių reakcijų metu išsiskiriančią energiją konvertuoja į elektros energiją. Jie gali būti mikrobiniai ar fermentiniai. Patys mikroorganizmai tampa tiesioginiu katalizatoriumi gliukozės oksidacijos reakcijoje. S1.1 paveiksle pateikiamas tipinis biokuro elementas, kuriame membrana (dažniausiai porėta polikarbonatinė plėvelė, turinti 3 mikronų dydžio poras, puikų cheminį bei šiluminį atsparumą) atskiria anodą, ant kurio yra imobilizuotos mielės ir katalizuojama gliukozės-deguonies reakcija (gliukozės oksidacija), ir katodą, kur vyksta redukcija. Oksidacijos reakcijos metu išlaisvinti elektronai gali būti perduodami elektrodui tiesiogiai arba per elektronų pernašos tarpininką. Jis yra medžiaga, turinti savybę oksiduotis ir redukuotis dalyvaudama tiek gyvuose organizmuose (lipofiliniai elektronų pernašos tarpininkai), tiek ant elektrodo esant tam tikram oksidacijos-redukcijos potencialui (hidrofiliniai elektronų pernašos tarpininkai). Elektros srovė teka dėl nuolat išlaisvinamų elektronų vykstant oksidacijos-redukcijos reakcijoms. Elektros krūvio judėjimo kryptis iš anodo katodui vyksta per išorinę grandinę. O reakcijos metu susidarę laisvieji protonai perduodami į terpę, kurioje yra katodas. Ant katodo tirpale esantis deguonis redukuojamas į vandenį. Tad svarbiausia ir dažniausiai analizuojama dalis yra anodas, kurį modifikuojant gaunamas didesnis elementų efektyvumas.

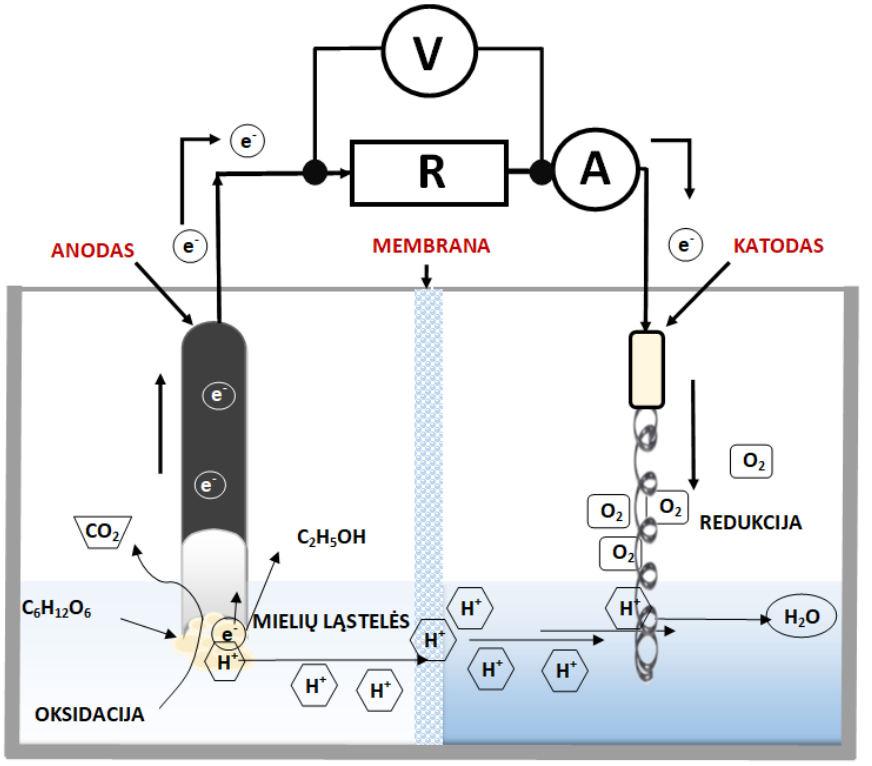

S1.1 pav. Tipinis biokuro elementas

Disertacijoje taip pat pateikiami mikrobinių kuro elementų praktinio pritaikymo būdai, kadangi dėl savo specifikos jie dažnai priskiriami alternatyviesiems energijos šaltiniams, kuriuos galima integruoti į organinių atliekų perdirbimo, taip pat komunalinių nuotekų, kuriose taip pat gausu organinių medžiagų, valymo sistemas. Ypatingo ir vis didėjančio mokslo bendruomenės dėmesio ši mokslo ir technologijų sritis susilaukė tik per pastaruosius du dešimtmečius.

Disertacijos darbe išnagrinėjamos kaip mikroorganizmai naudojamos komerciškai prieinamos sausos kepimo mielės *Saccharomyces cerevisiae*, kurios pasižymi dideliu atsparumu aplinkos poveikiui, lengvai prieinamos ir sąlygiškai nebrangios, todėl tikimasi, kad naudojant jas taps įmanoma prailginti biokuro elemento tarnavimo laiką. Mieles gaubia membrana ir sienelė, todėl reikia ištirti, kokios medžiagos galėtų pereiti membraną ir efektyviausiai reaguoti su ląstelėje esančiais fermentais.

Yra gana daug tokių medžiagų, tačiau beveik visos jos yra toksiškos, taigi reikia ištirti koncentracijas bei kitas sąlygas, kurioms esant ląstelė išlieka gyvybinga. Gana dažnai, siekiant efektyvesnio elektronų pernešimo iš ląstelės link anodo, yra naudojami antriniai elektronų pernešimo tarpininkai. Jų koncentracijos, poveikis ląstelei bei poveikis

paties biokuro elemento efektyvumui irgi nėra išsamiai ištirti. Todėl disertacijoje aprašyti biokuro elementų tyrimams pasirinkti elektronų pernašos tarpininkai: 9,10-fenantrenchinonas; 2-metil-1,4-naftochinonas; anglies nanovamzdeliai ir kalio heksaciano feroatas.

Galiausiai aptariamas pasirinktas atominių jėgos mikroskopijos metodas, kuris leidžia išanalizuoti pasirinktų medžiagų ir vykstančių reakcijų įtaką ląstelėms.

2. Tyrimams naudojamų medžiagų paruošimas ir metodika

Antrajame skyriuje apžvelgiamas medžiagų paruošimas ir visi tyrimams taikomi metodai. Pradžioje aprašomas grafito elektrodų, mielių ląstelių ir daugiasienių anglies nanovamzdelių suspensijos paruošimas. Taip pat aprašomas mielių ląstelių paruošimas eksperimentams su skirtingais elektronų pernašos tarpininkais ir daugiasieniais anglies nanovamzdeliais. Galiausiai pateikiamas nanodalelių elektrocheminių matavimų ir charakteristikų analizės aprašymas.

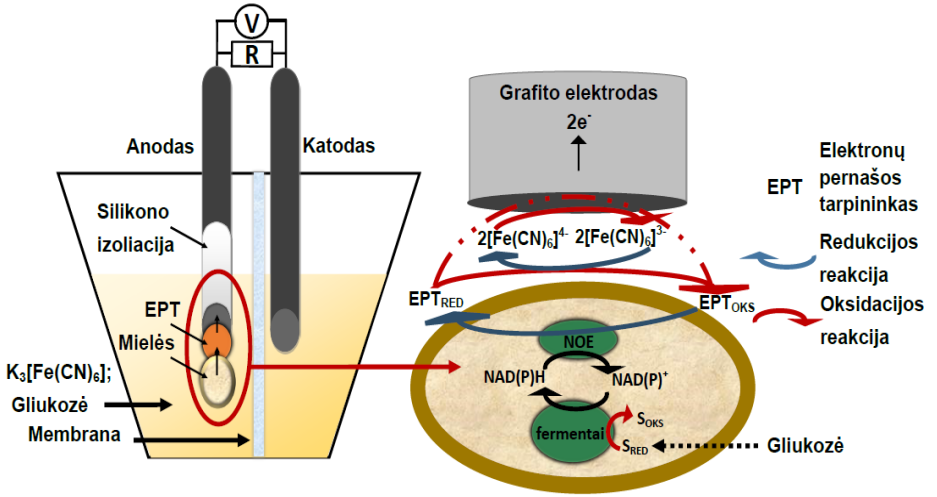

S2.1 pav. Tyrimams naudojamos celės ir reakcijų schema

Didžiąją dalį tyrimų sudarė elektrocheminiai matavimai, kurie atliekami potenciostatu „Autolab PGSTAT 30 Potentiostat/Galvanostat“ (Utrechtas, Olandija) ir „NOVA“ programa. Naudojant įrenginį matuojamos ciklinės voltamperogramos, o vėliau atidedami taškai: prie neigiamo potencialo, kur vyksta redukcija, ir prie teigiamo, kur vyksta oksidacija. Šios srovės reikšmės naudojamos grafikuose, kuriuose nurodomas srovės kitimas kintant tirpalo koncentracijai. Siekiant sugeneruoti daugiau galios, parenkamos sąlygos ir elektronų pernešimo tarpininkai bei jų koncentracija, kad būtų gaunama kuo didesnė elektros srovė.

Matavimo celė užpildoma (ne pilnai) acetatinio-fosfatinio buferinio tirpalo (pastovaus pH elektrolitas), o pasirinktos koncentracijos hidrofilinis kalio heksaciano feroatas bei gliukozė įpilami į tirpalą. Vienas iš pasirinktų lipofilinių elektronų pernašos tarpininkų (9,10-fenantrenchinonas; 2-metil-1,4-naftochinonas ar daugiasieniai anglies nanovamzdeliai) imobilizuojamas ant parengto švaraus elektrodo prieš ten pat imobilizuojant mielių ląsteles. Celėje dviejų rūšių mediatoriai reikalingi todėl, kad vienas iš jų – netirpus vandenyje, jis gali prasiskverbti pro ląstelės membraną ir sureagavęs su ląstelėje esančiais fermentais atiduoti elektronus kitam, ląstelės išorėje veikiančiam mediatoriui, kuris elektronus perneša į elektrodą (S2.1 paveikslo dešinioji pusė).

Metodikos dalyje taip pat aprašomas mikrobinių kuro elementų ląstelių tyrimams pagerinti sukurtas dinaminio modelio sudarymas. Pateikiant atominių jėgų mikroskopo veikimo tikslumo gerinimo metodiką pristatoma ir skenavimo eksperimentų, simuliavimo ir santykinės paklaidos apskaičiavimo etapai. Taip pat pabaigoje pateikiama kitų parametrų apskaičiavimo metodika. Antrajame skyriuje apžvelgiamas medžiagų paruošimas ir visi tyrimams taikomi metodai. Aprašomas grafito elektrodų, mielių ląstelių ir daugiasienių anglies nanovamzdelių suspensijos paruošimas. Taip pat aprašomas mielių ląstelių paruošimas eksperimentams su skirtingais elektronų pernašos tarpininkais ir daugiasieniais anglies nanovamzdeliais. Galiausiai pateikiamas nanodalelių elektrocheminių matavimų ir charakteristikų analizės aprašymas.

3. Eksperimentiniai mielių *Saccharomyces cerevisiae* taikymo biokuro elementuose tyrimai

Trečiajame skyriuje pateikiami mielių *Saccharomyces cerevisiae* taikymo biokuro elementuose eksperimentinių tyrimų rezultatai, kurie gauti remiantis 2 skyriuje pateiktais mielėmis modifikuoto biokuro elemento modeliavimo ir elektrocheminių tyrimų atlikimo metodais. S3.1 paveiksle pateikiama disertacijoje iškeltiems uždaviniams įgyvendinti sukurta tyrimų schema. Ji susideda iš dviejų dalių: pirmoji dalis sujungia pasirinktų medžiagų ir ląstelių analizę (raudonas rėmelis), antroji dalis pateikia sukurto biokuro elemento parametrų tyrimus (juodas rėmelis). Pirmame schemos lygmenyje pateikiamos tyrimo užduotys, o antrame lygmenyje – metodai joms įgyvendinti. Pirmoje dalyje pateikiami medžiagų ir ląstelių tyrimų metodai: ląstelių vizualizavimas, tinkamiausių ląstelių parinkimas, naudojamų medžiagų optimalios koncentracijos nustatymas, ląstelių gyvybingumas ir imobilizacijos kokybė. Antroje dalyje pateikiami mikrobinio kuro elemento savybių tyrimų metodai: medžiagų celėje įterpimo būdai, dviejų elektronų pernašos tarpininkų sistemos analizė, pačio mikrobinio kuro elemento efektyvumas ir ilgaamžiškumas.

Nuosekliai atliekant tyrimus ir atlikus rezultatų interpretavimą numatytų tyrimų planas ir darbų seka buvo koreguojami. Tik atlikus pirmąją tyrimų dalį nagrinėjančią medžiagų pasirinkimą, jų poveikį ir panaudojimo būdus, buvo galima sukurti biokuro elementą ir ištirti jo efektyvumą.

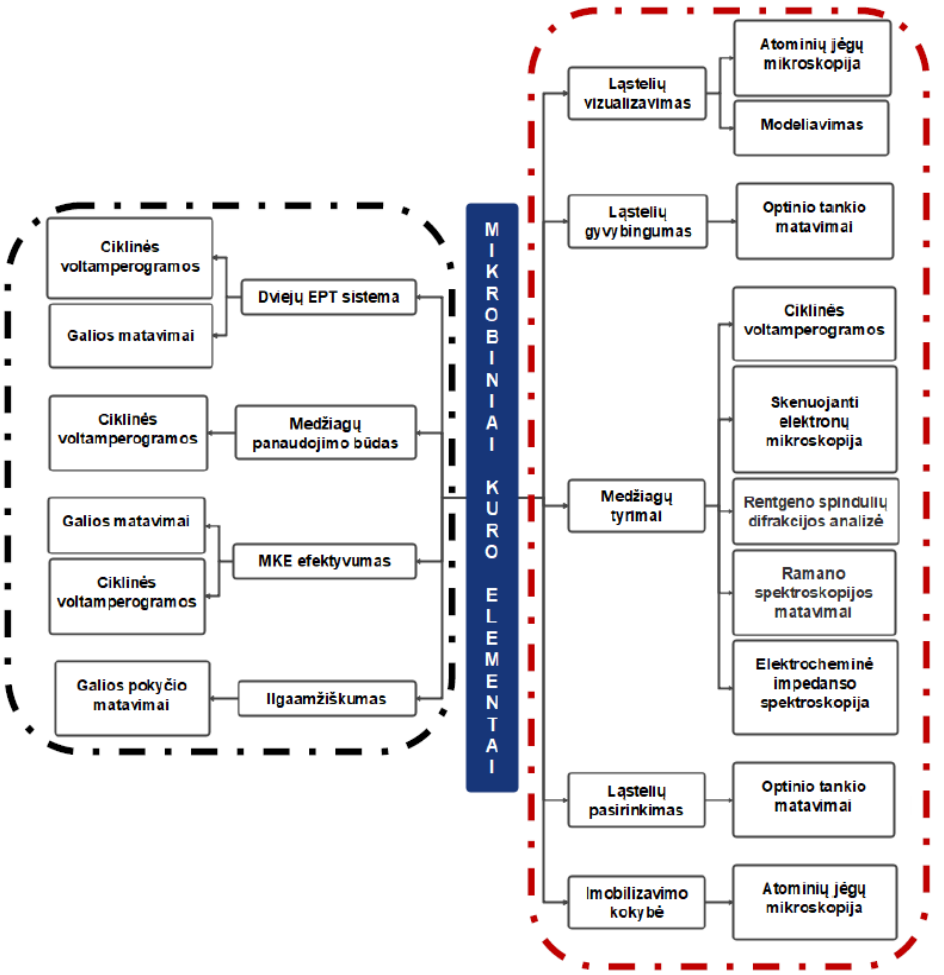

S3.1 pav. Atliktų tyrimų schema

S3.2 paveiksle pateikiamas kokybiškesnio vizualizavimo metodo sukūrimui sukurtas dinaminis modelis, kuris suteikia galimybę sureguliuoti atominių jėgų mikroskopo parametrus, tokius kaip adatos ir paviršiaus sąveikos jėga bei skenavimo greitis, atsižvelgiant į mėginio medžiagą ir adatos geometriją.

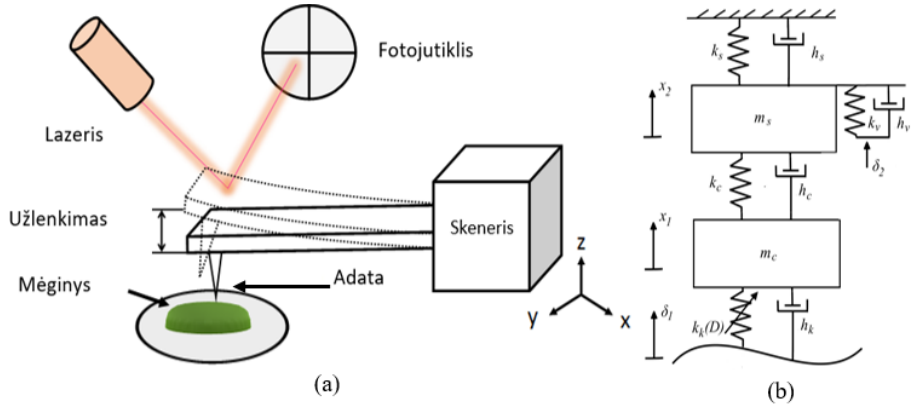

S3.2 pav. Dinaminio modelio informacija: (a) Supaprastinta AJM schema; (b) Dinamis mechaninės skenerio ir AJM adatos modelis. m_s – skenerio masė; k_s – skenerio standumo koeficientas; h_s – skenerio slopinimo koeficientas; m_c – adatos masė; k_c – adatos standumo koeficientas; h_c – adatos slopinimo koeficientas; δ_1 – koordinatė, nusakanti kinematinio žadinimo reikšmę atitinkančią mėginio paviršiaus formą; δ_2 – koordinatė, nusakanti valdymo sistemos poveikį; k_k – kontakto tarp adatos ir medžiagos standumo koeficientas; h_k – kontakto tarp adatos ir medžiagos slopinimo koeficientas; k_v, h_v – standumo ir slopinimo koeficientai nusakantys valdymo sistemos jautrumą, x_1 – adatos masės centro koordinatė; x_2 – skenerio masės centro koordinatė

Modelio adekvatumas įvertintas tarpusavyje palyginus modeliavimo ir eksperimento rezultatus pateikiamus S3.3 paveiksle. Skenuojant bandinį, skirtumas tarp modelio ir eksperimento rezultatų neviršija 3 % (esant 100 µm/s skenavimo greičiui ir 10 nN adatos prispaudimo jėgai).

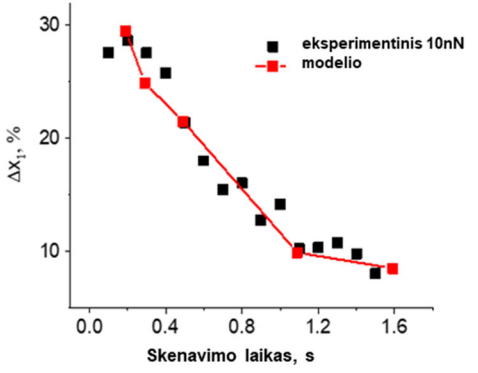

S3.3 pav. Santykinės paklaidos eksperimentinių ir gautų simuliuojant sukurtą modelį palyginimas. Skenavimo greitis 100 µm/s, užduota jėga 10 nN, paviršiaus medžiaga – silicis

Poveikio ląstelėms nustatymo tyrimai pateikiami S3.4 paveiksle, kuriame *Saccharomyces cerevisiae* kepimo mielių ir *Saccharomyces cerevisiae* 21PMR (MATα leu2 ura3-52) mielių augimo kreivės rodančios, kad kepimo mielės yra atsparesnės elektronų pernašos tarpininkų poveikiui skirtingame temperatūrų diapazone.

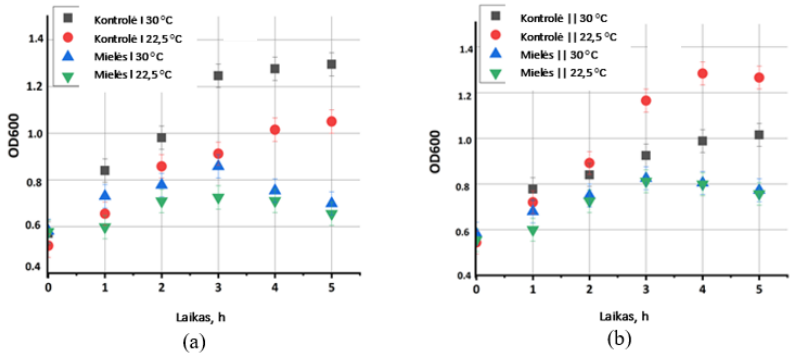

S3.4 pav. Optinio tankio (OD) kitimas nustatant mielių augimo kreives: (a) Augimo kreivių palyginimas: (i) Mielės I – *Saccharomyces cerevisiae* 21PMR (MATα leu2 ura3-52) mielių ląstelės su 3,75 mM menadiono (MD); Kontrolė I – *Saccharomyces cerevisiae* 21PMR (MATα leu2 ura3-52) mielių ląstelės buferiniame tirpale; (b) Augimo kreivių palyginimas: (ii) Mielės II – *Saccharomyces cerevisiae* kepimo mielių ląstelės su 3,75 mM MD; Kontrolė II – *Saccharomyces cerevisiae* kepimo mielių ląstelės buferiniame tirpale

S3.5 paveiksle pateikiamas medžiagų koncentracijų optimizavimas atliktas registruojant ciklines voltamperogramas ir stebint srovės tankio pokytį keičiantis elektronų pernašos tarpininkų koncentracijoms juos imobilizuojant ir naudojant tirpale – nustatyta optimali kiekvienos medžiagos koncentracija ir imobilizavimo pranašumas.

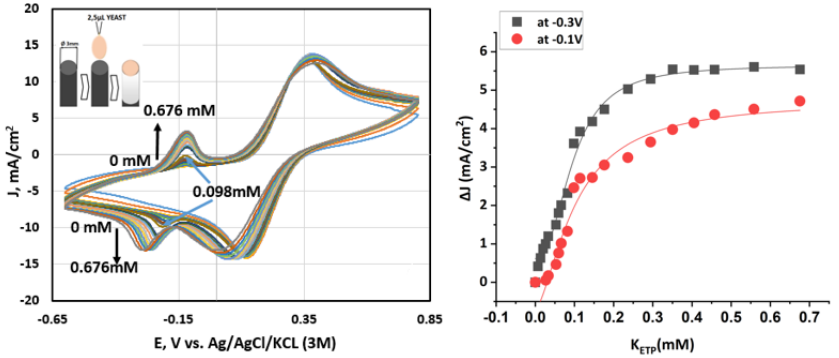

S3.5 pav. Medžiagų koncentracijų optimizavimas (a) Ciklinė voltamperograma, registruojama naudojant mielėmis modifikuotą grafito elektrodą ir keičiant 9,10-fenantrenchinono koncentraciją; (b) maksimalios srovės ties dviem potencialio vertėmis kitimas keičiantis PQ koncentracijai.

Atliekant biokuro elementų efektyvumo nustatymo tyrimus, kuriuose pritaikomi skirtingi elektronų pernašos tarpininkai, buvo analizuojame sugeneruojama galia, kuriuos didžiausios gautos galios rezultatai pateikiami S3.6 paveiksle.

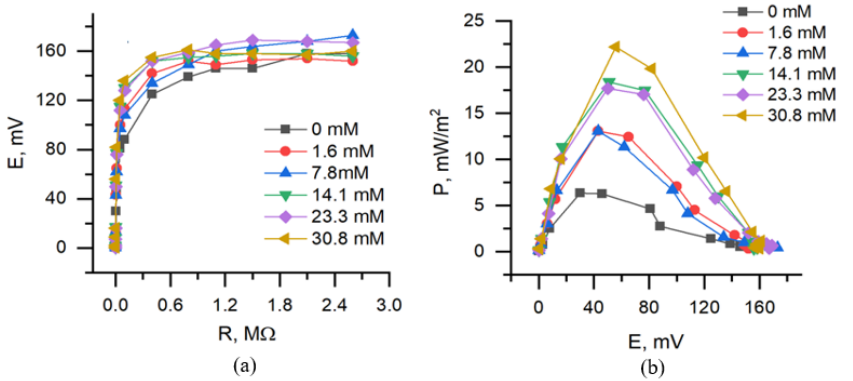

S3.6 pav. Sukurto biokuro elemento generuojamos galios duomenys: (a) Potencialo priklausomybė nuo apkrovos; (b) Apskaičiuoto galios tankio priklausomybė nuo potencialo, kai matavimo celėje (i) grafito elektrodas modifikuotas PQ ir mielėmis yra anodas ir (ii) nemodifikuotas grafito katodas įmerkti į fosfato-acetato buferinį tirpalą su 23 mM kalio heksaciano feroato ir skirtingos gliukozės koncentracijos: 0 mM, 1.6 mM, 7.8 mM, 14.1 mM, 23.3 mM and 30.8 mM

Atlikti pasirinktų medžiagų koncentracijos parinkimo, skirtingų ląstelių įvertinimo, ląstelių gyvybingumo ir generuojamos elektros srovės tankio bei galios tyrimai.

Bendrosios išvados

Apibendrinus literatūros analizės ir eksperimentinių tyrimų rezultatus, galima teigti, kad:

1. Atlikus naudojamų medžiagų optimalios koncentracijos parinkimo, skirtingų ląstelių įvertinimo, imobilizavimo įtakos ir ląstelių gyvybingumo tyrimus sukurta gyvų ląstelių kokybiškesnio vizualizavimo, gyvybingumo ir elektrocheminių savybių nustatymo metodika pagrįsta generuojamos elektros srovės tankio, ląstelės standumo ir optinio tankio matavimais. Tačiau ateityje rekomenduojama susitelkti į elektroporacijos metodo taikymą ląstelių modifikacijai nagrinėtomis medžiagomis ir jų naudojimo tyrimus.
2. Sukurtas atominių jėgų mikroskopo dinaminis modelis, skirtas parinkti įvesties parametrus individualiam eksperimentui, atsižvelgiant į adatos geometriją ir mėginio medžiagą. Modelio adekvatumas įvertintas tarpusavyje palyginus modeliavimo ir eksperimento rezultatus. Skenuojant bandinį, skirtumas tarp modelio ir eksperimento rezultatų neviršija 3 % (esant 100 µm/s skenavimo greičiui ir 10 nN adatos prispaudimo jėgai). Ateityje turėtų būti susitelkiama ties kitų atominių jėgų mikroskopo skenavimo režimų simuliavimu, modelio tikslinimu įvedant

daugiau laisvės laipsnių ir parametrų, stebint ne tik adatos poslinkį, bet ir pasisukimą bei pačio dinaminio modelio automatizavimą taikant mašininį mokymą siekiant pagreitinti modelio rezultatų gavimą.

3. Pagal sukurtą metodiką ištyrus lipofilinių elektronų pernašos tarpininkų ir (arba) daugiasienių anglies nanovamzdelių įtaką ląstelių gyvybingumui ir elektriniam aktyvumui, nustatyta, kad didžiausią srovės tankį užtikrina 9,10-fenantrenchinonas (10 000 mA/m^2), o ląstelių gyvybingumą visos medžiagos paveikia vienodai (OD 0,81±0,05). Ateityje galima nagrinėti kitų tyrimuose geriausius rezultatus parodžiusių medžiagų taikymo galimybes naudojant jas pagal disertacijoje pristatomą metodiką ir derinant su darbe pristatytais elektronų pernašos tarpininkais.
4. Tiriant sukurtą biokuro elementą įrodyta, kad pritaikant skirtingus elektronų pernašos tarpininkus sugeneruojamą biokuro elemento galią galima padidinti daugiau nei 50 kartų. Tačiau žvelgiant į ateities perspektyvas būtina apsvarstyti ne tik generuojamą galią, bet ir minimalų toksiškų medžiagų naudojimą bei lengvai prieinamų ir aplinkos poveikiui atsparių biokuro / ląstelių pasirinkimą. Taip pat siekiant pagerinti gaunamą galios rezultatą galima susitelkti ties elektrodų pakeitimu, taip pat siekti stabilaus ilgaamžiškumo.

Ateities tyrimai šioje srityje turėtų būti nukreipti į generuojamos galios didinimą išlaikant atsinaujinančių energijos šaltinių panaudojimą alternatyviosios energijos gavyboje.

Justė ROŽĖNĖ

APPLICATION OF *SACCHAROMYCES CEREVISIAE* YEAST IN BIOFUEL CELLS

Doctoral Dissertation

Technological Sciences,
Materials Engineering (T 008)

MIELIŲ *SACCHAROMYCES CEREVISIAE* TAIKYMAS BIOKURO ELEMENTUOSE

Daktaro disertacija

Technologijos mokslai,
medžiagų inžinerija (T 008)

2022 05 13. 15,75 sp. l. Tiražas 20 egz.
Leidinio el. versija *https://doi.org/10.20334/2022-023-M*
Vilniaus Gedimino technikos universitetas
Saulėtekio al. 11, 10223 Vilnius
Spausdino UAB „Ciklonas“,
Žirmūnų g. 68, 09124 Vilnius